Project ID: **54661**

Progress Report

Electrochemical Processes for In-situ Treatment of Contaminated Soils

Submitted to
Department of Energy

by:

C.P. Huang (Principal Investigator)
Daniel Cha (Co-Investigator)
Jih-Hsing Chang (Graduate Research Assistant)
Zhimin Qiang (Graduate Research Assistant)
Menghau Sung (Graduate Research Assistant)
Yu-Chun Chiang (Graduate Research Assistant)

Department of Civil and Environmental Engineering
University of Delaware
Newark, Delaware 19716

September 1998 to May 1999

TABLE OF CONTENTS

EXECUTIVE SUMMARY

Mechanisms of Electro-Osmotic Flow in Soils

The electro-osmotic (EO) flow rate is one of the major factors controlling influence the process performance. Many soil and solution parameters can affect the EO water transport. A number of theories about the EO flow in a capillary have been developed. However, there is no simple and acceptable correlation between the EO water transport and fundamental soil-water parameters, such as the soil water content, the soil surface charge density, and the electrolyte concentration. Consequently, we have tried to develop a semi-empirical equation, as a means to estimate the electro-osmotic water transport in the unsaturated soil. It is expected that the equation can provide a better foundation for the development of an in-situ remediation process for application to the vadose zone.

Electro-osmotic flow experiments were conducted under several conditions, namely, the solution pH, the electric field strength, the soil water content, and the electrolyte concentration. Results indicate that the EO flow is proportional to the extent of surface charge density and the intensity of electric field. This can be attributed to the negative charges on the soil surface. When an electric field is imposed to the soil-water system, the electrostatic force is the only driving force for the electro-osmotic flow. According to the Coulomb's law, the electrostatic force is a linear function of the intensity of electric field and the quantity of electric charges. Therefore, the EO flow is closely related to both the extent of surface charge density and the intensity of electric field.

The electrolyte concentration has no significant effect on the EO flow if the electrolyte ions do not interact with the soil (i.e., indifferent ions). The electrolyte concentration can only influence the zeta potential rather than the surface charge when there is no chemical reaction between the electrolyte and the soil. In other words, the electrolyte concentration effect compresses the thickness of the double layer but not change the surface charge density of the soil. Consequently, the electrolyte concentration effect is independent of the EO flow rate because the water flow is related to the surface charge density rather than the zeta potential.

The parabolic relationship between the EO flow and the water content was observed in this study. We used the infinite plate model to derive the correlation between the flow rate and the moisture of the soil. The basic assumption of the infinite model is that the shear stress at any surface element in the water layer is proportional to the rate of change of velocity across the element (i.e., the Newtonian fluid). The EO flow rate is theoretically proportional to the square

of the soil water content.

The following equation was developed: $Q = K\sigma_0(dE/dx)\omega^2$. Where Q, K, σ_0, dE/dx, and ω, are electro-osmotic flow rate, characterized coefficient, surface charge density, potential gradient, and soil water content, respectively. The characterized coefficient, K, is a collection of several physical properties of the soil including the total soil mass (M), the specific surface area ($\sum$), and the pore size (w) of the soil and fluid viscosity (η), that is $K = kwM^2/\eta\sum^2$.

Desorption of Selected Polycyclic Aromatic Hydrocarbons from Soils

In this study, six polycyclic aromatic hydrocarbons (PAHs) were selected as the target compounds, including naphthalene ($C_{10}H_8$), fluorene ($C_{13}H_{10}$), phenanthrene ($C_{14}H_{10}$), anthracene ($C_{14}H_{10}$), fluoranthene ($C_{16}H_{10}$), and pyrene ($C_{16}H_{10}$). The methanol served as a cosolvent to enhance the water solubility and the desorbed efficiency of PAHs. The extraction solution for desorption tests were obtained by mixing methanol and water at various molar ratios. The molar ratios of methanol to water were selected at 0, 0.3, 0.5, 0.8, and 1.0. To conduct the desorption tests, the weighed PAHs-spiked soil was put into a series of glass tubes. A cosolvent with a specific methanol-water ratio was added to each tube. After a pre-selected mixing time, the soil-solution mixtures were filtered and centrifuged. Collect the supernatant into a vial and mix with hexane. The hexane solution was then analyzed for the PAHs concentrations. Each desorption test was conducted in triplicate.

Results indicate that naphthalene, fluorene, and phenanthrene exhibit the identical desorptive trends at various cosolvent fractions. On the other hand, anthracene, fluoranthene and pyrene display similar desorption behavior due in part to their water solubilities being at the same order of magnitude. The amounts of PAHs compounds desorbed increase with increasing the molar ratio of cosolvent from 0 to 0.8. It is observed that the amount of PAHs desorbed reduced when the Log K_{ow} increased at zero molar ratio of the cosolvent. This can be attributed to the different hydrophobilities of the PAHs compounds. The hydrophobility of organic compound is generally considered as the driving force to distribute the organics from liquid phase into soil phase. In other words, the organic compound with a high octanol-water partition coefficient (Log K_{ow}) is difficult to be desorbed. However, as cosolvents fractions were at 0.5, 0.8 and 1.0, the desorbed amounts increase with increasing the value of Log K_{ow}. The extent of methanol must play an important role in the soil-PAHs-water system due to its cosolvent characteristics.

The kinetic behaviors of PAHs desorption exhibit the Langmuir-type characteristics,

which contain a fast followed a slow desorption. In addition, the equilibrium of desorption can be reached after 12-hour mixing for all PAHs. The equilibrium concentrations of phenanthrene are similar in the presence of cosolvent. The equilibrium concentration (25 μg/g) of anthracene at 0.3-cosolvent fraction is lower than that of other PAHs (75 μg/g). The molecular weight, the Henry's law constant, and the $\log K_{ow}$ of these two PAHs are similar except their water solubility. The different water solubility can be attributed to the difference between their molecular structures. Likewise, the equilibrium concentrations of fluoranthene and pyrene at various cosolvent fractions are different even both have same molecule formula.

Oxidation of Selected Organic Compounds by Fenton Process

In the previous report (1997-1998), we investigated the oxidation of naphthalene and halogenated hydrocarbons, including PCE, TCE and chloroform by Fenton process in batch, pseudo-continuous and continuous modes. The continuous mode process yields the best results. Another major category of toxic organic contaminants typically present at some specific DOE sites is polycyclic aromatic hydrocarbons (PAHs). They are generally found in the heavier fractions of petroleum. The weight percentage of aromatics (both monocyclic and polycyclic) in crude oil is around 30% (U.S. EPA, 1980). Accidental petroleum spills and leaking of underground petroleum storage tanks can seriously contaminate surrounding soils and groundwaters by PAHs. Thermal incineration also significantly contributes to PAHs contamination. In the current work, we have studied the oxidation of selected PAHs, namely, fluorene, phenanthrene, fluoranthene, pyrene and anthracene, by continuous mode Fenton process.

The major limiting factor of studying the oxidation of PAHs in aqueous solutions is their extremely low water solubility. This property not only makes chemical analysis difficult, but also requires a long time to prepare the reaction solutions due to the slow dissolution rate. All selected PAHs were analyzed by GC/MS after concentrated by hexane extraction. In order to accelerate dissolution, three media-assisted dissolution methods were investigated and compared. Methanol, glass-beads, and hexane were separately selected to enhance the dissolution of the model compound, phenanthrene. Results indicate that the hexane-assisted dissolution is the most practical method to obtain the PAHs-only reaction solutions quickly. Methanol is commonly used as a cosolvent to wash out hydrophobic compounds in subsurface in soil and groundwater remediation processes. The influence of methanol on the oxidation of selected PAHs was also investigated. These solutions were prepared by the methanol-assisted dissolution, with methanol

concentration being at 0.1% (v/v) or about 790 ppm, in the final reaction solutions.

We developed a kinetic model, $[RH]=[RH]_0 \exp(-k_{obs}t^2)$, to fit the experiment data. Where, *[RH]* and $[RH]_0$ are the residual and initial concentrations of organic compound, respectively; k_{obs} is the observed rate constant; t is the reaction time. The increasing rate of hydroxyl radical concentration can be calculated using $a = 2k_{obs} / k_3$. Where, a is the increasing rate of hydroxyl radical concentration, and k_3 is the second order rate constant of organic compound toward hydroxyl radical. This proposed kinetic model was employed to fit the experiment data for the oxidation of PCE, TCE and naphthalene. Results indicate that the values of the observed rate constant, k_{obs}, are 4.38 x 10^{-2}, 1.41 x 10^{-2}, 8.30 x 10^{-3}, 3.50 x 10^{-3} and 1.30 x 10^{-3} min^{-2} for PCE, 1.13 x 10^{-2}, 5.6 x 10^{-3}, 2.5 x 10^{-3}, 1.3 x 10^{-3} and 5.3 x 10^{-4} min^{-2} for TCE, and 4.19 x 10^{-2}, 2.95 x 10^{-2}, 1.93 x 10^{-2}, 6.1 x 10^{-3} and 3.1 x 10^{-3} min^{-2} for naphthalene at different dosage molar ratios of $[H_2O_2]/[Fe^{2+}]$ from 1:1 to 1:0.0625. Correspondingly, the calculated a values are 5.21 x 10^{-13}, 1.68 x 10^{-13}, 9.88 x 10^{-14}, 4.17 x 10^{-14} and 1.55 x 10^{-14} M/min for PCE, 9.42 x 10^{-14}, 4.67 x 10^{-14}, 2.10 x 10^{-14}, 1.05 x 10^{-14} and 4.4 x 10^{-15} M/min for TCE, and 1.40 x 10^{-13}, 9.83 x 10^{-14}, 6.43 x 10^{-14}, 2.03 x 10^{-14} and 1.03 x 10^{-14} M/min for naphthalene. By plotting k_{obs} vs. $[Fe^{2+}]/[RH]_0$, the linear relationship can be obtained for PCE, TCE and naphthalene. For PCE, there are two linear segments: K_{obs} = 0.0686 x $[Fe^{2+}]/[PCE]_0$ (0 $[Fe^{2+}]/[PCE]_0$ 0.2 M/M.min), and K_{obs} = 0.183 x $[Fe^{2+}]/[PCE]_0$ -0.0233 ($[Fe^{2+}]/[PCE]_0$ 0.2 M/M.min). For TCE, there is only one linear equation: K_{obs} = 0.0741 x $[Fe^{2+}]/[TCE]_0$, on the whole range of $[Fe^{2+}]/[TCE]_0$ studied (0 $[Fe^{2+}]/[TCE]_0$ 0.16 M/M.min). For naphthalene, there are two linear equations: K_{obs} = 0.130 x $[Fe^{2+}]/[Naph]_0$ (0 $[Fe^{2+}]/[Naph]_0$ 0.14 M/M.min), and K_{obs} = 0.053 x $[Fe^{2+}]/[Naph]_0$ + 0.013 ($[Fe^{2+}]/[Naph]_0$ 0.14 M/M.min).

In PAHs experiments, results indicate that all selected PAHs can be effectively oxidized by the Fenton's reagent without the interference of methanol. Experiment data can be fitted well by the above proposed kinetic model. The values of k_{obs} and a can be obtained by model fitting, e.g., 0.57 x 10^{-1} min^{-2} and 0.19 x 10^{-12} M/min for fluorene, 5.24 x 10^{-1} min^{-2} and 1.75 x 10^{-12} M/min for phenanthrene, 7.64 x 10^{-1} min^{-2} and 2.55 x 10^{-12} M/min for fluoranthene, 8.10 x 10^{-1} min^{-2} and 2.70 x 10^{-12} M/min for pyrene, and 0.57 x 10^{-1} min^{-2} and 0.19 x 10^{-12} M/min for anthracene, at $[H_2O_2]/[Fe^{2+}]$ molar ratio of 1:0.25. However, in the presence of methanol, the oxidation of selected PAHs is seriously inhibited. Though the reactivity of methanol toward hydroxyl radical is not as high as those of selected PAHs, it captures most of hydroxyl radicals due to its relatively high concentration. In order to improve the removal efficiency of target organic contaminant, both dosages of hydrogen peroxide and ferrous ion should be increased at the optimal $[H_2O_2]/[Fe^{2+}]$ molar ratio. Increasing the dosage of hydrogen peroxide or ferrous ion

alone has little effect on the removal efficiency. The optimal $[H_2O_2]/[Fe^{2+}]$ molar ratio is 1:0.125 for fluorene, phenanthrene and fluoranthene, and 1:0.5 for pyrene. No optimal $[H_2O_2]/[Fe^{2+}]$ molar ratio has been observed for anthracene, however. In the whole range of $[H_2O_2]/[Fe^{2+}]$ molar ratio studied, the oxidation efficiency of anthracene increases with decreasing $[H_2O_2]/[Fe^{2+}]$ molar ratio. It is noted that the saturated concentration decreases from fluorene, phenanthrene, fluoranthene, pyrene to anthracene, whereas the corresponding optimal $[H_2O_2]/[Fe^{2+}]$ molar ratio increases in the order: fluorene phenanthrene fluoranthene > pyrene > anthracene.

I. INTRODUCTION

I.1. Statement of Problem

Soils at typical DOE (Department of Energy) waste sites are known to be contaminated by a host of hazardous organic chemicals, heavy metals and radionuclides. Typical hazardous organic contaminants include chlorinated solvents such as trichloroethylene (TCE), tetrachloroethylene (PCE), chloroform, and carbon tetrachloride, and polycyclic aromatic hydrocarbons (PAHs) such as naphthalene, fluorene, phenanthrene, anthracene and pyrene. It is also known that major toxic heavy metals such as Pb, Cr, As, Zn, Cu, Hg, and Cd and major radionuclides such as Tritium, U, Sr^{90}, Pu, Cs^{137}, and Tc are also commonly present at some DOE waste sites. Some of these chemicals are relatively mobile and can migrate down to the vadose zone and/or the aquifer region.

Among these hazardous chemicals, the treatment of organic contaminants is the focus of this project. Heavy metals, as well as radionuclides, can be readily separated by various commercioally available methods once they are desorbed from the soil surface and collected in the solution phase,

Chlorinated hydrocarbons, commonly used as industrial solvents, are a significant category of hazardous organic compounds. Chlorination has become a widespread industrial practice because it yields compounds of lower flammability, higher density, high viscosity, and improved solvent properties compared to nonchlorinated solvents (Watts, 1997). In the 1970s, 46.5% chlorine gas was used for the production of chlorinated organic compounds in the United States (Higgins, 1989). Chlorinated solvents are mainly used for degreasing and cleaning a large range of products, from machine parts to computer chips. Tetrachloroethylene (PCE) is one of the most stable species of the chlorinated aliphatic solvents due to the total chlorination status. Its primary application has been in dry cleaning. About 80% of the cleaning industry uses PCE. Trichloroethylene (TCE) is an excellent solvent for a large number of natural and industrial materials. It is moderately toxic, nonflammable, and slowly oxidized. TCE has greatest use in the vapor degreasing of fabricated metal parts (Higgins, 1989). Chloroform has been used most frequently as a dry cleaning spot remover and for cleaning and degreasing machine and engine parts. Other applications include industrial intermediates, insecticides, and the purification of vitamines. Carbon tetrachloride was widely used in dry cleaning, metal degreasing, and fire extinguisher before 1970 in the United States. It was then banned because of its toxicity. For

some industrial purposes, carbon tetrachloride is stilled used as a reaction intermediate in the industrial synthesis of some organic chemicals. Because of its environmental persistence, it is still found in significant concentrations at some sites. Although these compounds are highly volatile, they can also migrate through the subsurface. The properties of chlorinated solvents that make them mobile in groundwater systems include high density, relatively high water solubility, and low biodegradability (Watts, 1997). They also adsorb to soil surfaces, resulting in a high contamination level at some specific sites. A survey of 7000 wells conducted in California from 1984 to 1988 showed that approximately 1500 of them had detectable concentrations of organic chemicals present. The most common chemicals detected were chlorinated hydrocarbons such as tetrachloroethylene, trichloroethylene, chloroform, 1,1,1-trichloroethane, and carbon tetrachloride (Mackay, 1990). In addition, at National Priorities List (NPL) sites the contaminants that are most frequently found include trichloroethylene (42%) and tetrachloroethylene (28%) (ATSDR, 1989).

Polycyclic aromatic hydrocarbons (PAHs) are found in the heavier fractions of petroleum products (e.g., lubricating oils, asphalt, and tarlike materials) as well as automobile exhaust. The leaking of petroleum underground storage tanks may result in serious contamination of subsurface soils with PAHs, and eventual contamination of groundwater. Though these tanks are made of relatively durable materials, unfortunately, soil is a corrosive environment and, after a certain peroid of time (from 5 to 25 years), the tanks rust, corrode, and leak (Shwendeman *et al*., 1987). Another major source of PAH contamination is gas plants, which produce gas from coal and oil. Soils around these gas plants are difficult to remediate because of high concentrations of PAHs, long chain aliphatics, and phenolics (Michelcic *et al*., 1988). It is well known that PAHs chemically induce cancer.

Public concerns focus on health effects such as cancer and other chronic illnesses. The importance of minimizing the effects of these typical hazardous wastes is obvious: approximately 33% of the United States cities use groundwater, while 95% of the rural United States population relies on groundwater for domestic use (Patrick, 1983). That is why most of chlorinated organics (such as tetrachloroethylene, trichloroethylene, chloroform, carbon tetrachloride), and PAHs (such as naphthalene, phenanthrene, pyrene, anthracene) are listed among U.S. EPA priority pollutants.

The removal of toxic organic chemicals from contaminated soils is a difficult task. The soil remediation processes are usually classified as in-situ and ex-situ applications. In-situ treatment is more attractive compared to ex-situ methods such as pump and treat and containment. Many methods have been suggested for the in-situ remediation of contaminated

soils, including vitrification, freezing, and bioremediation. However, vitrification and freezing only provide passive solution to the problem, and bioremediation is hindered by several engineering difficulties such as nutrient transport, metal toxicity, and microbial adaptability. Especially the presence of heavy metals, can render the bioremediation process infeasible. Therefore, in-situ remediation technologies that are easy for application, dependable, and effective are urgently needed.

I.2. Overview of Current Related Technologies

Since this research project deals with the development of in-situ treatment for the remediation of contaminated soils, an overview of current related technologies is necessary. Soil remediation methods can be classified as physical, biological, and chemical processes based on different principles involved.

A number of physical methods such as in-situ heating, freezing and vitrification are currently being developed for soil remediation. In-situ heating uses steam injection (Hoogendon, 1984) or radio frequency (RF) (Brideg and Strestly, 1984) to heat the contaminated soil. At high temperatures, ranging from 300 ~ 400 ^{o}C, organic chemicals are decomposed. Artificial soil freezing involves the installation of freezing loops in the ground and a self-contained refrigeration system. Toxic chemicals are immobilized at low temperatures. In-situ vitrification is done by passing an electrical current through the soil to convert the soil into a glassy material. Though physical in-situ remediation processes appear effective, its implementation is difficult. Furthermore, method such as vitrification renders the affected aquifer useless.

Bioremediation has received much attention in the field. It is done by injecting appropriate nutrients to the contaminated zone to stimulate microbial growth and as a means to degrade the organic contaminants. However, bioremediation can only degrade those organic compounds which are amenable to microbes. Several factors can affect the operation of the bioremediation process: nutrient, oxygen content, redox potential, pH, water saturation, hydraulic conductivity, osmotic pressure, temperature, growth inhibitors, predators, and the type and concentration of contaminants. Primary substrate must be provided if the organic contaminants are co-metabolized. Aerobes require oxygen, and anaerobes need nitrate or sulfate as electron acceptors. Optimum pH range for microbial activity is 6 to 8. The temperature is between 20 and 37 ^{o}C. Since subsurface temperature is generally around 10~15 ^{o}C, temperature is unfavorable for bioremediation. If the concentration of the target compound is low, the microbes may not be

stimulated to utilize the organic compound in question. Moreover, if other "preferred" carbon sources are present, the microorganisms may by-pass the target pollutants as food source. The ecological structure of the underground can cause severe problems to bioremediation process. Competition between different microbial species and salt concentrations can have a severe influence on the microbes of interest. Extensive research has been conducted to use isolates from the soil-water system (Stief, 1984; Mckinnon and Dykessen, 1984; Strier, 1980; Macay and Shiu, 1981; Wood, 1980; Martinez, 1986; Chivers, 1971). However, the sustainability of these enriched isolates in the natural environment remains unknown. Another crucial factor is the hydraulic conductivity of the soil-water system. The hydraulic conductivity must be large enough and the residence time short enough so that the nutrients added will be effective. Another complication is the presence of an anaerobic condition where heavy metals may be released, thereby posing as toxicants to the microbial activities. Recent development on bioremediation processes has been concentrated on the addition of oxidizing agents. Oxidizing agents such as H_2O_2, O_3 and air have been delivered to the soil-water system to enhance the microbial activity. However, due to the limited availability of oxygen in the subsurface system, the degradation of organics will be hindered.

Chemical in-situ treatment technology includes immobilization, extraction and detoxification. Precipitation, chelation and polymerization are major forms of immobilization. Extraction involves the flushing of contaminated soils with surfactants, dilute acids and bases, or water. Detoxification includes reduction, oxidation, neutralization (for heavy metals), and hydrolysis. Immobilization does not eliminate the contaminants permanently. Rather it releases the contaminants from their associated soil mass. Chemical oxidation and reduction change the oxidation state of the organic contaminants. Commonly used oxidizing agents include potassium permanganate, ozone, hydrogen peroxide and hypochlorite. Among these oxidants, ozone has received the greatest attention. However, the mechanism of ozonation was not fully understood until the last seventies when Hoigne and Bader (1978, 1983) proposed that ozone can have two reaction modes: direct and indirect reactions. The direct ozone reaction is highly selective and slow with rate constants on the order of 1 to 10^3 (M^{-1} sec^{-1}). The indirect reaction is nonselective and fast with rate constants on the order of 10^7 to 10^{10} (M^{-1} sec^{-1}). As a result, there is no complete mineralization and a variety of intermediates can be formed.

I.3. Objectives

By all account, in-situ remediation of contaminated soil is the most attractive approach. However, to be successful in in-situ remediation, one needs to address two basic engineering problems: (1) enhancing the release and subsequent transport of the contaminants from the soil surface to the solution phase, and (2) facilitating the detoxification of the released contaminants.

In this project, we concentrate on the study of electrokinetic process as a means to facilitate the removal of mixed contaminants, namely, organics and heavy metals, from soils. In order to effectively degrade the released organic contaminants, we use an advanced chemical oxidation process based on catalytic hydrogen peroxide.

Electrokintics has been widely applied in sludge dewatering, grout injection, in-situ generation of chemical reagents for electrolysis of contaminants, electro-osmosis flow barrier, and decontamination of soil and groundwater (Mitchell, 1986). The electrokinetic process relies on an external applied voltage to induce water movement in soil capillaries. The soluble cations in the water phase migrate to the cathode and the anions move toward the anode. Since the hydration spheres of cations are larger than those of most anions, more water mass is carried by cations than anions, a net flow of water will move from the anode toward the cathode. Consequently contaminants will be carried away from the soil to the cathodic chamber as a form of solvate in the net water flow. Acar and associates (1991) have demonstrated in laboratory and field studies that the removal of Pb(II) from soils. It is reported that 75~95% of Pb(II) can be transported across the test specimens at an energy consumption of 29~60 kWh/m^3 (Hamed *et al*., 1991). Lageman has reported successful treatment of soils contaminated by heavy metals in the Netherlands (1994). For the mobilization of non-polar organic compounds from the soil surface by electrokinetic force, it is noted that the electrostatic attraction becomes unimportant. In order to enhance the electrokinetic flow rate, it is necessary to increase the ionic strength and the zeta potential of the soil surface which can be accomplished by pH adjustment or the addition of surfactants.

The concept of "advanced chemical oxidation processes" (AOP) is defined as "the oxidation processes which generate hydroxyl radicals in sufficient quantity to affect water treatment" (Glaze *et al*., 1987). Due to its extremely high oxidation-reduction potential, hydroxyl radical can react with almost all organic compounds and some inorganic ions. Most of AOP systems use a combination of strong chemical oxidant, e.g. O_3 or H_2O_2, a catalyst, e.g. transition metal ions or photocatalyst, and with or without irradiation, e.g. ultraviolet (uv), ultrasound (us), or electron beam (eb). Huang *et al*. (1993) have discussed the merits and demerits of these various AOP processes and concluded that hydrogen peroxide-based AOP such as conventional Fenton and electro-Fenton processes are the most promising technologies.

These methods require no addition of obnoxious chemicals, easy for operation, effective, and economically attractive. Compared to ozone-based processes, hydrogen peroxide-based processes have better mass transfer efficiency and higher working safety. Of the two hydrogen peroxide-based processes, namely, conventional Fenton and electro-Fenton, the later process appears to be more advantageous than the conventional Fenton process due mainly to the fact that there is no need to purchase, transport, and store hydrogen peroxide with the electro-Fenton process.

In this project, electro-kinetic (EK) and electro-Fenton (EF) processes will be studied and integrated for in-situ treatment of soils containing mixed contaminants. It is to achieve the following objectives:

(a) To study important parameters controlling the mobilization and transport of selected organics and metals in soils by electrokinetic (EK) process.

(b) To study the important factors governing the oxidation of selected organic contaminants by the electro-Fenton (EF) process.

(c) To understand the mechanisms of the oxidation of selected organic contaminants by electro-Fenton oxidation process.

II. ELECTRO-OSMOTIC FLOW IN SOILS

II.1. Introduction

The electrokinetic behavior has been investigated since the very beginning of the 19th century. Many theories have been developed to explain the mechanism of electro-osmotic (EO) flow in the capillary and the porous media. Reuss, in 1809, found that the water flow could be induced through the capillary by applying an electric field. About half a century later, Wiedemann conducted a number of quantitative experiments and introduced one of the fundamental theories of electrokinetics. This theory states that the volumetric electro-osmotic flow is proportional to the applied current. In 1879, Helmholtz developed the double layer theory, which incorporated parameters of electrical and the electro-osmotic flow. Although the theory can not explain all electro-osmotic behaviors, it represents a relatively acceptable formulation of the electro-osmotic phenomenon in most capillary materials.

In 1903, Smoluchowski applied the double layer theory to account for the distribution of electro-osmotic flow on the capillary surface. Gouy introduced a concept of the potential and charge distribution in the fluid adjacent to the capillary wall in 1910. He computed the electric charge distribution in a diffuse layer. Debye and Huckel, in 1923, determined the ionic distribution in solutions of low ionic energy, by means of a linear simplification of the exponential Boltzmann ion energy distribution. In 1965, Esrig and Majtenyi applied the Buchingham π theorem to describe the electro-osmotic flow in porous media. They mathematical equation suggested that the average velocity of flow is proportional to the surface charge density of the porous media. Gray and Mitchell, in 1967, found a parabolic relationship between the water content and the electro-osmotic water transport in soils.

One of the earliest and still widely used models of electrokinetic processes was developed by Helmholtz (1879) and later refined by Smoluchowski (1914). This theory indicated that the electro-osmosis water transport in the capillaries or in soils could be described quantitatively. They assumed that the pore radii were relatively larger than the thickness of the diffuse double layer and all of the mobile ions were concentrated near the interface between water and the soil. These assumptions are acceptable when the soil with large pores is saturated with fresh water or dilute electrolyte solutions. On this basis, the velocity of electro-osmotic flow in soils, v_e, produced by an applied voltage, E, is given by:

$$v_e = \frac{D\zeta}{4\pi\eta}\frac{E}{L} \qquad [2.1]$$

where D = dielectric constant of the soil water

ζ = zeta potential

η = viscosity

L = electrode spacing

However, this model is not considered valid for small capillaries because the thickness of electric double layer and the capillary radius are at the same order of magnitude.

To describe the electro-osmosis phenomena in the case of very small capillaries (microcapillaries), a quantitative model was developed by Schmid (1950). He assumed that the excess cations balancing the negative charges of clay particles are uniformly distributed through the entire pore cross-section area. The equation of electro-osmotic flow is given by:

$$v_e = \frac{r^2 A_o F}{8\eta}\frac{E}{L} \qquad [3.2]$$

where r = radius of pore

A_o = volume charge density in the pore

F = Faraday constant (96,500 coulombs per equivalent)

Shimid considered this equation valid for capillaries with radii of less than about 500 .

In addition, Spiegler (1958) introduced a completely different concept to explain the electro-osmosis processes, which is based on ion-water-matrix frictional interactions. This concept is independent of any particular structure of the porous medium and can account for some of the observed discrepancies in the earlier theories. Spiegler's theory is conceptually useful. The quantitative predictions based on his theory require lengthy experimental measurements and computations (Gray and Mitchell, 1967).

For the application of the electro-osmotic flow in the vadose zone, the above models are not valid because the water molecule are not filled with the soil void (i.e., unsaturated). The practically used model of electro-osmotic flow through soil is described on a macroscopic scale by the following equation:

$$Q = k_e i_e A \qquad [2.3]$$

where Q = electro-osmotic flow rate

k_e = coefficient of electro-osmotic conductivity

i_e = applied electrical gradient

A = gross cross-sectional area perpendicular to water flow

The values of hydraulic conductivity of different soils can differ by several orders of magnitude; however, those of the coefficients of electro-osmotic conductivity are generally between 1×10^{-9} and 10×10^{-9} $m^2/(V \cdot s)$ and are independent of soil type (Mitchell 1993). Thus, an electrical gradient is a much more effective driving force than hydraulic gradient conductivity. Nevertheless, there is no simple and acceptable correlation between electro-osmotic water transport and fundamental soil-water parameters (such as the water content of the soil, the soil surface charge density, and the electrolyte concentration) has been advanced. One of the difficulties in developing a universal correlation is the wide variance of electrokinetic behavior exhibited by clay-water-electrolyte systems.

Consequently, we have tried to develop a semi-empirical equation, which can estimate the electro-osmotic water transport in the unsaturated soil. Several factors were considered including the solution pH value, the soil surface charge density, the intensity of electric field, the soil water content, and the electrolyte concentration. It is expected that the equation can provide a better foundation for the development of an in-situ remediation process for application to the vadose zone.

II.2. Methods and Materials

Soil samples were collected from a specific waste site. The characteristics of soil including particle size distribution, pH, ECEC (effective cation exchange capacity), organic matter, soil moisture, hydraulic conductivity, zeta potential, pH_{zpc}, and specific surface area were analyzed. Table 2.1 shows the results and analytical methods used. The chemicals as electrolytes were purchased from Aldrich Co (Milwaukee, WI). The purity of sodium chloride and sodium acetate is around 99.0%.

Table 2.1. Physical-chemical characteristics of the soil sample

Physical-chemical characteristics	Result	Method
Sand (%)	14.0	Hydrometer
Silt (%)	38.0	Hydrometer
Clay (%)	48.0	Hydrometer
pH	7.6	In 0.01M $CaCl_2$
ECEC (meq/100g)	20.5	The sum of exchangeable K,Ca,and Mg
Organic Matter(%)	1.69	Heating at 105 ^{o}C for 2 hours, then at 360 ^{o}C for 2 hours
Moisture (%)	13.6	Heating at 105 ^{o}C for 24 hours
Hydraulic Conductivity (10^{-8}cm/s)	2.49	Constant-head
pH_{zpc}	2.34	pH meter and Zetameter
Specific Surface Area (m^2/g)	0.4	Coccine Dye Adsorption

ECEC: effective cation exchange capacity

Figure 2.1 shows the sketch of the laboratory electro-osmosis reactor. The electro-osmosis cell, consists of an acrylic unit with a central cylinder of 11.5 cm in length and 8.9 cm in internal diameter. The volume of both the cathode and the anode compartments are 700 mL. To separate the soil from the water solution, a set of two nylon meshes (Spectrum model PP, mesh opening 149 μm) with a filter paper (Whatman No. 1) in between are used as a membrane in each of the electrode reservoirs. Graphite disks (Carbon of America; grade 2020; 3.25 inches

in diameter) are utilized as electrodes placed at each compartment near the central cylinder, right behind the membranes.

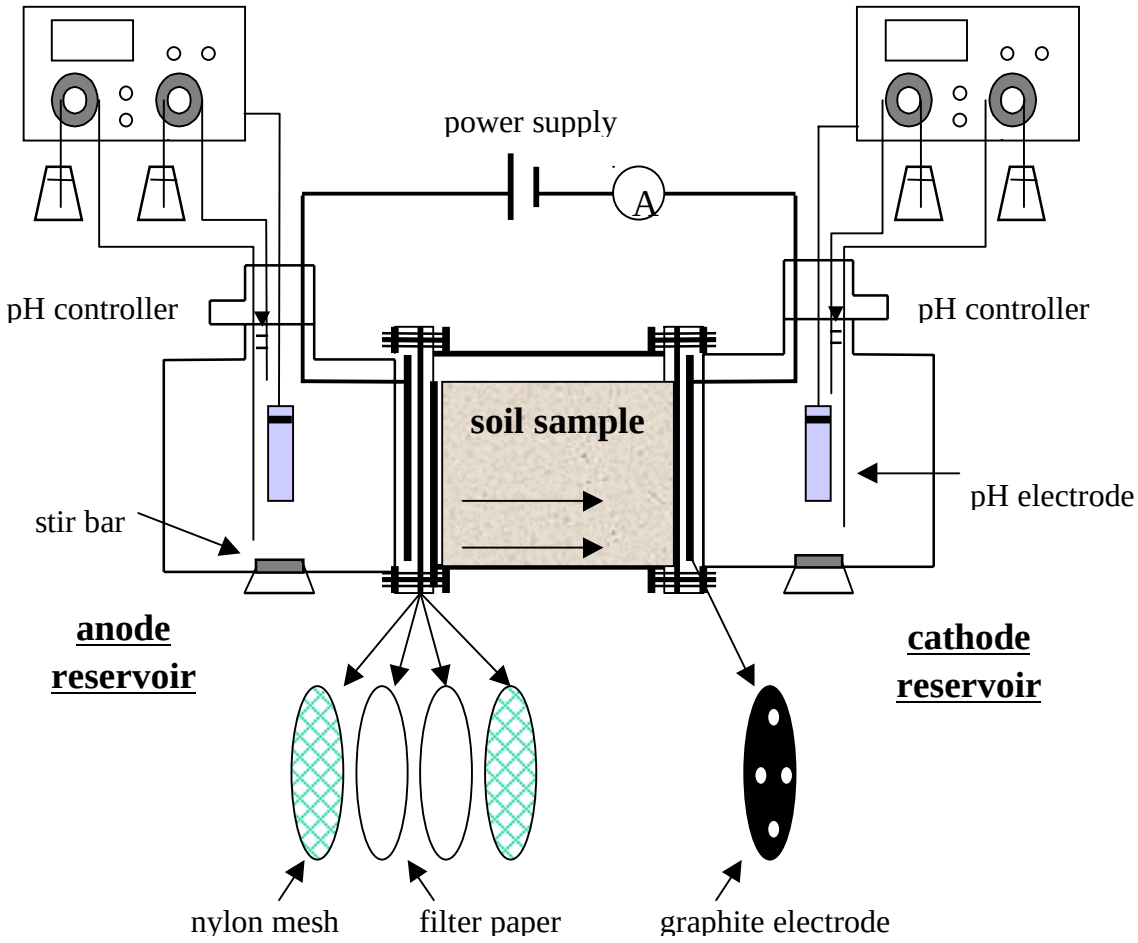

Figure 2.1. Schematic diagram of the electro-osmosis reactor

The electro-osmotic flow experiments were conducted by changing the pH of the working solution, the electrolyte type and its concentration, the water content of soils, and the intensity of electric field. Table 2.2 shows the experimental conditions of electro-osmotic flow tests. The electrodes were connected to a regulated DC power supply (Vector-VID instrument division; model WP-705B). During these tests, parameters such as amount of water flow per day, the intensity of electric current and field, pH of catholyte and anolyte were monitored as a function of time. At the end of a pre-selected time period, the soil sample in the cell were sliced into 10 equal sections. The pH value and the water content of the soil were measured.

Table 2.2. Experimental conditions of electro-osmotic flow tests

Test Number	pH Value of Solution	Intensity of Electric Field (V)	Electrolyte Type and Its Concentration	Initial Water Content (%)
1	4	12	10^{-3}M NaCl	20
2	6	12	10^{-3}M NaCl	20
3	7	12	10^{-3}M NaCl	20
4	9	12	10^{-3}M NaCl	20
5	*	6	10^{-2}M CH_3COONa	20
6	*	12	10^{-2}M CH_3COONa	20
7	*	24	10^{-2}M CH_3COONa	20
8	*	12	10^{-3}M NaCl	20
9	*	12	10^{-3}M CH_3COONa	20
10	*	12	10^{-2}M CH_3COONa	20
11	*	12	$5x10^{-2}$M CH_3COONa	20
12	*	12	10^{-1}M CH_3COONa	20
13	*	12	10^{-2}M CH_3COONa	5
14	*	12	10^{-2}M CH_3COONa	10
15	*	12	10^{-2}M CH_3COONa	15
16	*	12	10^{-2}M CH_3COONa	20
17	*	12	10^{-2}M CH_3COONa	25

*: uncontrolled pH

II.3. Results and Discussions

In typical soil-water system, the surface charge of the soil is always negative, which induces the excess counter-ions (cations) distribution in a thin water layer adjacent to the soil surface. When an electric field is imposed to the soil-water system, the cations will migrate to the cathode and the anions migrate to the anode, respectively. The water momentum (or frictional drag) produced by cations and anions, which develops a net driving force due to the excess charge distribution on the soil surface. Accordingly, a water flow (i.e., electro-osmosis) will transport in one direction from the anode to the cathode. Note that no electro-osmosis occurs in the free electrolyte solution because the cations and anions are present in equivalent concentrations. In other words, the applied electric field imparts equal and opposite momentum to both cations and anions in the bulk solution. Therefore, the net transfer of water momentum is zero and no water molecules are transferred by the action of the migrating ions.

The electrostaticforce is the only driving force for the electro-osmotic flow in the soil-water system, which provides the momentum to migrate the ions. According to the Coulomb's law, the electrostaticforce is a function of the intensity of electric field and the amount of charges. As a result, the variables, applied field (potential gradient) and the excess charges on the soil-water interface, must be included in modeling the water flow. Furthermore, these excess charges must be equivalent to the soil surface charges due to the electroneutrality. Hence, Esrig and Majtenyi (1965) derived a model, which shows that the average velocity of electro-osmotic flow is proportional to the applied field and the surface charge density for porous media. Some models also suggested that the distribution of the excess ions on the soil-water interface can affect the EO flow. Both concepts together with the experimental results were used to discuss the EO flow phenomena in the unsaturated soils.

II.3.1. pH Effect

Figure 2.2 presents the daily flow as a function of time at various pH conditions. Results show that the EO water flow rate decreases with decreasing solution pH value and ceases to exist at pH around 2.2. The reduced EO flow can be attributed to the decrease of surface charge density of soils. When the proton concentration increases in the solution the soil surface charge is rendered more positive. Therefore, the electrostatic driving force of the water momentum reduces and the EO flow decreases. The magnitude of the surface charge density at different pH can be obtained by the zeta potential. For symmetrical electrolytes, the surface charge density

can be written as follows (Hunter, 1981):

$$\sigma_0 = 11.74 c^{1/2} \sinh(19.46 z \psi_0) \qquad [2.4]$$

where σ_0 = surface charge density ($\mu C/cm^2$)

c = electrolyte concentration (M)

z = valance of electrolyte ion

ψ_0 = zeta potential (Volt)

Figure 2.3 presents the zeta potential of soil particles as a function of pH at various electrolyte concentrations. Results show the absolute value of zeta potential decreases with decreasing the pH value and the pH_{ZPC} is around 2.2 at the electrolyte concentration of 10^{-3}M. In addition, figure 2.4 presents the pH value of the soil as a function of normalized distance. The average pH value of soil can be obtained from this graph, then, the zeta potential at different pH value can be calculated. According to equation 2.4, the surface charge density of soil can be determined at the various pH conditions. The relationship between the EO flow rate and the surface charge density (at different pH) is shown in figure 2.5 and results indicate that the EO flow is proportional to the surface charge density.

II.3.2. Electric Field Effect

Figure 2.6 presents the daily flow as a function of time under different applied electric voltages. Results show that the EO flow rate increases with increasing the intensity of electric field. As mentioned above, the electric potential is assumed to be proportional to the EO flow. Figure 2.7 demonstrates this linear relationship between the flow rate and the electric field. However, it is observed that the EO flow rate decreases with increasing the operation time. Since the solution pH was not controlled in these tests, the protons produced from the anode reduce the surface charge density of the soil. Hence, the EO flow in the soil decreases gradually. Figure 2.8 presents the pH value at anode as a function of time. Results show that the pH of the working solution at anode decreases with increasing the operation time, which illustrate the pH value of the soil decreases as well.

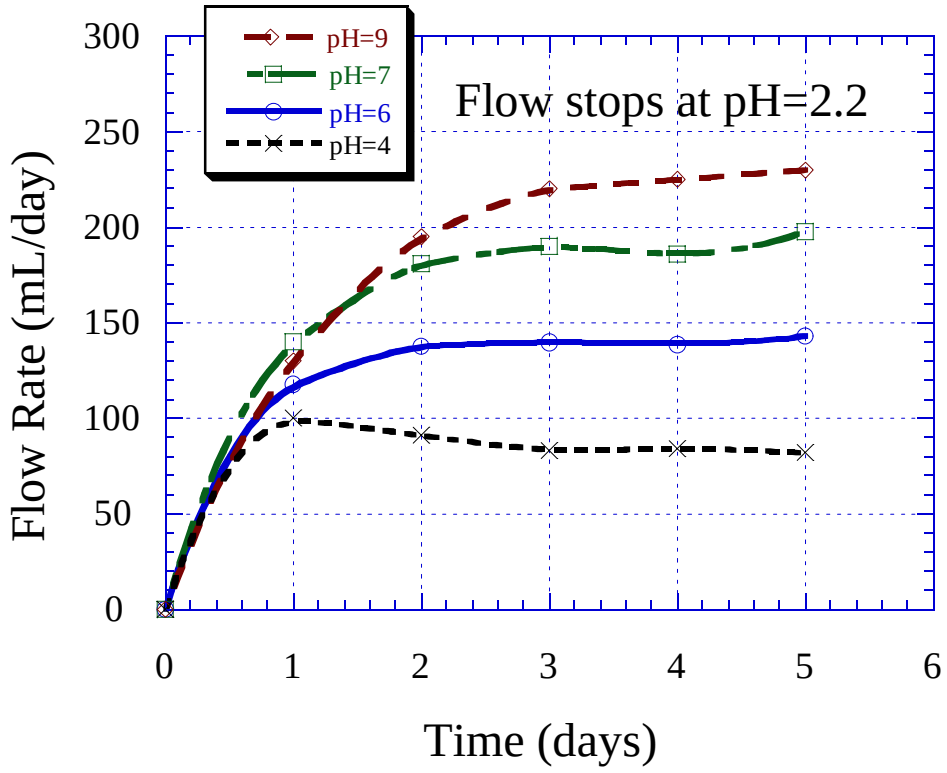

Figure 2.2. **Influence of the pH on the electro-osmotic flow rate. Experimental conditions: electrolyte concentration = 10^{-3} M NaCl; voltage = 12 V; water content = 23% (w/w).**

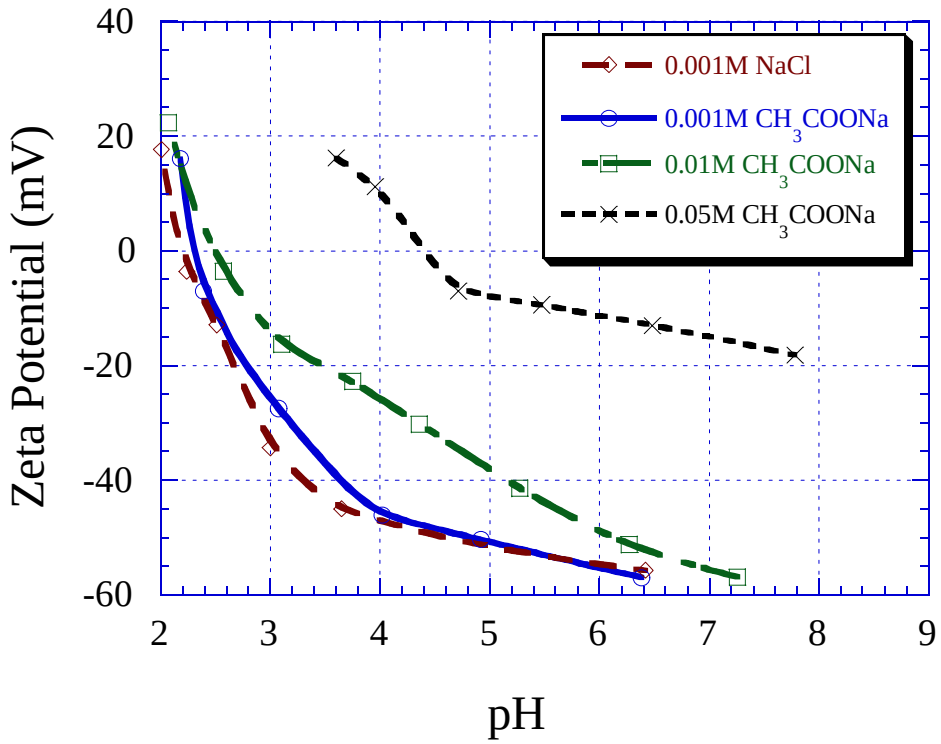

Figure 2.3. The zeta potential of soil particles as a function of pH at various electrolyte concentrations.

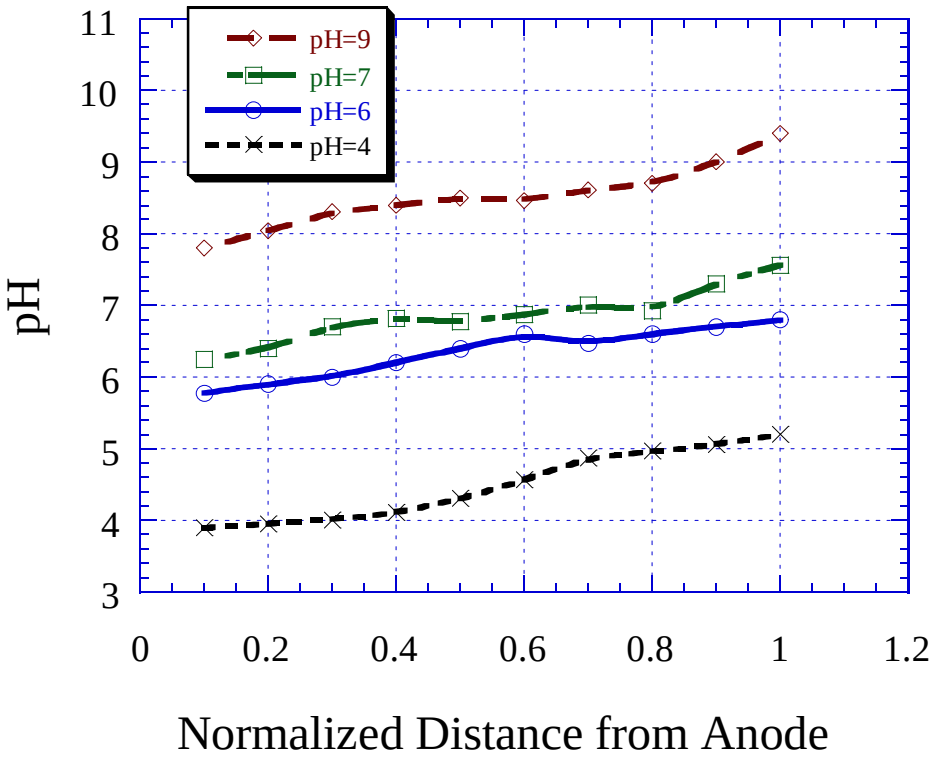

Figure 2.4. **The pH value of the soil as a function of normalized distance. Experimental conditions: electrolyte concentration = 10^{-3} M NaCl; voltage = 12 V; water content=23% (w/w).**

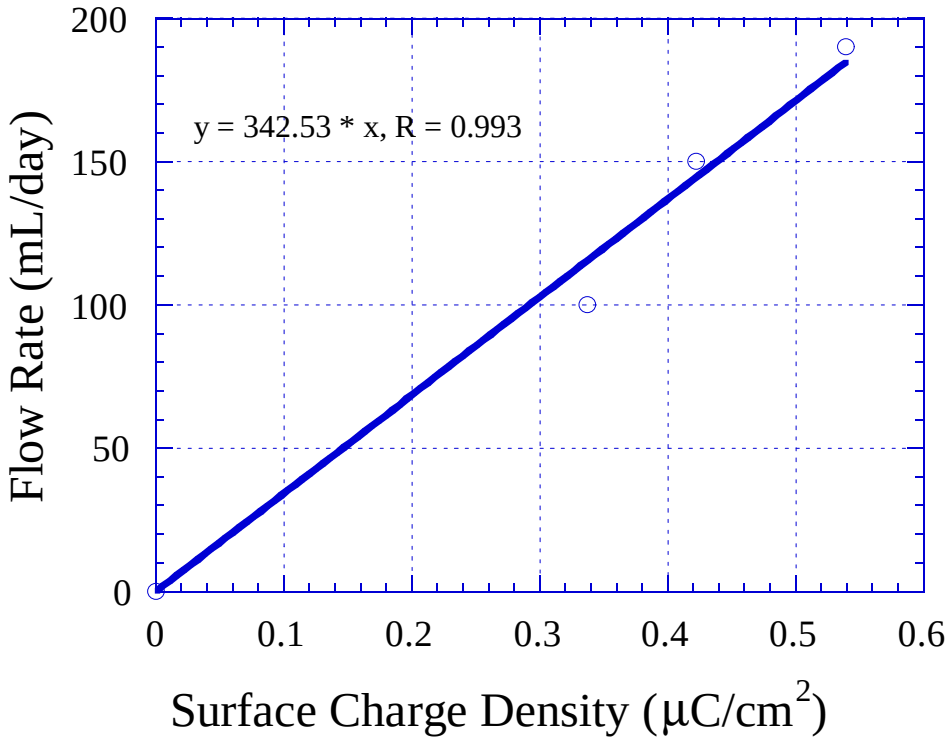

Figure 2.5. The electro-osmotic flow rate as a function of the surface charge density.

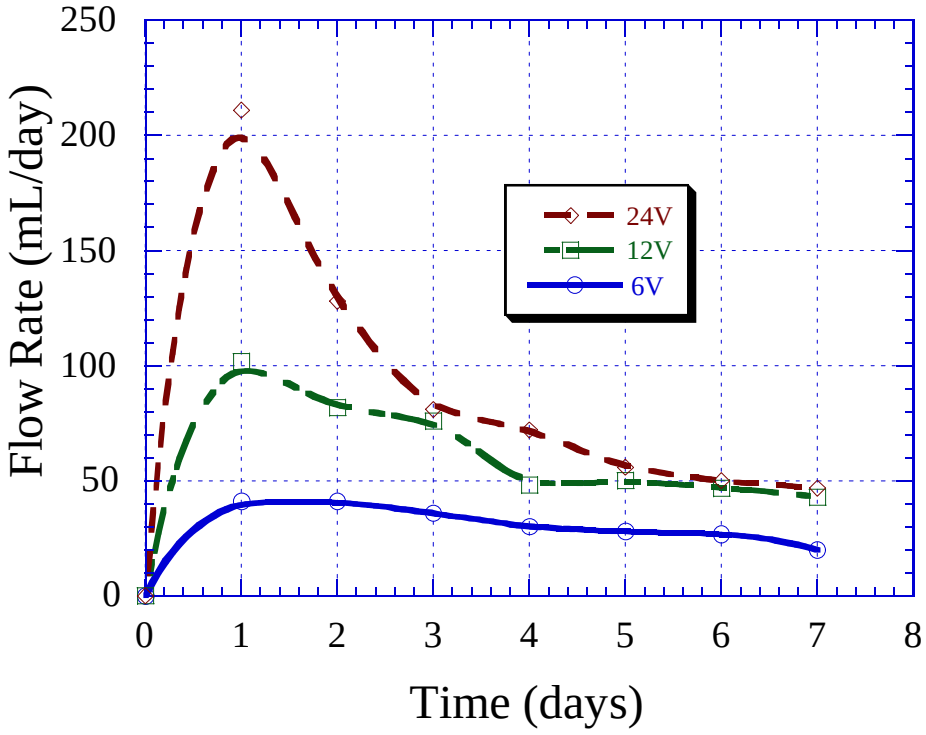

Figure 2.6. **Influence of the intensity of electric field on the electro-osmotic flow rate. Experimental conditions: electrolyte concentration = 10^{-2} M CH_3COONa; water content = 20% (w/w).**

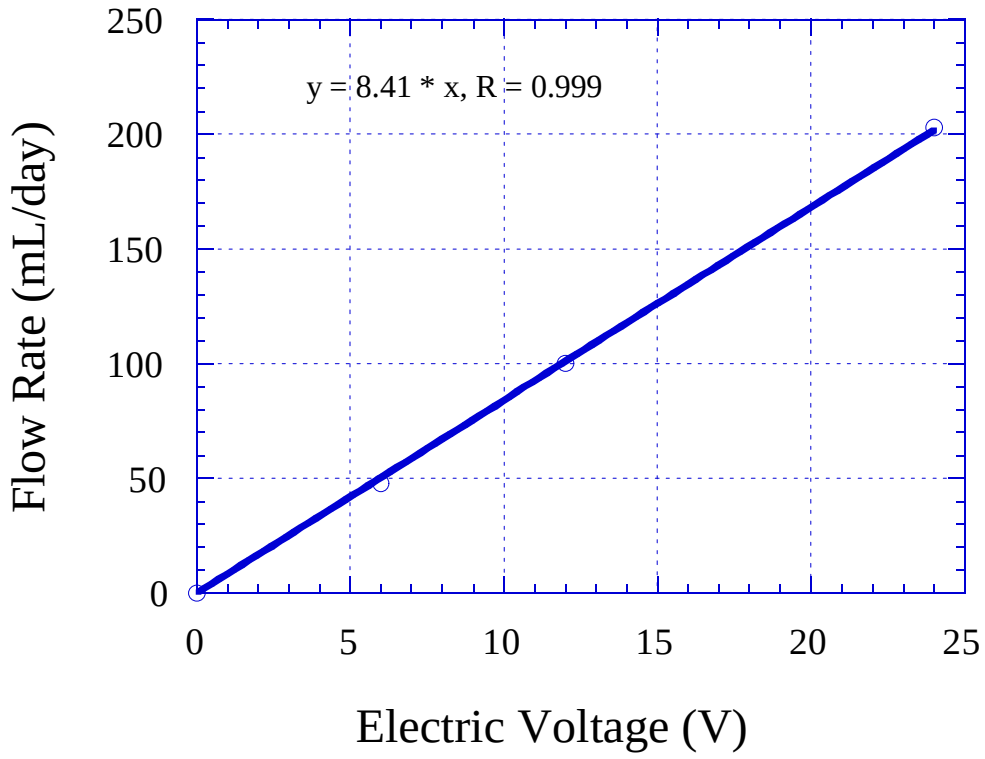

Figure 2.7. The electro-osmotic flow rate as a function of the applied voltage.

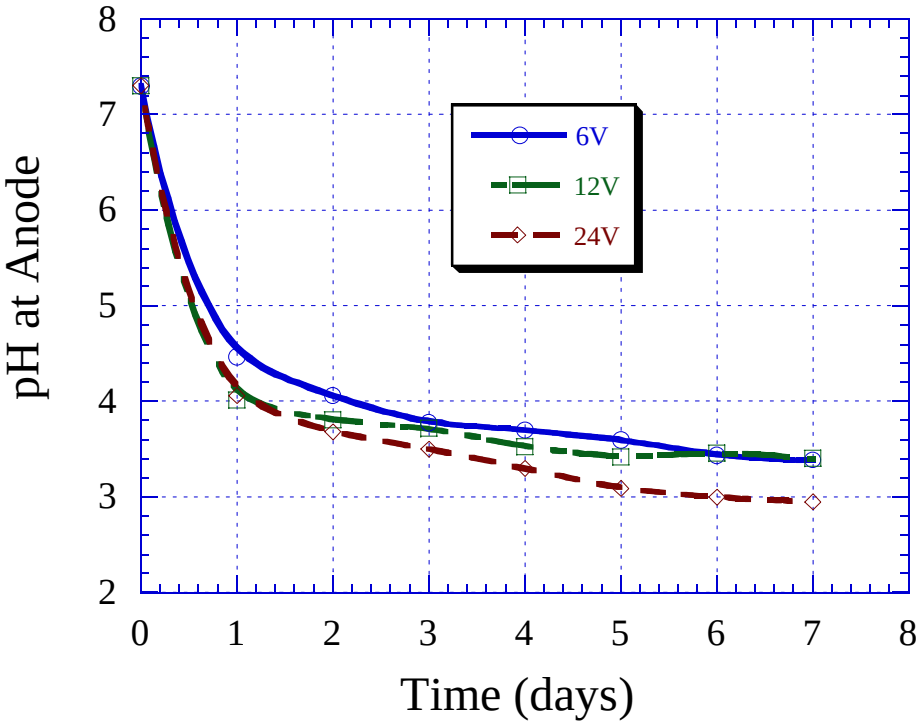

Figure 2.8. **The pH value at anode as a function of time at various intensities of electric field. Experimental conditions: electrolyte concentration = 10^{-2} M CH_3COONa; water content = 20% (w/w).**

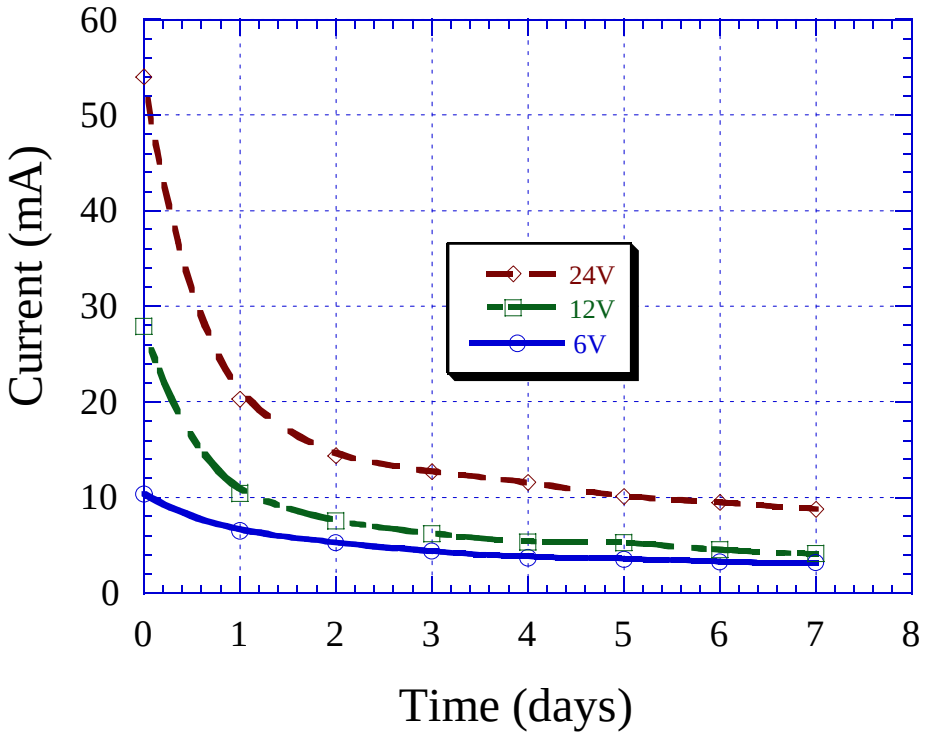

Figure 2.9. **The electric current as a function of time at various intensities of electric field. Experimental conditions: electrolyte concentration = 10^{-2} M CH_3COONa; water content = 20% (w/w).**

Figure 2.9 shows the electric current as a function of time under various values of electric field. Results indicate that the electric current decreases with increasing time. The current is produced due to the ion migration. In the electro-osmosis system filled with soil particles and water solution, protons and hydroxide ions are generated by water electrolysis reactions. Concurrently, the electrolyte ions are consumed on the electrode (i.e., oxidation and reduction reactions). Therefore, parameters such as the electric field, the electrolyte concentration, the valance of ion, the ion adsorption, and the rate of the electrolysis reaction might influence the current magnitude. In an ionic conductor, the current can be written by:

$$I = -AF\frac{d\phi}{dx}\sum|z_i|u_i c_i \qquad [2.5]$$

where I = current

A = cross section area

F = Faraday constant

$d\phi/dx$ = potential gradient

z_i = the valance of ion

u_i = mobility of ion

c_i = ion concentration

In the beginning of the operation time, the electrolyte ions are the dominant charge carriers due to their relatively high concentrations. According to equation 2.5, the current is proportional to the applied electric field. Figure 2.10 shows the relationship between the current and the electric voltage and results demonstrate this theoretical proportionality.

Figure 2.11 shows the logarithmic value of current versus the operation time. Results indicate that the current decreases in two kinetic steps and can be fitted by the first order rate law, respectively. During the first day treatment, the current reduced in a relatively high rate. Then, the decreasing rate changes to a relatively low value. In addition, the slopes of these straight lines are parallel to each other (i.e., the apparent rate constant is independent of the intensity of the electric field).

II.3.3. Electrolyte Concentration Effect

Figure 2.12 presents the influence of the electrolyte concentrations on the electro-osmotic flow rate. Results show that the electrolyte concentration has no effect on the EO flow rate during the one-day treatment. Besides, the EO flow rate decreases with the increase of operation

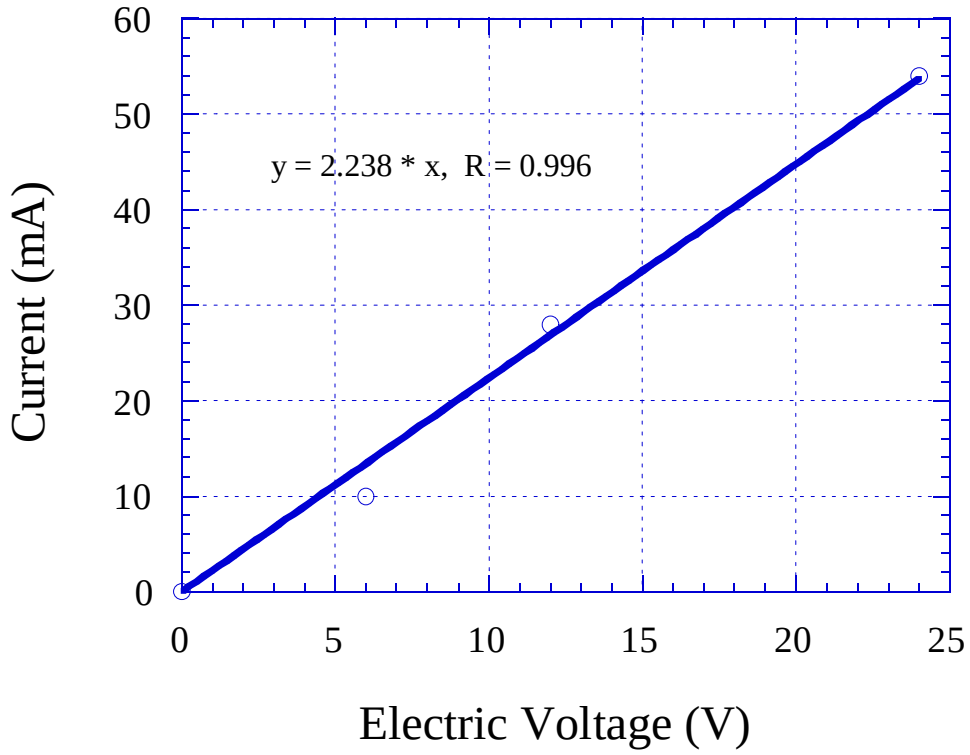

Figure 2.10. The current as a function of the applied voltage.

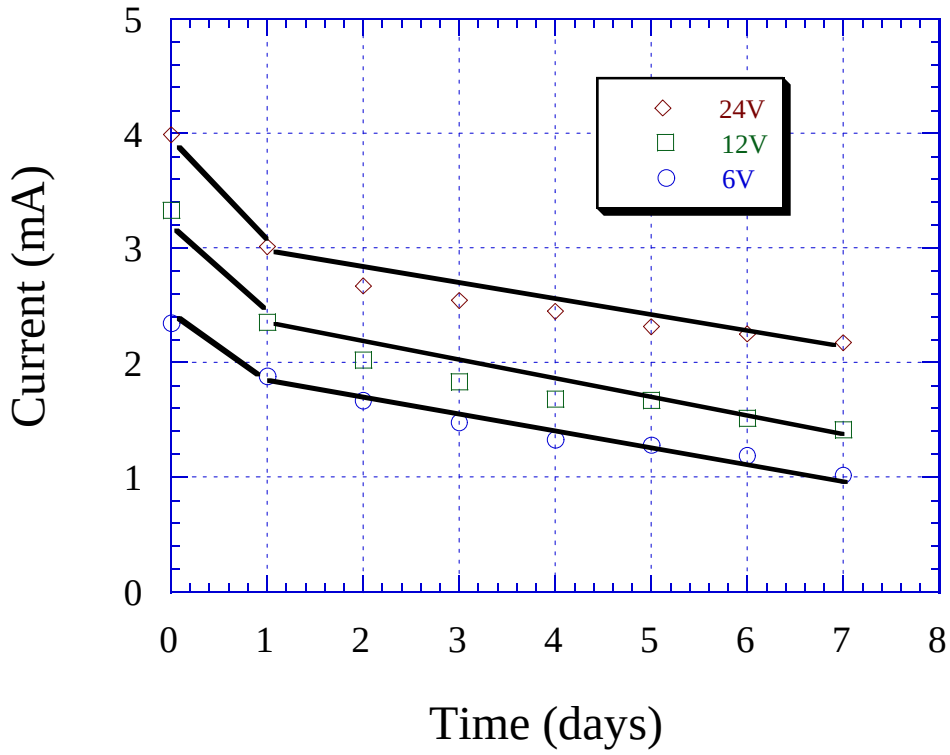

Figure 2.11. The logarithmic value of electric current as a function of time at various intensities of electric field.

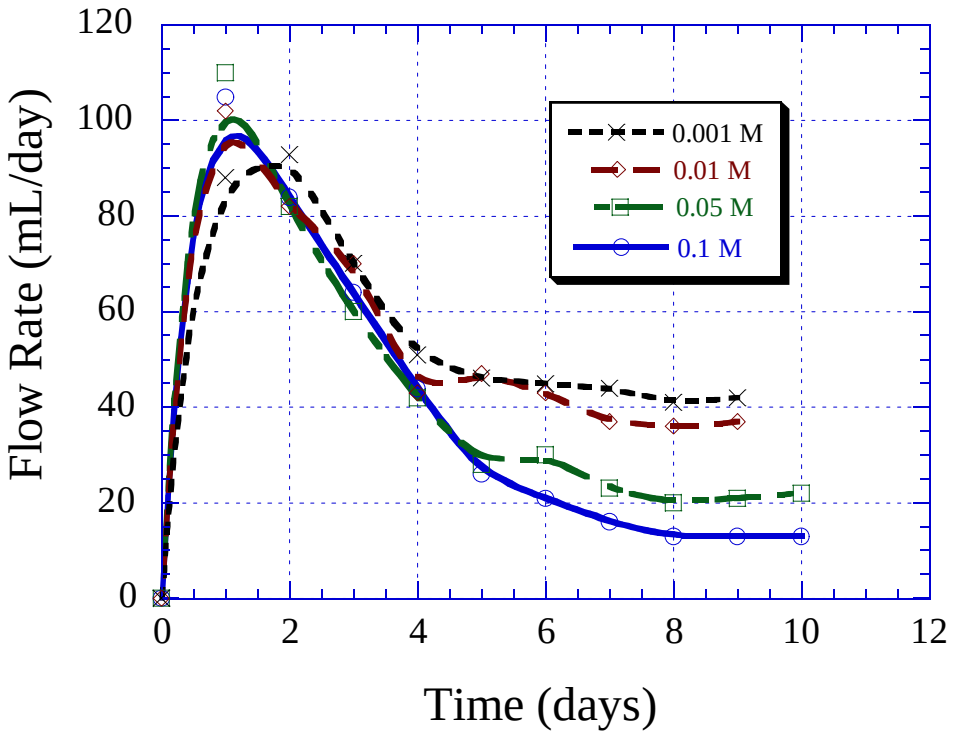

Figure 2.12. Influence of the electrolyte concentrations on the electro-osmotic flow rate. Experimental conditions: voltage = 12 V; water content = 20% (w/w).

time which is due to the acidification of soils. According to figure 2.2, it is seen that the EO flow rate approaches to a steady state as the electrolyte concentration increased by the addition of the pH control solution, i.e. strong acid/base. This observation also implies that the electrolyte concentration has no effect on the EO flow if the electrolyte ions have no interaction with the soil (i.e., indifferent ions). However, the electrolyte type and concentration can influence the zeta potential and the distribution of the cations on the soil surface. For instance, some electrolyte can be adsorbed on the soil, which results in the change of the zeta potential and the surface charge density of the soil. The electrolyte concentration can influence the zeta potential rather than the surface charge. The Gouy-Chapman model of the electrical double layer predicts an increase in zeta potential with increase in concentration of indifferent electrolyte (Hunter, 1981). In other words, the concentration effect compresses the thickness of the electrical double layer but can not change the surface charge density of the soil. Consequently, varition in electrolyte concentration has no effect on the EO flow rate because the flow is only related to the surface charge density rather than the zeta potential.

From figure 2.11, we observed that the flow rate decreases with increasing the electrolyte concentration after several-days treatment. The phenomena can be explained by adsorption of the electrolyte ions. According to figure 2.3, the electrolyte (sodium acetate) has chemical reaction with soil surface, which results in an increase in pH_{zpc} upon the increase of electrolyte concentration. The solution pH value at the anode shown in figure 2.13 presents the differences of pH value at various electrolyte concentrations. Based on these data (figure 2.3 and 2.13), we found that the order of the zeta potential is 10^{-3} M > 10^{-2} M > $5x10^{-2}$ M > 10^{-1} M at given pH. This implies the surface charge density follows the same order as the zeta potential. Therefore, the EO flow decreases with increasing electrolyte concentration. Figure 2.14 presents the electric current as a function of time at various electrolyte concentrations. Results shows that the current decreases with increasing the operation time. This phenomenon is similar to those shown in figure 2.9 and might be fitted by first order rate law.

II.3.4. Water Content Effect

Figure 2.15 presents the water content of the soil as a function of the normalized distance after treated for a given period of time. Results show that the final water content is different from the initial one. This can be attributed to the varition in soil packing conditions, which results in different infiltration rate during EO tests. Therefore, as the EO system reached a hydraulic steady state, the water content of soil varies from 5% to 26%, 10% to 20%, 15% to

16%, 20% to 20%, and 25% to 23%, respectively. Figure 2.16 presents the EO flow rater as a function of time at various soil water contents. Results show that the flow rate increases with increasing the soil water content. Gray and Mitchell (1967) found that the parabolic relationship between the EO flow and the water content in the soil-water system. This EO phenomenon was also observed in this study (figure 2.17).

When the EO system is applied to the unsaturated soil, the water flow behavior is different from the saturated capillary system. The water molecule oriented on the soil surface is considered as the main resistance for the drag force. It is assumed that this frictional stress decreases with increasing the thickness of the water layer. For the unsaturated soil-water system, the water layer is extremely thin, generally ranging from 10^{-10}cm to 10^{-8}cm. Thus, all water molecules exhibit the frictional interaction with the soil surface. For the saturated water-capillary system, the radii of capillaries are relatively large, ranging from 10^{-1}cm to 10^{-3}cm. Most water in the capillary has no physical and chemical interaction with the capillary wall. In addition, the cross-section area of the water transport flux is different for these two systems. The cross-section area of the water transport flux in saturated capillary can be considered circular, which is not the case in the unsaturated soil system. Consequently, the circular capillary model (used to predict the water flow in the saturated capillary system) is not able to describe the EO flow in the unsaturated soil. The infinite plate model is much acceptable compared with the circular capillary model. The basic assumption of the infinite model is that the shear stress at any surface element in the water layer is proportional to the rate of change of velocity across the element (i.e., the Newtonian fluid). The constant of proportionality is the coefficient of viscosity of the fluid. The shear stress equation is written as follows:

$$\tau = \eta(dv/d\theta) \qquad [2.6]$$

where τ = shear stress

η = viscosity of fluid

v = velocity of fluid

θ = thickness of water layer

For the calculation of the EO flow rate, the equation is given by:

$$Q = vA = v\theta w \qquad [2.7]$$

where Q = Electro-osmotic flow rate

A = the cross section area of the EO flow

θ = thickness of the water layer

w = width of the cross-section area

Since, the thickness can be expressed as following equation:

$$\theta = V/\Sigma \qquad [2.8]$$

where V = volume of the fluid

Σ = specific surface area of soils

By substituting equation 2.8 into equation2.7, the flow rate can be obtained as follows:

$$Q = vVw/\Sigma \qquad [2.9]$$

By substituting equation 2.8 into equation 2.6, one has:

$$\tau = \eta(v / \theta) = \eta v\Sigma/V$$

Rearranging the above equation yield the following equation:

$$v = \tau V/\eta\Sigma \qquad [2.10]$$

By substituting equation 2.10 into 2.9, the flow rate can be expressed as:

$$Q = vVw/\Sigma = V^2 \tau w/\eta\Sigma^2 \qquad [2.11]$$

Since the shear force can be assumed to be proportional to the electric force induced by the surface charge density and the applied electric field, the following equation can be obtained:

$$k\sigma_0(dE/dx) = \tau \qquad [2.12]$$

where k = frictional coefficient

σ_0 = surface charge density

E = the intensity of electric field

x = total length of water layer

By substituting equation 2.12 into equation 2.11, the flow rate formula is written as follows:

$$Q = k\sigma_0(dE/dx)V^2w/\eta\Sigma^2 = k'\sigma_0(dE/dx)V^2 \qquad [2.13]$$

where $k' = kw/\eta\Sigma^2$

Since $\omega = \rho V/M \qquad [2.14]$

where ω = water content of the soil

ρ = fluid density

M = soil mass

Consequently, the EO flow equation is finally given by:

$$Q = k'\sigma_0(dE/dx)\omega^2M^2 = K\sigma_0(dE/dx)\omega^2 \quad [2.15]$$

where K is a characterized coefficient ($K = kwM^2/\eta\Sigma^2$).

This characterized coefficient, K, collects several physical properties of the soil such as the total soil mass (M), the specific surface area (Σ), and the pore size (w). In addition, K value also represents the variable of the fluid viscosity (η). According to this equation, the EO flow rate is proportional to the square of the water content (i.e., $Q \propto \omega^2$). This theoretical result is consistent with the analytical data shown in figure 2.17.

Figure 2.18 and 2.19 present the pH at the anode and the cathode as a function of time at various water contents, respectively. Results show that the water content of the soil can not influence the pH value of working solution at the anode and the cathode. In other words, the water content of the soil is independent of the rate of the water electrolysis reaction at each electrode. Figure 2.20 shows the pH value of the soil as a function of normalized distance at various water contents. Results indicate that the water content of the soil has no obvious impact on the soil. Figure 2.21 presents the current as a function of time at various water contents. Results imply that the water content of the soil has no significant effect on the current in the EO system.

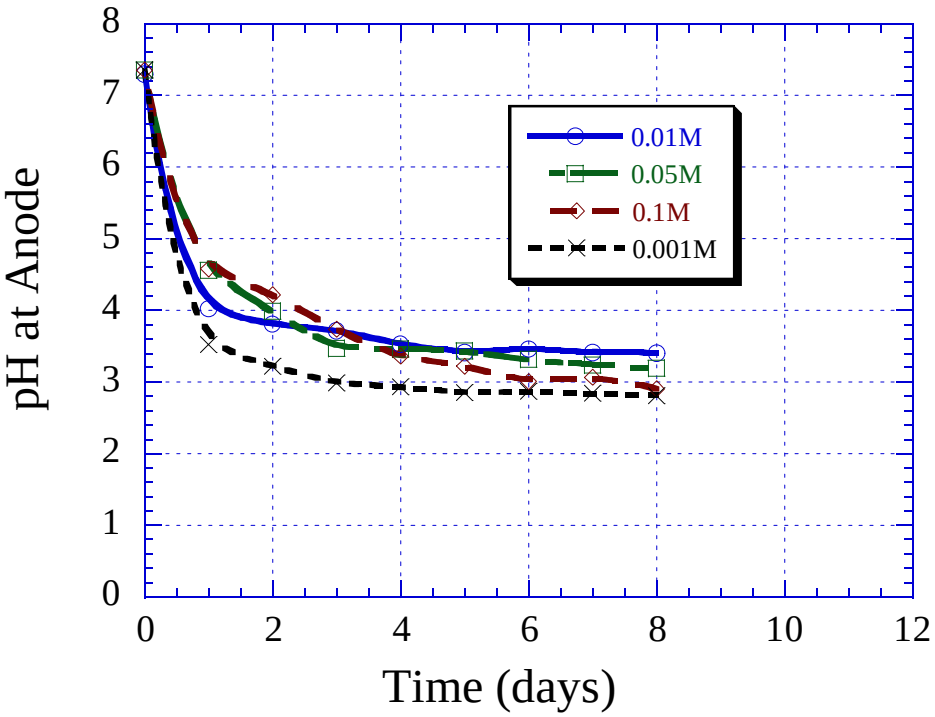

Figure 2.13. The pH value at anode as a function of time at various electrolyte concentrations. Experimental conditions: voltage = 12 V; water content = 20% (w/w).

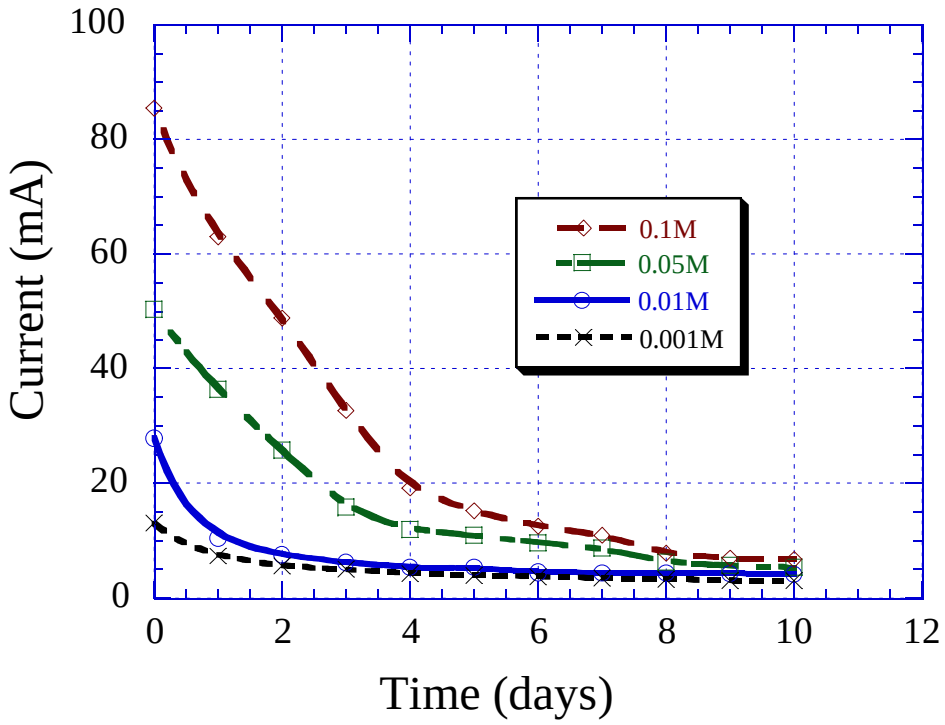

Figure 2.14. The electric current as a function of time at various electrolyte concentrations. Experimental conditions: voltage = 12 V; water content = 20% (w/w).

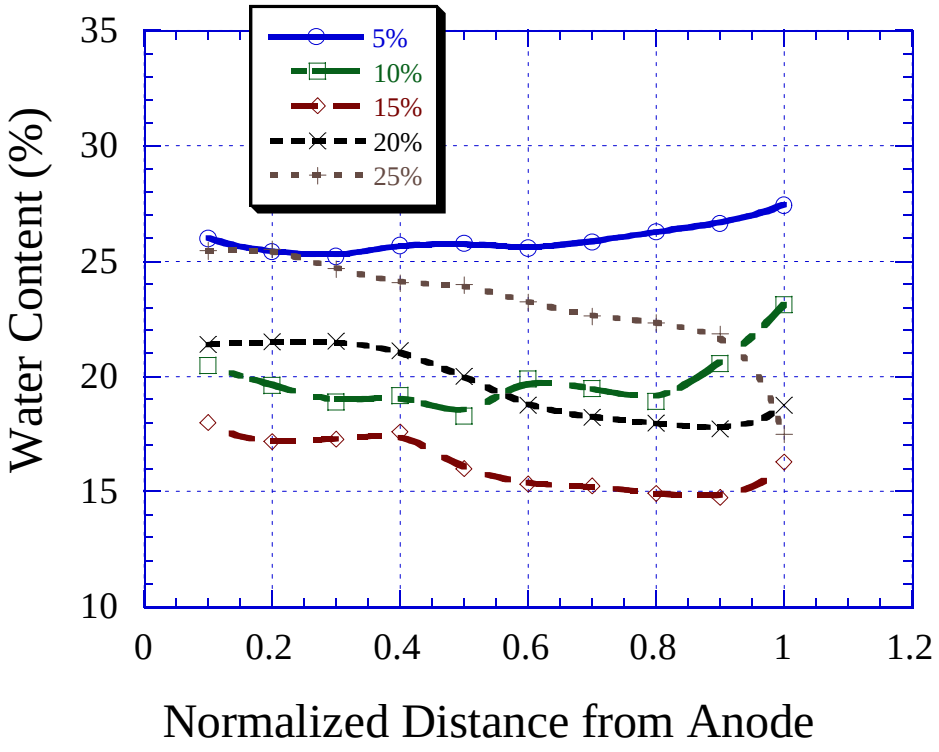

Figure 2.15. The final water content as a function of normalized distance at various initial water contents packed in the soil. Experimental conditions: electrolyte concentration = 10^{-2} M CH_3COONa; voltage = 12 V

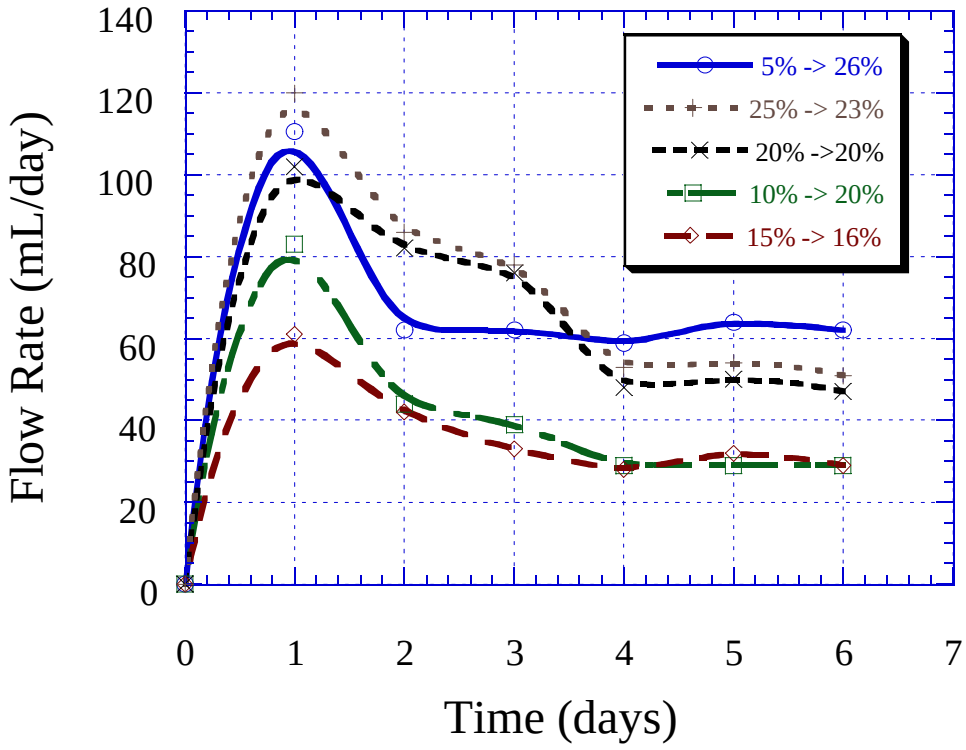

Figure 2.16. Influence of the water content on the electro-osmotic flow rate. Experimental conditions: electrolyte concentration = 10^{-2} M CH_3COONa; voltage = 12 V.

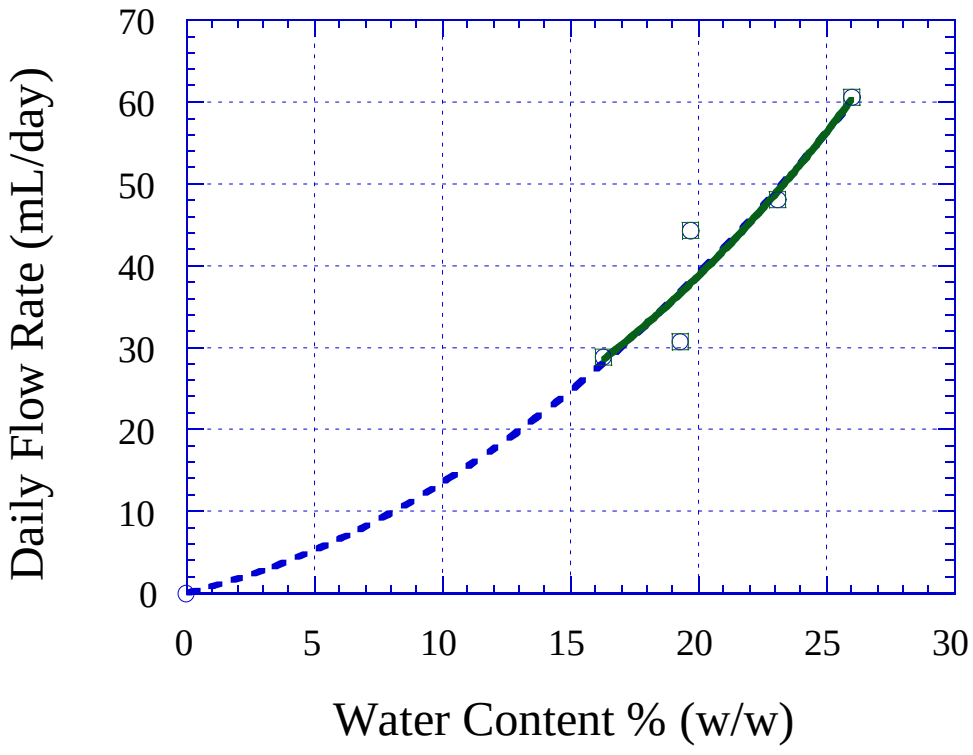

Figure 2.17. The electro-osmotic flow as a function of water content of the soil. Experimental conditions: electrolyte concentration = 10^{-2} M CH_3COONa; voltage = 12 V.

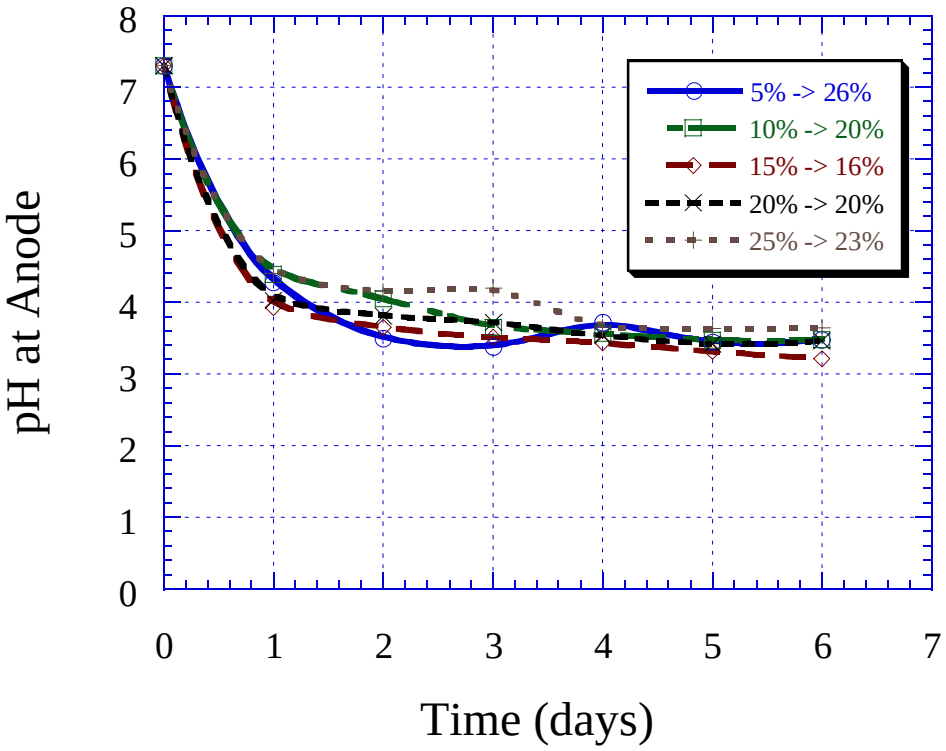

Figure 2.18. The pH value at anode as a function of time at various water contents. Experimental conditions: electrolyte concentration = 10^{-2} M CH_3COONa; voltage = 12 V.

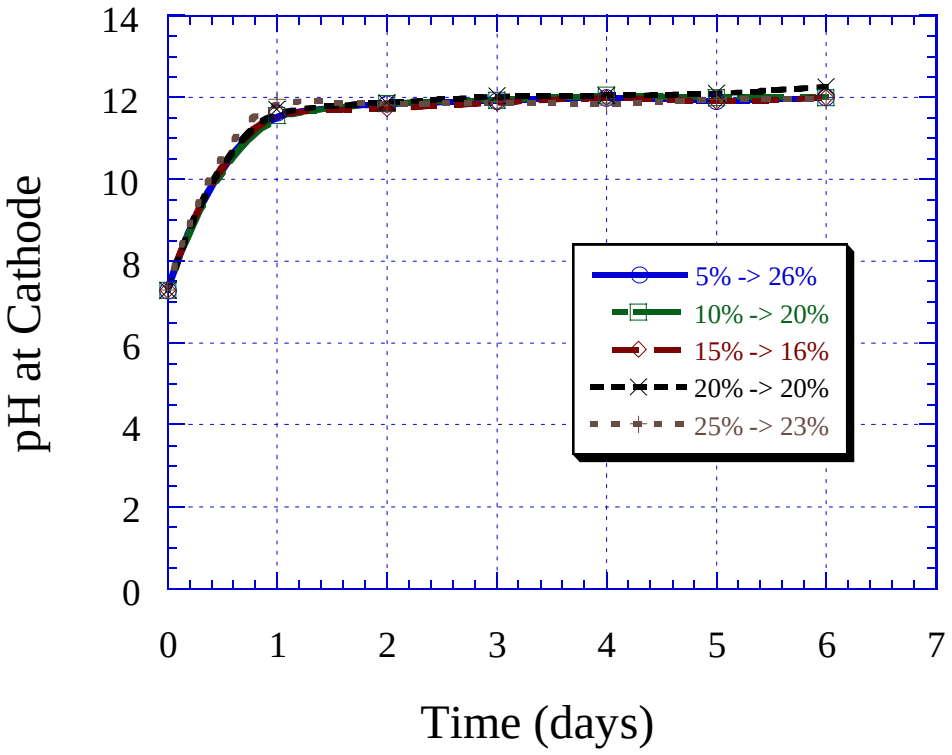

Figure 2.19. The pH value at cathode as a function of time at various water contents. Experimental conditions: electrolyte concentration = 10^{-2} M CH_3COONa; voltage=12 V.

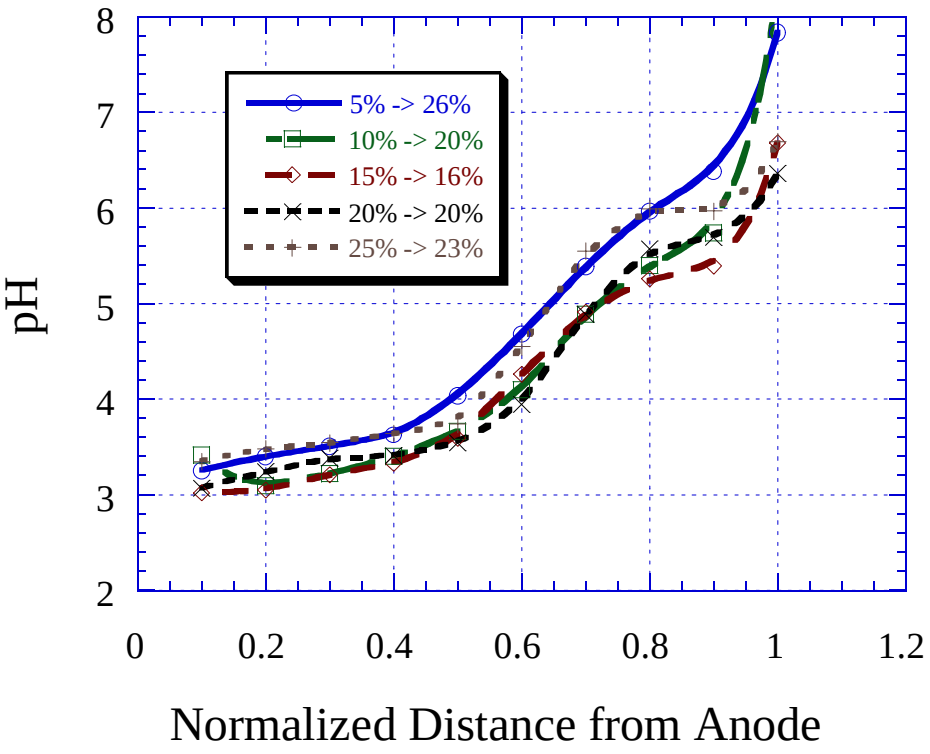

Figure 2.20. The pH value of the soil as a function of normalized distance. Experimental conditions: electrolyte concentration = 10^{-2} M CH_3COONa; voltage = 12 V.

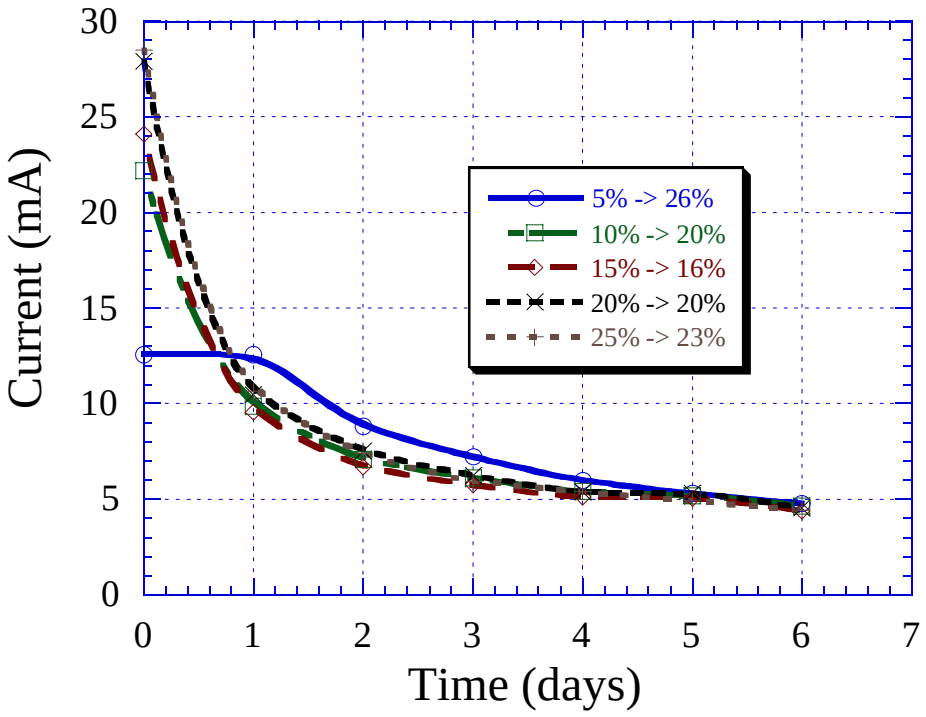

Figure 2.21. The electric current as a function of time at various water contents. Experimental conditions: electrolyte concentration = 10^{-2} M CH_3COONa; voltage = 12 V.

III. DESORPTION OF SELECTED POLYCYCLIC AROMATIC HYDROCARBONS IN SOILS

III.1. Introduction

Desorption of hydrophobic organic compounds (HOCs) from soils is of great environmental concerns. The release of HOCs can impact the entire cosystem. Accordingly, understanding and the prediction of desorption phenomenon is key to the design of effective remediation methods. For polycyclic aromatic hydrocarbons (PAHs), Gauthier et al. (1987) suggested that the degree of aromaticity in soil humic materials at normalized soil organic carbon levels control the sorptive uptake.

For reversible reaction, the desorbed organic concentrations at equilibrium generally depend on the sorption concentrations at equilibrium achieved. However, some researchers have reported the presence of irreversible reaction (Kan et. al., 1994; Pavlovstathis and Jaglal, 1991; Steinberg et. al., 1987). Many mechanisms have been proposed to interpret the resistance to desorption, e.g. penetration into the less accessible organic matrix (Carmichael et al., 1997), irreversible adsorption (Kan et al., 1998), chemisorption (Burgos et al., 1996), heterogeneous adsorption (Weber and Huang, 1996), or slow time-dependent processes (Carroll et al., 1994). Sorption and desorption of HOCs typically consist of a significantly slow fraction following an initially rapid release due to diffusion limitations (Pavlovstathis and Jaglal, 1991). Fu et al. (1994) reported that about 50 % of the total amount of phenanthrene were partitioned onto the sediments in the first minute of reaction time, which was indicative of a physical adsorption. Werth and Reinhard (1997) observed trichlorothylene desorption on a silica gel and some sediments. They suggested that the fast desorption is controlled by diffusion through aqueous filled mesopores; while the slow desorption is controlled by activated diffusion in micropores.

In order to improve the removal efficiency of remediation process, the organic cosolvents have received attention because they can enhance the solubility of HOCs. Walters and Guiseppi-Elie (1988) found that the sorption rate of dioxins from water/methanol mixtures on soil was faster at higher volume fraction of organic cosolvent. Brusseau et al. (1991) worked on the sorption kinetics of HOCs at mixed solvents and also reported that the reverse sorption rate constant increases log-linearly with increasing volume fraction of organic cosolvent. In addition, these sorption kinetics with cosolvent were speculated to be controlled by diffusion of sorbate within the matrix of sorbent organic matters.

Presently, sorption-desorption kinetic models can be generally categorized into several kinds based on the controlling mechanisms, such as first-order rate models, two-site rate models, pore-diffusion models, surface-diffusion models, or combined pore and surface-diffusion models (Miller and Pedit, 1992). Table 3.1 summaries some common sorption-desorption models have been developed.

Table 3.1. Summary of Sorption Kinetic Models

Kinetic Models	Conc/mass Flux	Equations	References
One-site model (First-order rate model) $S \xrightarrow{k_d} C$	$\frac{dY}{dt} = k(Y_{\max} - Y)$	$Y=Y_{max}[1-\exp(-kt)]$	Lapidus & Amundson (1952)
Two-site model $S_1 \xleftarrow{F,K_p} C \xleftarrow{k_d} S_2$	$S_1 = FK_pC$ $\frac{dS_2}{dt} = k_1S_1 - k_dS_2$	No analytical solution	Brusseau (1991)
Radialdiffusion penetration retardation (pore diffusion) model $S' \xleftarrow{K_p} C' \xrightarrow{D_{eff}} C$	$\frac{\partial S(r)}{\partial r} = D_{eff}\left[\frac{\partial^2 S(r)}{\partial r^2} + \frac{2}{r}\frac{\partial S(r)}{\partial r}\right]$	$\frac{C_t}{C_e} = f\left(\frac{D_{eff}\,t}{r^2}\right)^{1/2}$ †	Wu & Gschwend (1986) Steinberg et al. (1987)
Dual-resistance surface diffusion model $S' \xrightarrow{D_s} C'_s \xrightarrow{k_b} C$	$\frac{dC}{dt} = -\frac{3k_bM_S}{RV\rho}(C - C_S) - k_aC$	No analytical solution	Miller & Pedit (1992)
Gamma model	$f(k) = \beta^{\alpha}k^{\alpha-1}\exp(-\beta k)/\Gamma(\alpha)$ $M(t) = \int_0^{\infty} Mf(k)\exp(-kt)dk = M\left(\frac{\beta}{\beta+t}\right)^{\alpha}$	$Y = Y_{\max}\left[1-\left(\frac{\beta}{\beta+t}\right)^{\alpha}\right]$	Connaughton et al. (1993)
Modified one-site model	$\frac{dY}{dt} = kt^n(Y_{\max} - Y)$	$Y = Y_{\max}\left[1-\exp\left(-\frac{k}{n+1}t^{n+1}\right)\right]$	

† $\frac{C_t}{C_e} = (1+\alpha)\left[1 - \frac{\gamma_1}{\gamma_1+\gamma_2}e\,erfc\left\{\frac{3\gamma_1}{\alpha}\left(\frac{D_{eff}\,t}{a^2}\right)^{1/2}\right\} - \frac{\gamma_2}{\gamma_1+\gamma_2}e\,erfc\left\{-\frac{3\gamma_2}{\alpha}\left(\frac{D_{eff}\,t}{a^2}\right)^{1/2}\right\}\right] + higher\ terms$ (Crank, 1975)

III.2. Methods and Materials

The soil samples for desorption tests were the same as those of EO tests. Six kinds of polycyclic aromatic hydrocarbons (PAHs) were selected in this study, including naphthalene ($C_{10}H_8$), fluorene ($C_{13}H_{10}$), phenanthrene ($C_{14}H_{10}$), anthracene ($C_{14}H_{10}$), fluoranthene ($C_{16}H_{10}$), and pyrene ($C_{16}H_{10}$). They were purchased from Aldrich Chemical Company (Milwaukee, WI). The purity of the organic compounds is around 97 %. Table 3.2 shows the characteristics of these target compounds, which include the molecular weight, the water solubility, the henry's constant, and the octanol-water partition coefficient (log K_{ow}).

Table 3.2. Characteristics of polycyclic aromatic hydrocarbons (PAHs)

Compound Name	Molecular Formula	Molecular Weight	Water Solubility (mg/L, at 298 K)	Henry's Constant, (atm/mol/L, at 298 K)	Log K_{ow} (at 298 K)
Naphthalene	$C_{10}H_8$	128.2	31.9	4.27×10^{-1}	3.36
Fluorene	$C_{13}H_{10}$	166.2	1.84	7.24×10^{-2}	4.18
Phenanthrene	$C_{14}H_{10}$	178.2	1.09	2.57×10^{-2}	4.57
Anthracene	$C_{14}H_{10}$	178.2	0.059	2.29×10^{-2}	4.54
Fluoranthene	$C_{16}H_{10}$	202.3	0.233	1.05×10^{-2}	5.22
Pyrene	$C_{16}H_{10}$	202.3	0.134	8.9×10^{-3}	5.13

The extract solution, hexane (C_6H_{14}) with an assay of 99.9 %, was produced by Fisher Scientific Company (Pittsburgh, PA). The cosolvent, methanol (CH_3OH) with an assay of 99.9 %, is purchased from Fisher Scientific Company as well.

III.2.1. Soil Sample Preparation

Weighed 20 mg PAHs compound and dissolved into 100 mL hexane. This served as a spiking solution with a concentration of 0.2 g/L. Then, an aliquot of the spiking solution was added into an appropriate amount of air-dried soil samples. The mixed soil-solution samples were shaken with a rotary blender (Norton model, 4490s) for one day. Afterward, the spiked soils were put in a hood to evaporate the hexane. After the preparation procedure, the PAHs-spiked soil samples were stored in the refrigerator (Lab-Line Environeers, model 340) at 4 ^{0}C prior to desorption tests.

III.2.2. Batch Desorption Experiments

The cosolvents (i.e., the extraction solution) for desorption tests were obtained by mixing methanol and water at various molar ratios. In this study, the molar ratios of methanol to water selected were at 0, 0.3, 0.5, 0.8, and1.0, respectively. To conduct the desorption tests, the weighed 2g PAHs-spiked soil was put into a series of glass tubes (Teflon-sealed caps). A 10 mL cosolvent with a specific methanol-water ratio was added to each tube. These tubes, then, were mixed in an oscillatory shaker (Precision Scientific, model 102) at 100 times per minute under room temperature. After a pre-selected mixing time, the soil-solution mixtures were filtered by a glass microfiber filter (Whatman, 934-AH). Then, a centrifuge (Precision Scientific, model K-9) was used to centrifuge the filtrate at 3000 rpm for 10 minutes. Sample 5 mL supernatant into a vial and mix with 5 mL hexane for 24 hours. The hexane solution was then analyzed for the PAHs concentration. Each desorption test was conducted in triplicate.

A variable-wavelength ultraviolet (UV) spectrophotometer (Hewlett Packard, model 8452A Diode Array Spectrophotometer) was used to quantify the PAHs concentrations. The wavelength used for each PAH was determined by selecting for maximum UV absorbance. Table 3.3 lists the wavelength applied to each PAHs compound.

Table 3.3. Wavelength for PAHs measurement by UV spectrophotometer

PAHs Species	Wavelength (nm)
Naphthalene ($C_{10}H_8$)	275
Fluorene ($C_{13}H_{10}$)	300
Phenanthrene ($C_{14}H_{10}$)	293
Anthracene ($C_{14}H_{10}$)	354
Fluoranthene ($C_{16}H_{10}$)	342
Pyrene ($C_{16}H_{10}$)	318

III.3. Results and Discussion

Figure 3.1 and 3.2 show the desorbed concentration of six PAHs versus the methanol mole fraction after mixing for four days. In figure 3.2, the amount of desorbed PAHs was divided by the total amount of spiked concentration to eliminate the deviations of experimental processes. Results show that naphthalene, fluorene and phenanthrene could be categorized into one group according to their desorption profile. The desorption curve of naphthalene is lower than the other two PAHs compounds. This might be attributed to evaporation during experimental processes, since naphthalene has the highest Henry's constant (4.27×10^{-1} atm/mol/L, at 298 K). On the other hand, anthracene, fluoranthene and pyrene display similar desorption characteristics at 0.5, 0.8 and 1.0 cosolvent fractions. At 0.3 cosolvent fraction, fluoranthene appears to be desorbed greater than anthracene. There is a distinct discrimination among PAHs species at the 0.3-cosolvent fraction. In addition, the desorbed amounts for all PAHs increase with increasing the molar ratio of cosolvent from 0 to 0.8 instead of 1.0.

Figure 3.3 shows the ratio of desorbed PAHs concentration as a function of the octanol-water partition coefficient (Log K_{ow}). Results show that the desorbed amount of PAHs decreased when the Log K_{ow} increased. This can be attributed to the different hydrophobilities of the PAHs compounds. The hydrophobility of organic compound is generally considered as the driving force to distribute the organics from liquid phase into soil phase. In other words, the organic compound with a high octanol-water partition coefficient (Log K_{ow}) is difficult to be desorbed. However, as cosolvents fractions were at 0.5, 0.8 and 1.0, the desorbed amounts increase with increasing the value of Log K_{ow}. The extent of methanol must play an important role in the soil-PAHs-water system due to its cosolvent characteristics.

Based on the above results, naphthalene, fluorene and phenanthrene display similar desorptive characteristics. Accordingly, the phenanthrene was chosen to be the representative of this group for additional desorption kinetics tests. Figure 3.4, 3.5, 3.6, and 3.7 show the desorbed concentration of phenanthrene, anthracene, fluoranthene and pyrene as a function of time, respectively. Results show that the kinetic behavior of PAHs desorption exhibites a Langmuir-type desorption characteristic, which consists of a fast desorption followed by a slow desorption process. In addition, the equilibrium desorption can be reached after 12-hour mixing for all four PAHs studied. In figure 3.4, the equilibrium concentrations of phenanthrene at various cosolvent fractions are similar. The equilibrium concentration (25 μg/g) of anthracene at 0.3-cosolvent fraction is lower than that of other PAHs studied (75 μg/g). The molecular

weight, the Henry's law constant, and the $\log K_{ow}$ of these two PAHs are similar except their water solubility. The different water solubility can be attributed to the difference between their molecular structures. Likewise, the equilibrium concentrations of fluoranthene and pyrene at various cosolvent fractions are different even both have the same molecule formula.

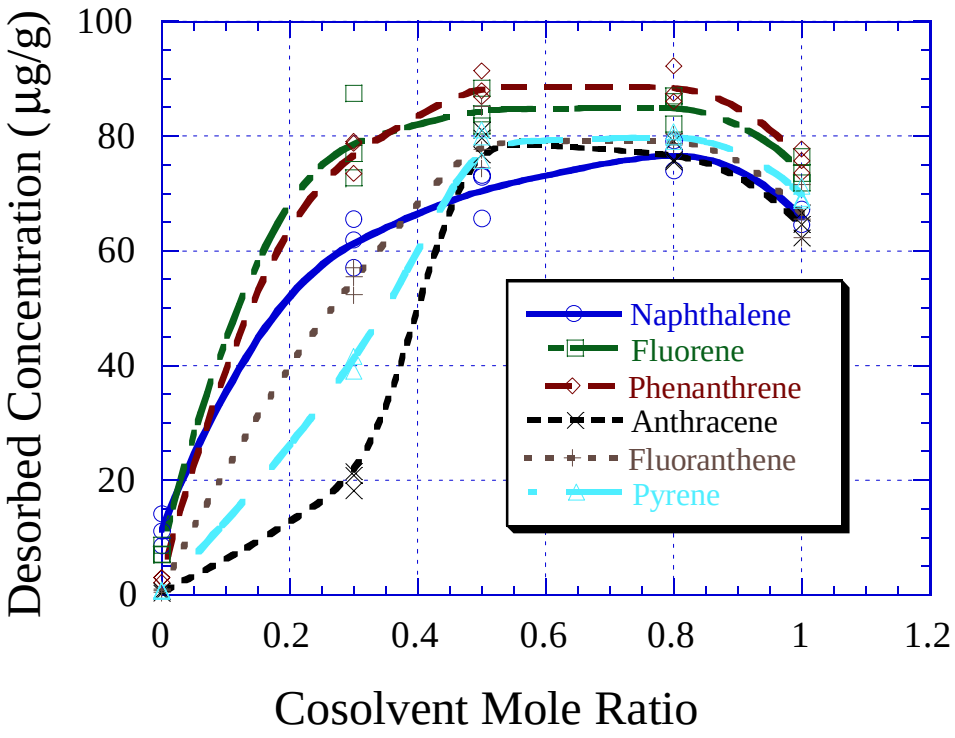

Figure 3.1. **The desorbed concentration as a function of cosolvent mole ratio for PAHs compounds. Experimental conditions: desorption time = 4 days, mixing rate = 100 oscillations per minute.**

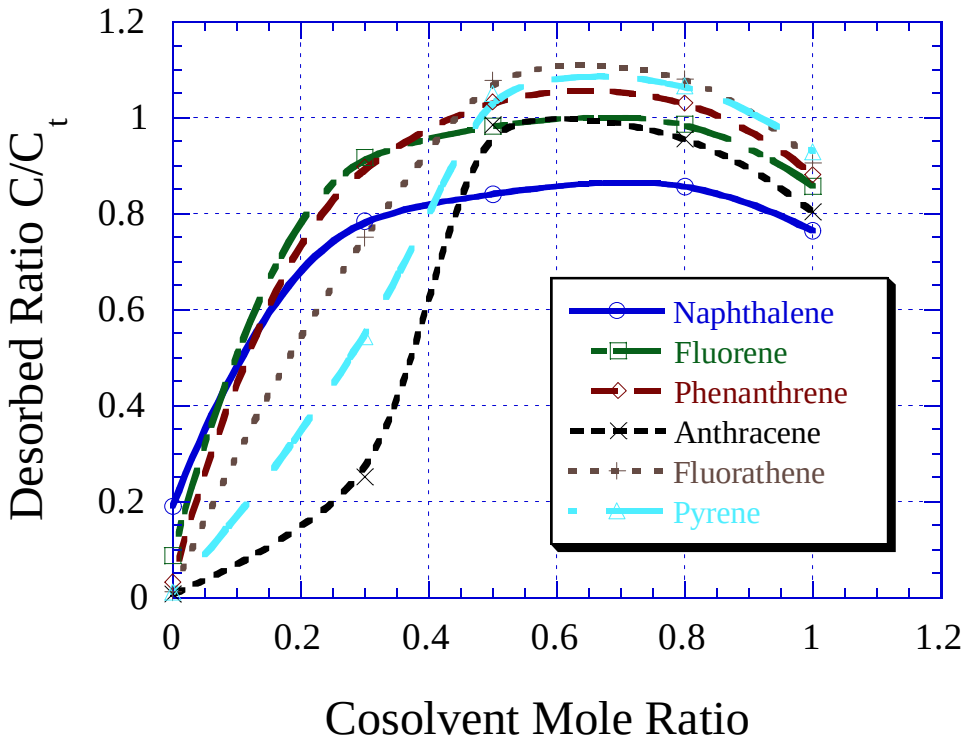

Figure 3.2. **The desorbed concentration ratio as a function of cosolvent mole ratio for PAHs compounds. Experimental conditions: desorption time = 4 days, mixing rate = 100 oscillations per minute.**

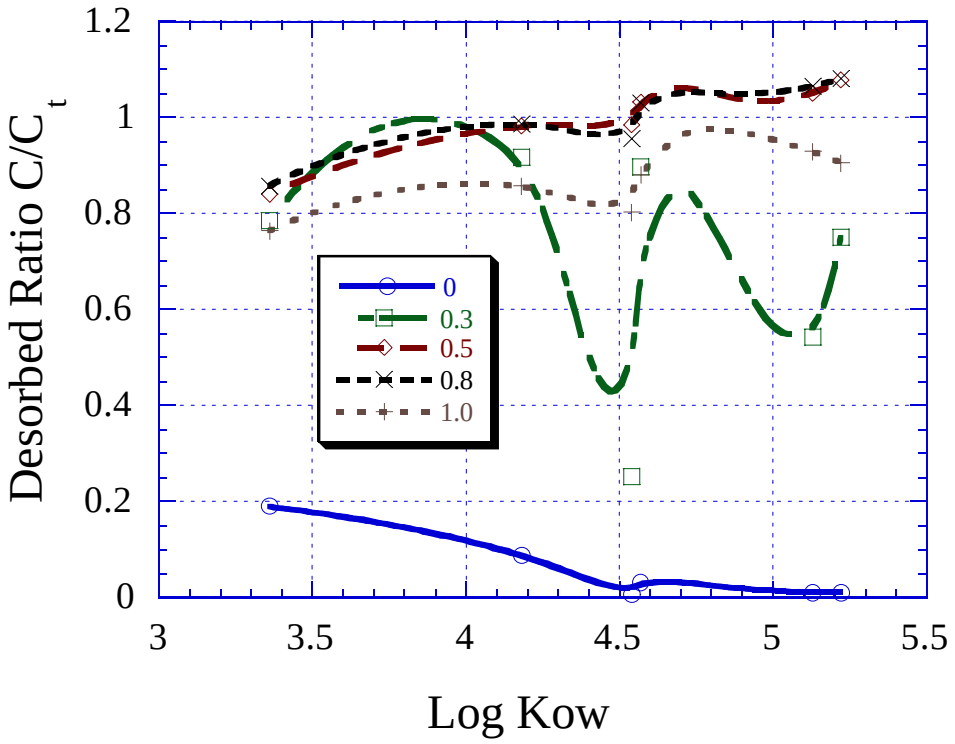

Figure 3.3. The ratio of desorbed PAHs concentration as a function of the octanol-water partition coefficient.

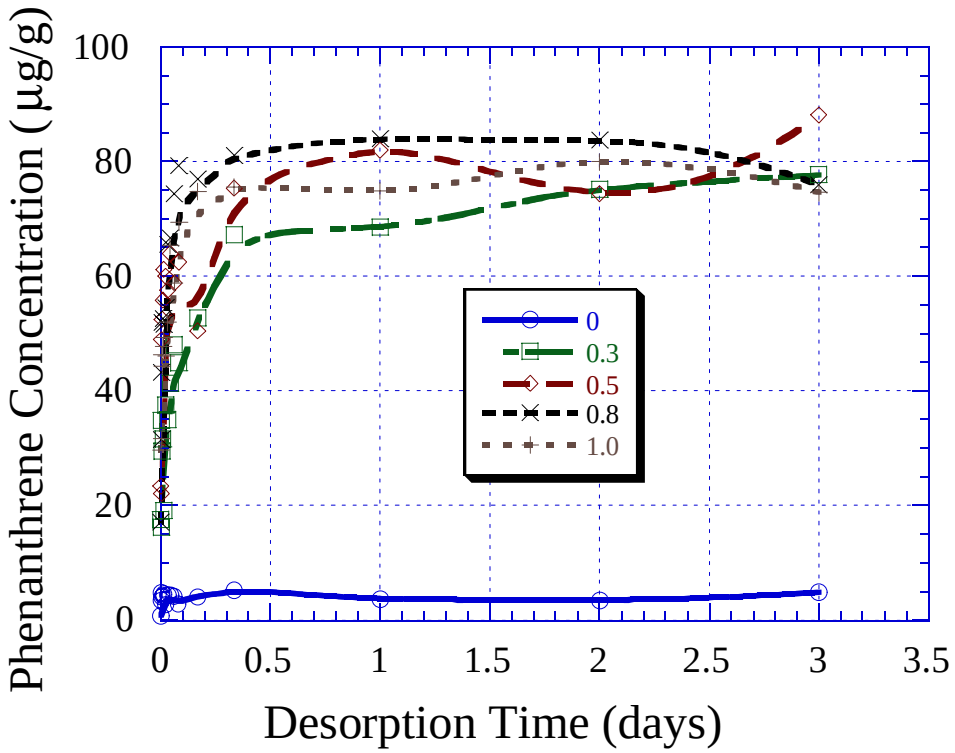

Figure 3.4. **The concentrations of phenanthrene as a function of the desorption time. Experimental conditions: mixing rate = 100 oscillations per minute, initial concentration = 100 µg/g.**

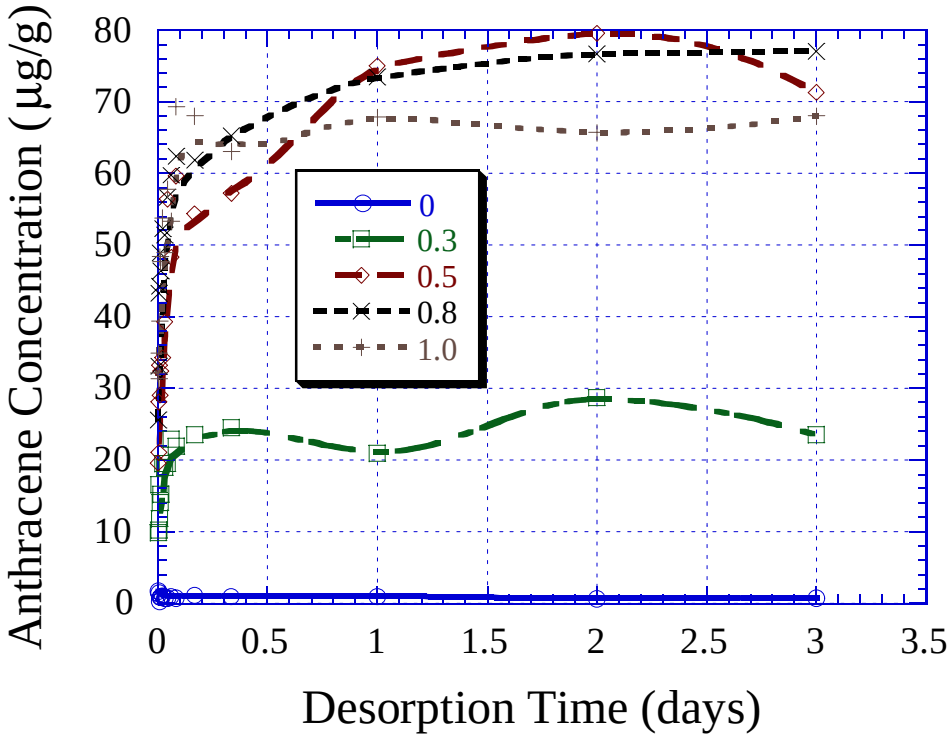

Figure 3.5. **The concentrations of anthrancene as a function of the desorption time. Experimental conditions: mixing rate = 100 oscillations per minute, initial concentration = 100 µg/g.**

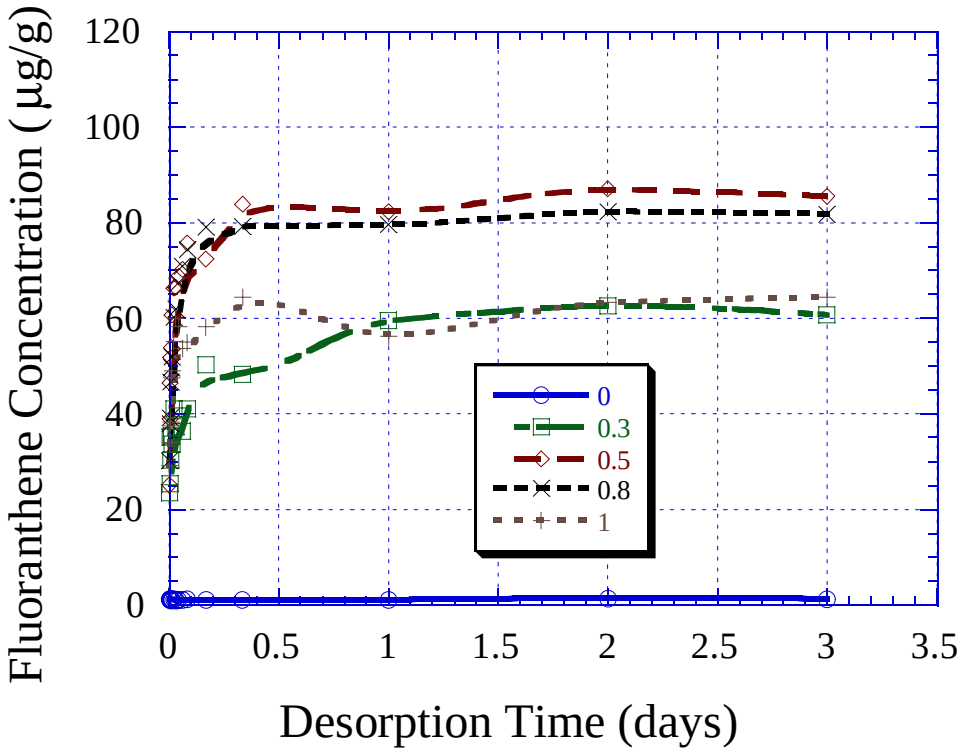

Figure 3.6. **The concentrations of fluoranthene as a function of the desorption time. Experimental conditions: mixing rate = 100 oscillations per minute, initial concentration = 100 µg/g.**

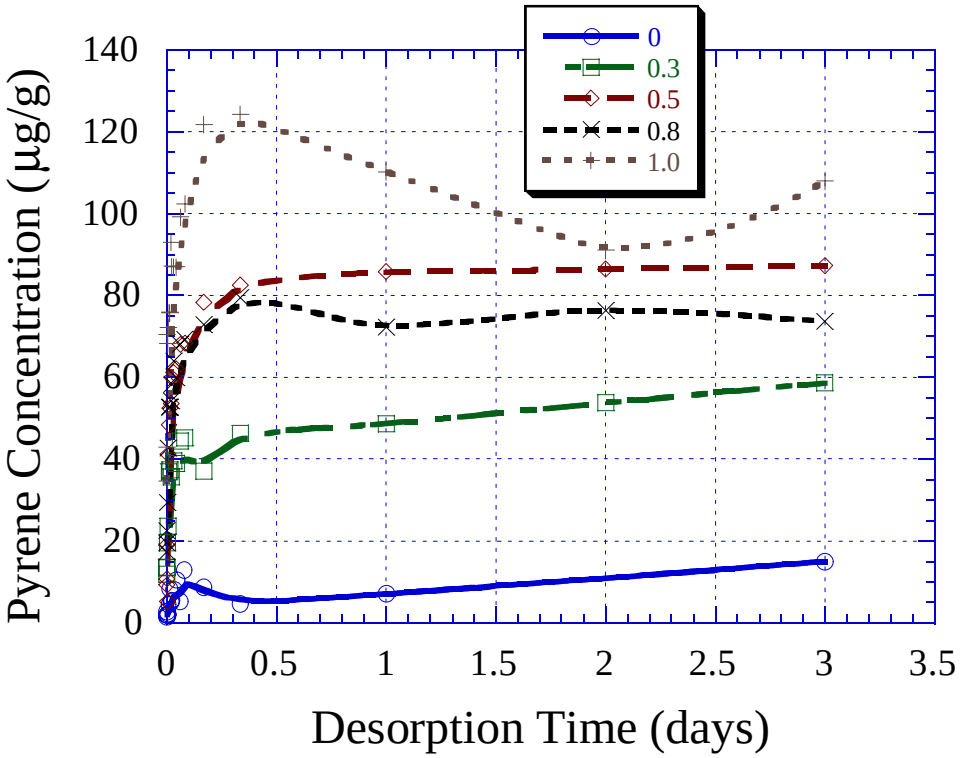

Figure 3.7. **The concentrations of pyrene as a function of the desorption time. Experimental conditions: mixing rate = 100 oscillations per minute, initial concentration = 100 µg/g.**

IV. OXIDATION OF SELECTED ORGANIC COMPOUNDS BY FENTON PROCESS

IV.1. Introduction

IV.1.1. Properties of Selected Organic Compounds

It is expected that two major categories of organic contaminants are typically present in the soils at specific DOE sites: 1) halogenated hydrocarbons, including tetrachloroethylene (PCE), trichloroethylene (TCE), chloroform, carbon tetrachloride; and 2) polycyclic aromatic hydrocarbons (PAHs), including naphthalene, fluorene, phenanthrene, fluoranthene, pyrene and anthracene. Careless disposal of hazardous organic compounds, accidental petroleum spills, and leaking of underground petroleum storage tanks can seriously contaminate surrounding soils and groundwaters by these toxic organic contaminants.

Some important properties of these selected organic compounds are listed in Table 4.1. The properties of these organic compounds, especially the volatility (expressed by the Henry's Law constant) and the water solubility, are essential not only to the reactor design and process control, but also to the chemical analysis. According to Table 4.1, all halogenated hydrocarbons are highly volatile; naphthalene is semi-volatile; while other PAHs are considered as relatively nonvolatile. Though the evaporation speed of naphthalene is not very high, the reaction condition such as vigorously stirring may accelerate its escaping from the aqueous solution. Based on the volatility and the water solubility, these organic compounds can be divided into two sets: 1) highly volatile or semi-volatile organic compounds (correspondingly, they have a high or relatively high water solubility, see Table 4.1), including all halogenated hydrocarbons studied and naphthalene; and 2) nonvolatile organic compounds (correspondingly, they have an extremely low water solubility), including all PAHs except naphthalene.

In the last annual report (1997-1998), we studied the oxidation of naphthalene and halogenated hydrocarbons, including PCE, TCE and chloroform by Fenton process in batch, pseudo-continuous and continuous modes. Continuous mode yields the best results. In the current work, we have studied the oxidation of selected PAHs, including fluorene, phenanthrene, fluoranthene, pyrene and anthracene by Fenton process in continuous mode.

Table 4.1. Important properties of selected PAHs and halogenated hydrocarbons (Schwarzenbach *et al.*, 1993).

Compound Name	Molecular Formula	Molecular Structure	Molecular Weight	Water Solubility @ 25 °C (mg/L)	Henry's Constant, $\log K_H$ @ 25 °C (L atm mol^{-1})	Log K_{ow} @ 25 °C
Naphthalene	$C_{10}H_8$	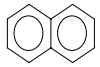	128.2	31.9 (30.0-34.4)	-0.37 (-0.31 exp.)	3.36
Fluorene	$C_{13}H_{10}$	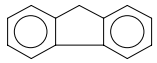	166.2	1.84 (1.69-1.98)	-1.14 (-1.00 exp.)	4.18
Phenanthrene	$C_{14}H_{10}$	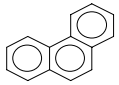	178.2	1.09 (0.994-1.29)	-1.59 (-1.45 exp.)	4.57
Anthracene	$C_{14}H_{10}$	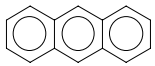	178.2	0.059 (0.045-0.073)	-1.64	4.54
Fluoranthene	$C_{16}H_{10}$	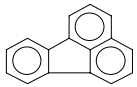	202.3	0.233 (0.206-0.26)	-1.98	5.22
Pyrene	$C_{16}H_{10}$	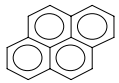	202.3	0.134 (0.132-0.135)	-2.05 (-1.96 exp.)	5.13
Tetrachloroethylene (PCE)	C_2Cl_4	$CCl_2=CCl_2$	165.8	275 (150-400)	1.44	2.88
Trichloroethylene (TCE)	C_2HCl_3	$CHCl=CCl_2$	131.4	1,312 (1,100-1,470)	1.03	2.42
Chloroform	$CHCl_3$	$HClC-CCl_2$	119.4	7,870 (7100-9300)	0.60 (0.59 exp.)	1.93
Carbon Tetrachloride	CCl_4	Cl_2C-CCl_2	153.8	911 (757-1,160)	1.38 (1.33 exp.)	2.73

IV.1.2. Proposed mechanisms of Conventional Fenton Process

Fenton's reagent consists of H_2O_2 and Fe^{2+} ion. In acidic conditions, H_2O_2 decomposes to hydroxyl radical and hydroxide ion under the catalysis of Fe^{2+} ion. Hydroxyl radical is an intermediate species characterized by an unpaired electron. The one-electron deficiency of hydroxyl radical results in its transient and highly oxidizing characteristics, with a redox potential being only next to elemental fluorine. Hydroxyl radical can nonselectively oxidize most of organic compounds as well as quite a few inorganic chemicals. This intermediate species can attack target organic contaminants, CO_3^{2-}, HCO_3^-, Cl^-, and even H_2O_2 and Fe^{2+}, as illustrated in Figure 4.1.

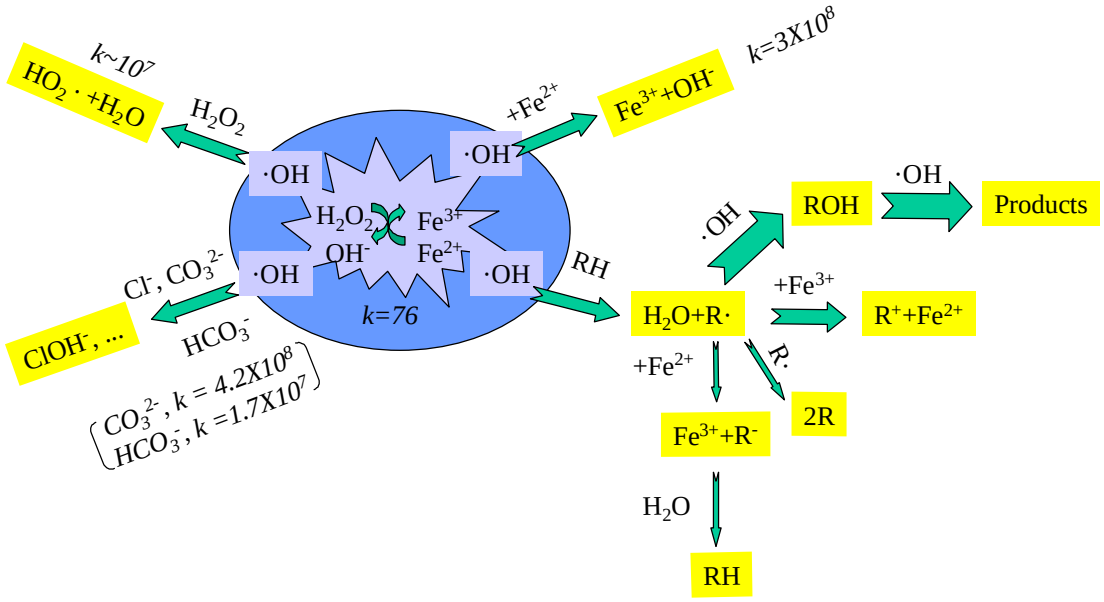

Figure 4.1. Illustration of Proposed Mechanisms of Fenton Process

The proposed reaction mechanisms are indicated by a series of chain reactions (Walling, 1975, 1976):

$$Fe^{2+} + H_2O_2 \rightarrow Fe^{3+} + \cdot OH + OH^- \ , \quad k_1 \qquad [4.1]$$

$$Fe^{2+} + \cdot OH \rightarrow Fe^{3+} + OH^- \ , \quad k_2 \qquad [4.2]$$

$$RH + \cdot OH \rightarrow R\cdot + H_2O,\ k_3 \quad [4.3]$$

$$R_1\cdot + Fe^{3+} \rightarrow R_1^{+} + Fe^{2+},\ k_{31} \quad [4.4]$$

$$2R_2\cdot \rightarrow R_2 - R_2,\ k_{32} \quad [4.5]$$

$$R_3\cdot + Fe^{2+} \rightarrow Fe^{3+} + R_3^{-} \xrightarrow{H_2O} R_3H,\ k_{33} \quad [4.6]$$

$$H_2O_2 + \cdot OH \rightarrow HO_2\cdot + H_2O,\ k_4 \quad [4.7]$$

where, k_1 = 76 (M^{-1} Sec^{-1}),
k_2 = $3x10^8$(M^{-1} Sec^{-1}),
k_4 = 2~$4.5x10^7$ (M^{-1} Sec^{-1}),
RH = target organic compounds.

Reaction 4.1 is a chain initiation step, producing hydroxyl radical. Hydroxyl radical so produced attacks organic compounds, producing organic radicals, as shown in reaction 4.3. These free organic radicals can be further transformed through three different pathways (Walling *et al*., 1970). $R_1\cdot$ radical is further oxidized by ferric ion, transforming into an organic cation; $R_2\cdot$ radical dimerizes; $R_3\cdot$ radical is first reduced by ferrous ion, and then the resulting organic anion is reverted to original form by hydroxylation. Side reactions occur at the same time, for example, hydroxyl radical reacts with H_2O_2 and Fe^{2+}. H_2O_2 is oxidized to superhydroxyl radical (reaction 4.7), an intermediate species with a redox potential less than that of hydroxyl radical, and Fe^{2+} is oxidized to Fe^{3+} (reaction 4.2). Both H_2O_2 and Fe^{2+} consume hydroxyl radical, and these two competition reactions are inevitable. However, most organic compounds react with hydroxyl radical at a rate constant of $K._{OH} > 10^9$(M^{-1} Sec^{-1}). Compared to the rate constants of H_2O_2 and Fe^{2+}, the competition reactions are not significant unless the concentration ratio of [H_2O_2]/[RH] or [Fe^{2+}]/[RH] is too high.

Due to the nonselective oxidation feature of hydroxyl radical, Fenton process has been widely used to oxidize hazardous organic compounds. This chemical oxidation process has the following advantages: no chlorinated organic compounds formed as in chlorination or hypochlorination, no mass transfer limitation due to its homogeneous catalytic nature, and cheap and nontoxic ferrous sulfate and hydrogen peroxide (Huang *et al.*, 1993). The hydroxyl radical combines with carbon in the organic compounds by attacking and substituting some functional groups (such as halogen elements, double bonds, and aromatic rings), converting many organic compounds to harmless carbon dioxide and water.

IV.1.3. Current Objectives

As described above, PAHs are typical toxic organic contaminants at specific DOE sites. Though extensive research has been carried out to study the oxidation of PAHs with ozone (Legube *et al.*, 1984, 1986; Bailey *et al.*, 1964; Cornell *et al.*, 1984), most of these experiments were conducted in organic solvents at high PAHs concentrations. One of the limiting factors of studies in aqueous solutions is the analytical problem associated with the extremely low water solubility of PAHs. The considerably slow dissolution rate of PAHs into water is another experimental problem. Methanol, acetone and octane were frequently used to increase the solubility of PAHs in liquid phase. However, the interference of the organic solvents on the oxidation efficiency of target PAHs was still unclear. To date, few literatures can be found on the oxidation of PAHs by Fenton's reagent.

In this study, we investigated the oxidation of selected PAHs, i.e., fluorene, phenanthrene, fluoranthene, pyrene and anthracene by continuous-mode conventional Fenton process. In order to prepare the reaction solutions more quickly, several media-assisted dissolution methods were investigated to increase the dissolution rate of PAHs in water. Furthermore, we used methanol as the model organic solvent to study its influence on the oxidation efficiency of selected PAHs. Experimental data were fitted by an exponential kinetic model, and the hydroxyl radical concentrations in the reaction solutions was estimated.

IV.2. Methods and Materials

IV.2.1. Reaction System

A similar reaction system was employed for the oxidation of selected nonvolatile organic contaminants (fluorene, phenanthrene, fluoranthene, pyrene and anthracene) by continuous-mode conventional Fenton process as was previously used for the oxidation of volatile organic contaminants (PCE, TCE, chloroform and naphthalene). The schematic diagram of the reaction system is illustrated in Figure 4.2. The only difference is that all PAHs oxidation experiments were carried out under ambient room temperature (23.5 ^{o}C) without solution temperature control. Since the volatility of the selected PAHs is negligible, the glass reactor was filled with 500 mL reaction solution, and the left 100 mL was headspace. Though PAHs prefer to partition on the reactor walls due to their high hydrophobicity (expressed by Log K_{ow}, as shown in Table 4.1), completely stirring of the reaction solution can eliminate this side effect. Two fine-

flowrate dosage pumps were used to continuously deliver hydrogen peroxide and ferrous sulfate into the reactor. Both hydrogen peroxide and ferrous sulfate solutions were kept in acidic conditions in a refrigerator (4 $^{\circ}$C). At low pH values, the natural decomposition of hydrogen peroxide and the oxidation of ferrous ions by dissolved oxygen can be minimized. Constant solution pH was maintained using a pH controller through the intermittent addition of NaOH or $HClO_4$ solutions.

IV.2.2. Chemical and Analysis

All selected PAHs, i.e., fluorene (98%), phenanthrene (98%), fluoranthene (98%), pyrene (98%) and anthracene (97%) were purchased from the Aldrich Chemical Company (Milwaukee, WI). They were used without further purification. Hydrogen peroxide and ferrous sulfate were purchased from the Fisher Scientific Company with a purity of 31.5% and 98%, respectively.

The selected PAHs were first extracted by hexane and then analyzed by GC/MS (GC, Hewlett Packard, 5890, Series II; MS, Hewlett Packard, 5972 Series, mass selective detector). A HP capillary column (cross-linked 5% Ph Me silicon, 30m x 0.25mm x 0.25μm film thickness) was used for separating organic compounds in GC. The extremely low water solubilities of all selected PAHs make chemical analysis difficult. Though GC/FID is capable of determining many hydrocarbons, its detection limit (250 ppb) can not satisfy the determination of PAHs studied even after concentrating PAHs by hexane extraction. However, PAHs can produce very stable molecular ions under the electron impact in MS due to their benzene-ring structures. This characteristic makes GC/MS more sensitive for detecting PAHs, usually with a detection limit of 50~100 ppb. The concentrating factors of hexane extraction are compound specific, i.e., depending on their different water solubilities. Fluorene, phenanthrene, fluoranthene, pyrene and anthracene were concentrated by 2.5, 2.5, 5, 20, 20 times, respectively. Experiments proved that the extraction recovery efficiencies were all greater than 95%.

IV.2.3. Reaction Solution Preparation

For the selected PAHs, due to their extremely low water solubility, it may take a long time to dissolve them into the distilled water up to saturation. Therefore, we need to develop a practical method for quick dissolution of PAHs. In order to accelerate the dissolution, three media-assisted dissolution methods were investigated and compared. Methanol, glass-beads and

hexane were separately selected to enhance the dissolution of the model PAH compound, phenanthrene.

Methanol assisted dissolution. Due to the dissolution and analytic problems associated with low solubility of PAHs in water, many PAHs degradation experiments, e.g., ozonation, were carried out in organic solvents. Sturrock *et al.* (1963) studied the oxidation of phenanthrene with ozone treatment in 1/1 water/methanol solution. Ilnitsky *et al.* (1968) ozonated benzo(a)anthracene, dibenzo(ah)anthracene, pyrene and benzo(a)pyrene in acetone and acetone-octane solutions. Moriconi and coworkers (1967, 1968) conducted ozonation of several PAHs in methylene chloride solution. In addition, methanol has been quite frequently used as a cosolvent to enhance the mobility of hazardous hydrophobic organic contaminants in soil and groundwater remediation processes. The presence of methanol in aqueous solution may significantly hinder the successive oxidation of target organic contaminants by advanced chemical oxidation processes. In order to speed up the dissolution of PAHs and investigate the influence of methanol on the oxidation of PAHs by Fenton's reagent, methanol was used for the reaction solution preparation. Phenanthrene was first dissolved in methanol so that each mL of methanol contained an amount of phenanthrene a little higher than its water solubility. Then, 1 mL of methanol solution was spiked into 1 L distilled water. After vigorously stirring for 1 hour, followed by vacuum filtration to remove possible crystal residue, the reaction solution was obtained. It was used within 2 hours after preparation. The volume fraction of methanol in the final reaction solution is 0.1%.

Glass beads assisted dissolution. According to dissolution theory, small crystals can be dissolved into water much easily than big ones due to the higher surface area. It is expected that the phenanthrene dissolution can be accelerated if it is adsorbed in molecular form on the large surface area of glass beads. A certain amount of phenanthrene in methanol solution was spiked to a certain weight of glass beads. After completely mixing, the spiked glass beads were placed in the hood to let the methanol evaporate. Two hours later, the dried glass beads were put into a 1 L glass flask filled with distilled water for phenanthrene dissolution. The flask was vigorously stirred so that the glass beads were suspended in the solution. By determining the concentration of phenanthrene as a function of time, the dissolution kinetics could be obtained. Figure 4.3 shows the dissolution kinetics of phenanthrene assisted by 10 g glass beads at different initial surface concentrations. Results indicate that the dissolution rate increases with increasing initial surface concentration of phenanthrene. At four hours, the relative aqueous concentrations (normalized to phenanthrene water solubility) obtained were about 40%, 80% and 90% for 1.5, 3.0 and 4.5 mg of initial surface concentration, respectively. The dissolution rate is linearly

proportional to the initial surface concentration when the amount of spiked phenanthrene was below 3.0 mg. Above this value, the increment of the dissolution rate is not significant. Figure 4.4 shows the dissolution kinetics of a certain amount of phenanthrene (4.5mg) assisted by different amounts of glass beads (5, 10 and 20 g). Also, a blank experiment was carried out to determine the dissolution kinetics without the assistance of glass beads. Results show that the amount of glass beads only affects the initial dissolution rate, and there is almost no difference after three hours. The relative aqueous concentrations of phenanthrene obtained at 4 hours were around 80~90%. However, the blank experiment indicates that the dissolution of phenanthrene is considerably slow. After six hours, the relative aqueous concentration was only 25%. It may take one or two weeks to get a nearly saturated reaction solution. The effect of glass beads on the dissolution of phenanthrene is thus obvious. After completing dissolution, vacuum filtration was necessary to remove phenanthrene crystal residues and some suspended glass beads to get the final reaction solution. There was no methanol detected by GC/FID in the final reaction solution. Though glass beads could significantly accelerate the dissolution of PAHs, we found that the vacuum filtration was relatively difficult. It is assumed that broken glass fragments and fine phenanthrene crystals block the filter paper (0.45 μm).

Hexane assisted dissolution. Phenanthrene was first dissolved in hexane so that each mL of hexane contained 2 mg phenanthrene. Then, 1 mL of hexane solution was spiked into 1 L distilled water which was preheated to 75~80 ^{o}C. There are two purposes of preheating: 1) increasing the evaporation of hexane from the flask; and 2) increasing the initial dissolution rate of phenanthrene at high temperatures. After vigorously stirring for twenty minutes, all hexane evaporated. The dissolution kinetics of phenanthrene is shown in Figure 4.4. Results indicate that at two hours, a relative aqueous concentration of about 85% can be obtained. As same as in the glass beads assisted dissolution method, vacuum filtration was used to remove phenanthrene crystal residues to get the final reaction solution. Our experiments showed that the vacuum filtration was very fast, the blocking problem was negligible.

Hexane assisted dissolution method can produce pure PAHs solutions (without any organic solvent like methanol) much faster than the glass beads method. In our experiments, all PAHs reaction solutions without methanol were prepared by this method. For the experiments that studied the methanol influence on the oxidation of selected PAHs, the reaction solutions were prepared by the methanol assisted dissolution method. In the final reaction solution, methanol occupied 0.1% (v/v), about 790 ppm.

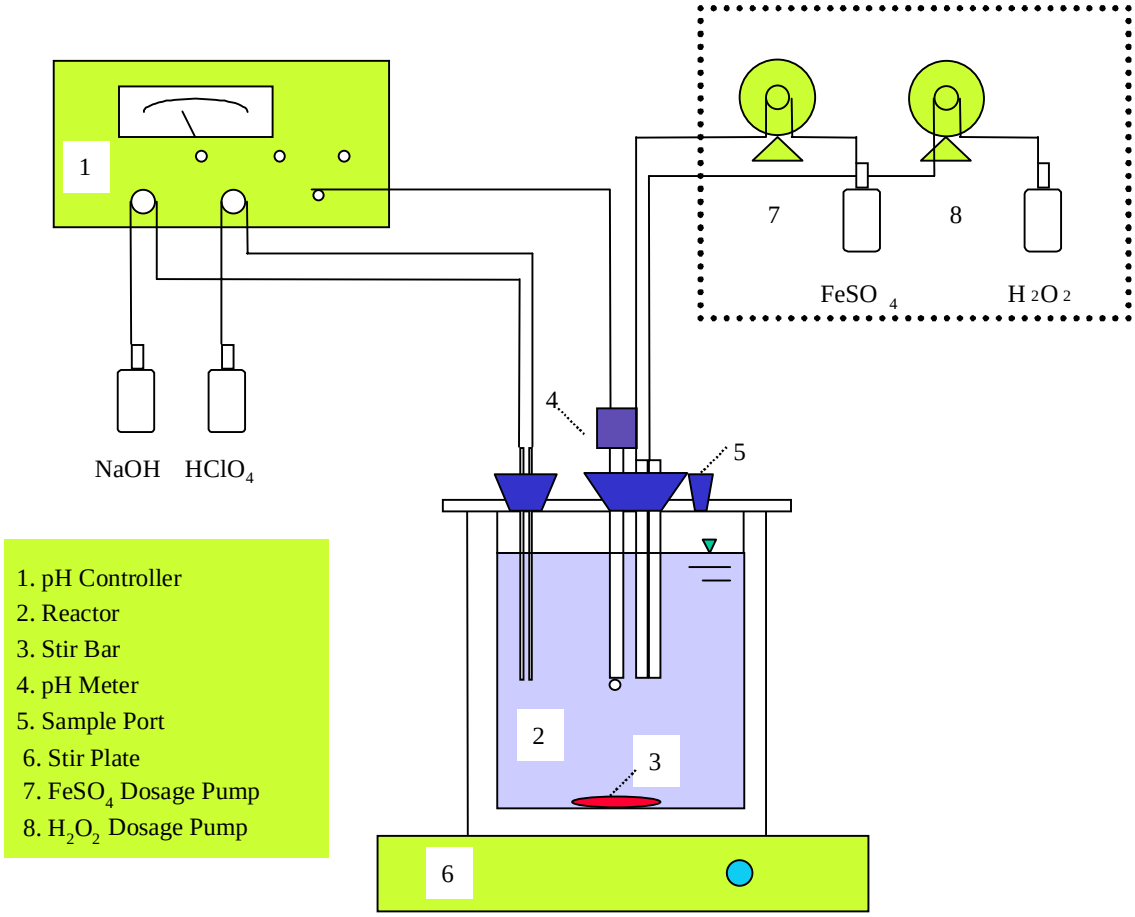

Figure 4.2. Schematic diagram of conventional Fenton process.

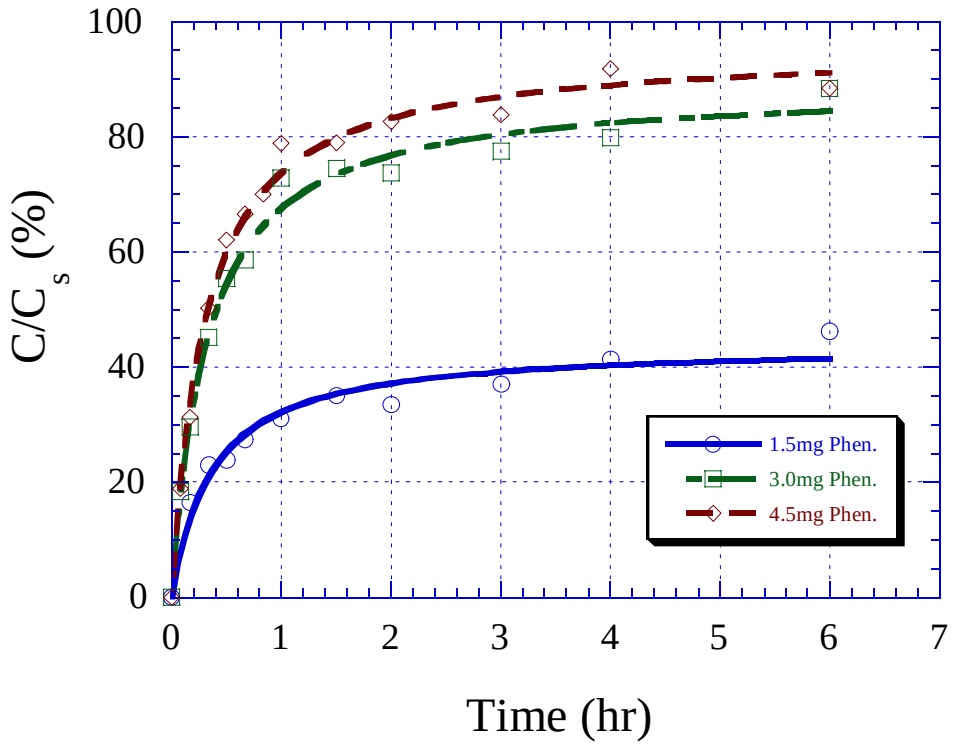

Figure 4.3. **Glass beads assisted dissolution of phenanthrene at different spiked initial concentrations. Experimental conditions: glass beads weight = 10g; room temperature (23.5 °C); ionic strength = 0.05M $NaClO_4$.**

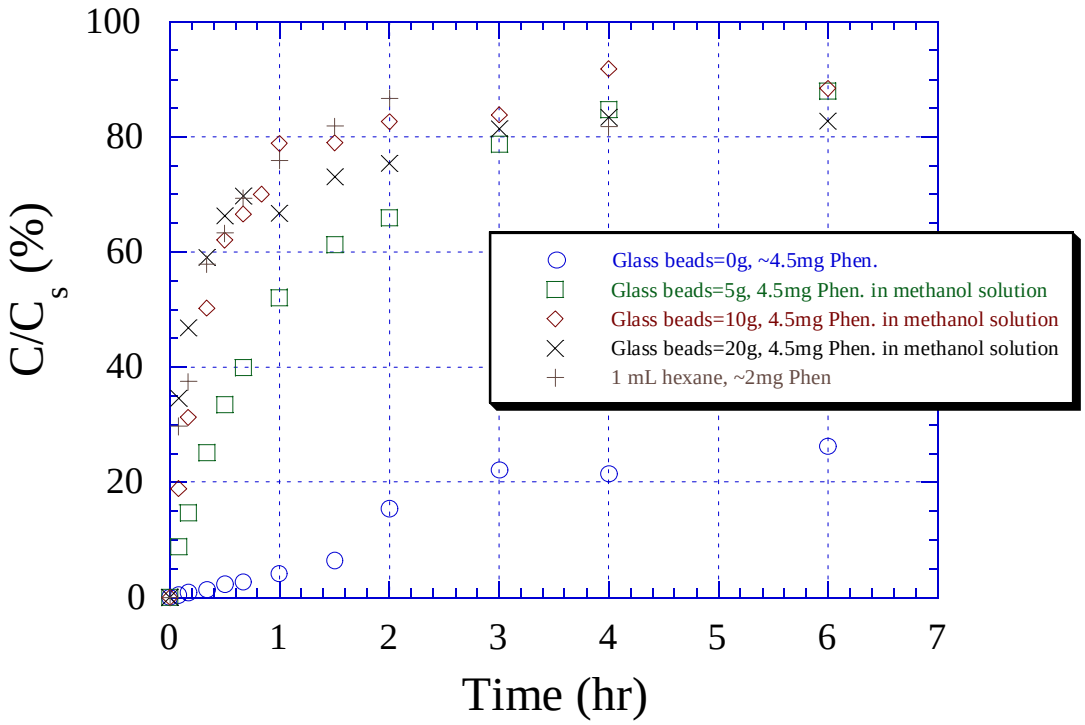

Figure 4.4. Comparison of different methods for phenanthrene dissolution. Experimental conditions: room temperature (23.5 °C); ionic strength = 0.05M $NaClO_4$.

IV.3. Results and Discussion

IV.3.1. Theoretical Consideration of Kinetic Modeling

An innovative competition method has been developed by Walling and coworkers (1970, 1975) to determine the rate constant of organic compound toward hydroxyl radical in aqueous solution instead of the traditional radiation chemistry method. This theory offers the advantage that it is not necessary to analyze the organic compound of interest, but rather involves simple measurement of ferrous ions regardless of the substrate tested. In batch experiment, a small amount of hydrogen peroxide is added into the reactor that contains premixed organic compound and ferrous ion solution. After the oxidation reaction completes, the residue concentration of ferrous ion is determined. By varying the initial molar ratio of organic compound to ferrous ion, a series of consumption percentages of ferrous ion can be determined. Since both ferrous ion and organic compound compete for hydroxyl radical and the rate constant of ferrous ion is already known (k_2 = 3 x 10^8 M^{-1} Sec^{-1}, Reaction 4.2), the rate constant of organic compound can be calculated by taking ferrous ion as a reference chemical.

Usually, the concentration of organic radical in reaction solution is very low, the dimerization shown by reaction 4.5 is unimportant. Also, the oxidation ability of organic radical is generally not very strong, therefore reaction 4.6 is not significant. Moreover, since hydrogen peroxide has only a relatively small rate constant of 2~4.5 x 10^7 M^{-1} Sec^{-1} in comparison with ferrous ion and organic compound, reaction 4.7 can be neglected. For the purpose of simplicity, we only use the four major chain reactions (Reaction 4.1 ~ 4.4) to deduce the kinetic models.

Considering only reactions 4.1 ~ 4.4, one gets the decomposition of ferrous ion, hydrogen peroxide and organic compound as a function of time:

$$-\frac{d[Fe^{2+}]}{dt} = k_1[Fe^{2+}][H_2O_2] + k_2[Fe^{2+}][\cdot OH] - k_{31}[Fe^{3+}][R\cdot] \qquad [4.8]$$

$$-\frac{d[H_2O_2]}{dt} = k_1[Fe^{2+}][H_2O_2] \qquad [4.9]$$

$$-\frac{d[RH]}{dt} = k_3[RH][\cdot OH] \qquad [4.10]$$

The concentrations of hydroxyl radical and organic radical may also be reaction time dependent, as shown in equations 4.11 and 4.12:

$$\frac{d[\cdot OH]}{dt} = k_1[Fe^{2+}][H_2O_2] - k_2[Fe^{2+}][\cdot OH] - k_3[RH][\cdot OH] \quad [4.11]$$

$$\frac{d[R\cdot]}{dt} = k_3[RH][\cdot OH] - k_{31}[R\cdot][Fe^{3+}] \quad [4.12]$$

By the steady-state assumption commonly employed, the concentration of hydroxyl radical does not change with reaction time. Equation 4.10 can be simplified by a pseudo-first order kinetic expression:

$$-\frac{d[RH]}{dt} = k_{obs}[RH] \quad [4.13]$$

where, k_{obs} equals $k_3[\cdot OH]$. The value of k_{obs} can be achieved by fitting experiment data. Since the value of k_3 has been obtained from the competition method, it is easy to estimate the concentration of hydroxyl radical in the reaction solution. In natural water system, hydroxyl radical is produced by photolysis of nitrate ions (Schwarzenbach *et al.*, 1993). Its concentration usually ranges from 10^{-18} M to 10^{-16} M. In advanced chemical oxidation processes, the concentration of hydroxyl radical can be increased to 10^{-14} ~ 10^{-11} M. Though the second order rate constant of organic compound is very high, usually in the range of 10^9 ~ 10^{10} M^{-1} Sec^{-1}, the value of k_{obs} is relatively small due to the extremely low concentration of hydroxyl radical. For engineering application, k_{obs} is more practical than k_3 since hydroxyl radical concentration varies with different advanced oxidation processes.

IV.3.2. Kinetic Modeling of Oxidation of PCE, TCE and naphthalene

As mentioned above, the decomposition of organic contaminant by Fenton's reagent can be expressed by a pseudo-first order kinetic model in batch experiment. A steady-state assumption is adopted for hydroxyl radical concentration in the reaction solution. We have proved in the annual report (1997 ~ 1998) that continuous mode Fenton process is more efficient for oxidizing organic contaminants than the traditional batch mode. In this system, the steady-state assumption may be no longer appropriate since hydrogen peroxide and ferrous ion are continuously delivered into the reactor at a constant dosage rate. Equations 8 and 9 need to be modified as follows:

$$-\frac{d[Fe^{2+}]}{dt} = k_1[Fe^{2+}][H_2O_2] + k_2[Fe^{2+}][\cdot OH] - k_{31}[Fe^{3+}][R\cdot] - Q_{Fe} \quad [4.14]$$

$$-\frac{d[H_2O_2]}{dt} = k_1[Fe^{2+}][H_2O_2] - Q_{H_2O_2} \quad [4.15]$$

where, $Q_{H_2O_2}$ and Q_{Fe} are the dosage rates of hydrogen peroxide and ferrous ion, respectively.

In contrast to most other oxidants, reactions of hydroxyl radical with organic compounds containing unsaturated structures, such as double bonds and benzene rings, generally proceed with rate constants approaching the diffusion-controlled limit (10^{10} $M^{-1}Sec^{-1}$). Therefore, the oxidation rate constant of organic compound is usually limited by the rates of hydroxyl radical generation and competition by other hydroxyl radical scavengers in the reaction solution rather than by its intrinsic reactivity with the oxidant. In a completely mixed reaction system, the diffusion means that organic molecule travels a certain distance to contact hydroxyl radical. Once they meet together, chemical reaction occurs immediately. More time is consumed on the "travelling" than on the chemical reaction. The nonselective oxidation nature of hydroxyl radical makes it to react with the first chemical that it encounters on the travelling way. Reactions 4.1 ~ 4.4 described above only generalize the major reactions occurring in Fenton's system. Other radicals such as $HO_2\cdot$ and $O_2\cdot^-$ also play a role accounting for the decomposition of organic contaminant. Moreover, new mechanisms about Fenton oxidation are still being proposed and investigated. In the continuous mode Fenton process, it is expected that the hydroxyl radical concentration changes as a function of reaction time since both hydrogen peroxide and ferrous ion are continuously supplied. For the purpose of simplicity, we assume that the hydroxyl radical concentration is a linear function of reaction time, i.e.,

$$[\cdot OH] = at \quad [4.16]$$

where, a is the increasing rate of hydroxyl radical concentration. This assumption satisfies the initial condition, i.e., $[\cdot OH] = 0$ at $t = 0$. Now equation 4.10 needs to be modified,

$$-\frac{d[RH]}{dt} = ak_3[RH]t \quad [4.17]$$

At a constant dosage rate of Fenton's reagent, the value of a is constant. By merging a and k_3 and integrating equation 4.17, we get

$$[RH] = [RH]_0 \exp(-k_{obs} t^2) \quad [4.18]$$

$$a = \frac{2k_{obs}}{k_3} \quad [4.19]$$

where, $[RH]_0$ is the initial concentration of organic compound.

Equation 4.18 is the basic kinetic expression that is employed to model our experiment data for the oxidation of PCE, TCE and naphthalene. The second order rate constants of PCE, TCE and PAHs toward hydroxyl radical have been achieved using radiation method. Watts (1998) compiled these values as 2.8 x 10^9, 4.0 x 10^9 and ~10^{10} $M^{-1}Sec^{-1}$ for PCE, TCE and PAHs, respectively. Then using equation 4.19 we can calculate the value of *a*, the increasing rate of hydroxyl radical concentration.

PCE. The oxidation of PCE at different molar ratios ($[H_2O_2]/[Fe^{2+}]$) of Fenton's reagent is shown in Figure 4.5. Results indicate that as the dosage rate of hydrogen peroxide is kept constant, the oxidation efficiency increases with increasing dosage rate of ferrous ion. The experiment data can be well fitted by the proposed kinetic model (equation 4.18), especially at high ferrous ion dosage rates. The values of the observed rate constant, k_{obs}, are 4.38 x 10^{-2}, 1.41 x 10^{-2}, 8.3 x 10^{-3}, 3.5 x 10^{-3} and 1.3 x 10^{-3} min^{-2} at varying Fe^{2+} dosage rates, i.e., 1.16, 0.578, 0.289, 0.145, 0.072 (x 10^{-4}) M/min, respectively. Due to the high volatility of PCE, it is impossible to prepare reaction solutions with a constant initial concentration. There is always a little variation of initial concentration between different reaction solutions. Generally, k_{obs} is also related to the initial concentration of organic compound. Therefore, we plot k_{obs} vs. the molar ratio of Fe^{2+} dosage rate to PCE initial concentration, as shown in Figure 4.6. The plot shows two linear segments: y = 0.0686x and y = 0.183x - 0.0233. Below 0.2 M/M.min of $[Fe^{2+}]/[PCE]_0$, k_{obs} increases with a slope of 0.0686 min^{-1}. While above this value, k_{obs} increases with $[Fe^{2+}]/[PCE]_0$ more rapidly, with a slope of 0.183 min^{-1}. Since both $k_{3,PCE}$ (2.8 x 10^9 $M^{-1}Sec^{-1}$) and k_{obs} are known, we can easily calculate the values of *a* at different Fe^{2+} dosage rates based on equation 4.19, such as 5.21 x 10^{-13}, 1.68 x 10^{-13}, 9.88 x 10^{-14}, 4.17 x 10^{-14} and 1.55 x 10^{-14} M/min, correspondingly. And then using equation 4.16, the concentration of hydroxyl radical can be estimated. Figure 4.7 shows that hydroxyl radical concentration increases in linear proportion to reaction time. At 30 minutes of reaction time, it ranges from 5 x 10^{-13} M to 1.6 x 10^{-11} M.

TCE. The influence of molar ratios ($[H_2O_2]/[Fe^{2+}]$) of Fenton's reagent on the oxidation of TCE is shown in Figure 4.8. Similar as in the oxidation of PCE, TCE is decomposed more efficiently with increasing dosage rate of ferrous ion. Using equation 4.18 to fit the experiment

data, we can get the values of k_{obs} as 1.13 x 10^{-2}, 5.6 x 10^{-3}, 2.5 x 10^{-3}, 1.3 x 10^{-3} and 5.3 x 10^{-4} min^{-2} at different Fe^{2+} dosage rates, correspondingly. Results also indicate that better data fitting can be achieved at higher Fe^{2+} dosage rates. The plot of k_{obs} vs. $[Fe^{2+}]/[TCE]_0$ (Figure 4.9) shows that the observed rate constant is linearly proportional to $[Fe^{2+}]/[PCE]_0$ in the whole x axis range, with a slope of 0.0741 min^{-1}. Since $k_{3,TCE}$ equals 4.0 x 10^9 $M^{-1}Sec^{-1}$, the corresponding values of *a* at different Fe^{2+} dosage rates can be calculated, such as 9.42 x 10^{-14}, 4.67 x 10^{-14}, 2.10 x 10^{-14}, 1.05 x 10^{-14} and 4.4 x 10^{-15} M/min. Figure 4.10 shows the linear increase of hydroxyl radical concentration in reaction solutions. It ranges from 1.8 x 10^{-13} M to 3.8 x 10^{-12} M at the end of reaction (40 minutes) for different dosages of ferrous ion.

Naphthalene. All PAHs can react with hydroxyl radical very fast, with a diffusion-controlled rate constant of ~10^{10} $M^{-1}Sec^{-1}$. The high reactivity of PAHs toward hydroxyl radical is ascribed to their electron-rich structures, i.e., multiple benzene rings. The initial oxidation step is often the addition of hydroxyl radical into one of the benzene rings. Figure 4.11 shows the oxidation of naphthalene at different $[H_2O_2]/[Fe^{2+}]$ ratios. Experiment data fitting gives the values of k_{obs}, such as 4.19 x 10^{-2}, 2.95 x 10^{-2}, 1.93 x 10^{-2}, 6.1 x 10^{-3} and 3.1 x 10^{-3} min^{-2} corresponding to different Fe^{2+} dosage rates. The plot of k_{obs} vs. $[Fe^{2+}]/[Naph]_0$ (Figure 4.12) shows two linear segments: y = 0.130x and y = 0.0530x + 0.0130. Below 0.14 M/M.min of $[Fe^{2+}]/[Naph]_0$, k_{obs} increases with a slope of 0.130 min^{-1}. Above this value, k_{obs} increases more slowly, with a slope of 0.053 min^{-1}. Actually, the slope is not only influenced by $[Fe^{2+}]/[RH]_0$ or $[H_2O_2]/[RH]_0$ (almost constant in our experiments), but also compound specific. There are different slopes for PCE, TCE and naphthalene. However, the difference is considerably small. All slopes fall in the range of 0.05 ~ 0.18 min^{-1}. Taking $k_{3,Naph}$ = 1 x 10^{10} $M^{-1}Sec^{-1}$, the increasing rates of hydroxyl radical concentration can be obtained, such as 1.40 x 10^{-13}, 9.83 x 10^{-14}, 6.43 x 10^{-14}, 2.03 x 10^{-14} and 1.03 x 10^{-14} M/min, corrspondingly. Figure 4.13 shows the increase of hydroxyl radical concentration as a function of reaction time at different Fe^{2+} dosage rates. It ranges from 2.1 x 10^{-13} M to 2.8 x 10^{-12} M at the end of reaction.

All the kinetic information about the oxidation of PCE, TCE and naphthalene is summarized in Table 4.2.

Table 4.2. Kinetic data for oxidation of PCE, TCE and naphthalene by Fenton's reagent

$[H_2O_2]/[Fe^{2+}]$(M/M) *		1:1	1:0.5	1:0.25	1:0.125	1:0.0625
PCE	k_{obs} (10^{-2} min^{-2})	4.38	1.41	0.83	0.35	0.13
	a (10^{-14} M/min)	52.10	16.80	9.88	4.17	1.55
TCE	k_{obs} (10^{-2} min^{-2})	1.13	0.56	0.25	0.13	0.053
	a (10^{-14} M/min)	9.42	4.67	2.10	1.05	0.44
Naph	k_{obs} (10^{-2} min^{-2})	4.19	2.95	1.93	0.61	0.31
	a (10^{-14} M/min)	14.00	9.83	6.43	2.03	1.03

* H_2O_2 dosage rate = 1.16 x 10^{-4} M/min;
$FeSO_4$ dosage rates = 1.16, 0.578, 0.289, 0.145, 0.072 (x 10^{-4}) M/min;
corresponding to molar ratios of 1:1, 1:0.5, 1:0.25, 1:0.125, 1:0.0625 (M/M), respectively.

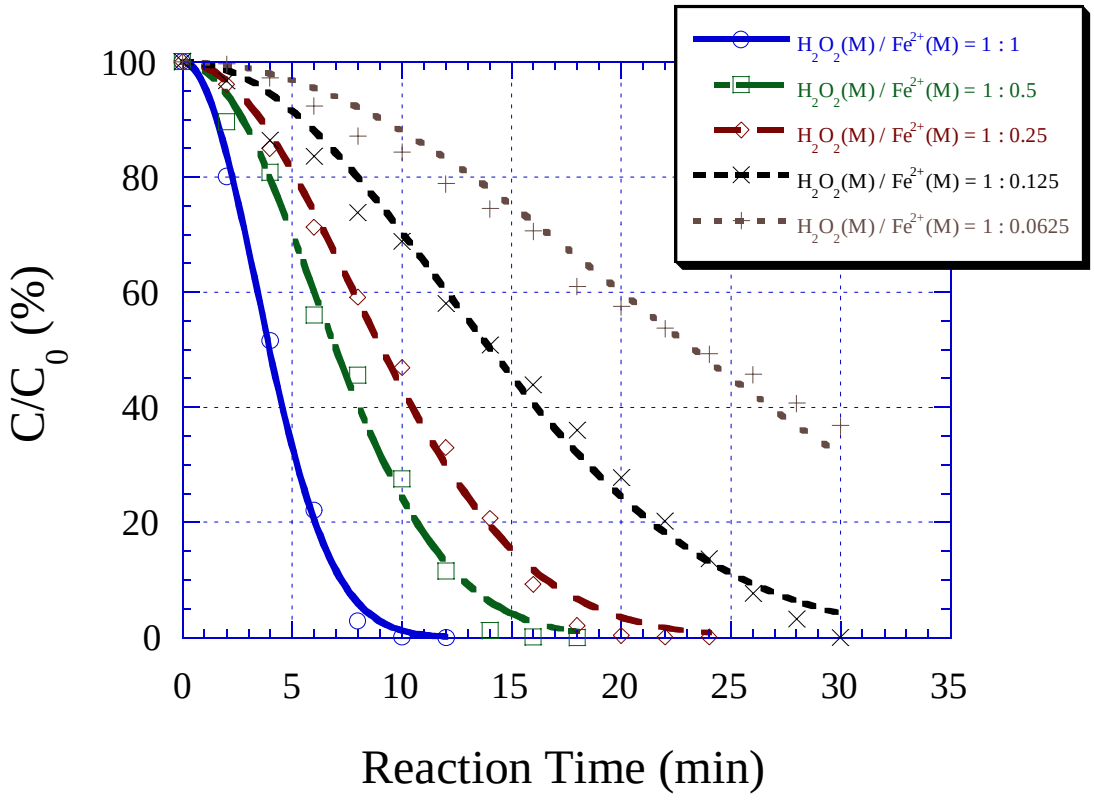

Figure 4.5. **Influence of molar ratio ($[H_2O_2]/[Fe^{2+}]$) on the decomposition of PCE by Fenton's reagent. Experimental conditions: room temperature (23.5 °C); pH = 3; ionic strength = 0.05M $NaClO_4$; H_2O_2 dosage rate = 1.16 x 10^{-4} M/min; $FeSO_4$ dosage rates = 1.16, 0.578, 0.289, 0.145, 0.072 (x 10^{-4}) M/min, corresponding to the molar ratios of 1:1, 1:0.5, 1:0.25, 1:0.125, 1:0.0625, respectively.**

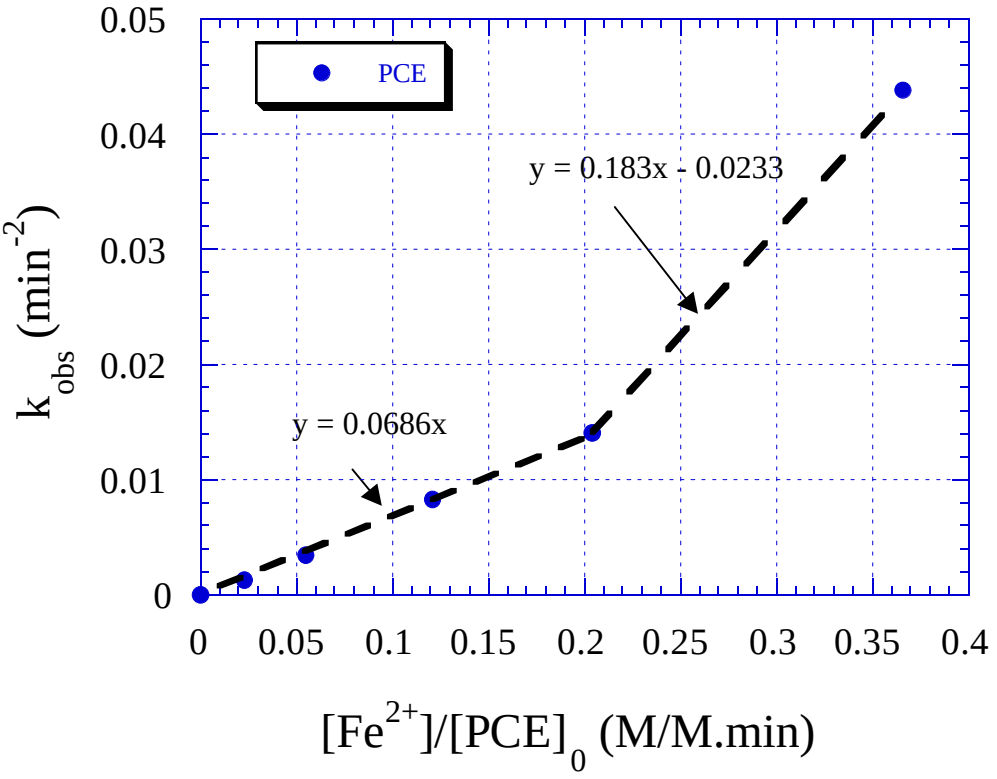

Figure 4.6. **Effect of $[Fe^{2+}]/[PCE]_0$ on the observed rate constant, k_{obs}, in the oxidation of PCE by Fenton's reagent.**

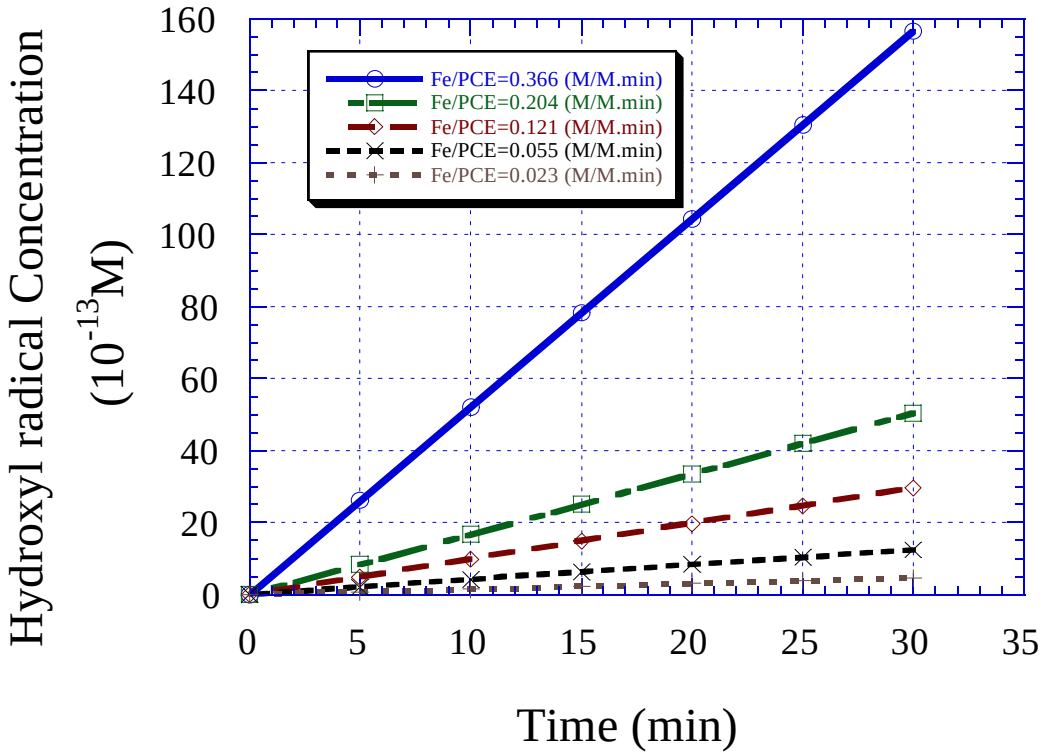

Figure 4.7. Hydrogen radical concentration as a function of reaction time in the oxidation of PCE by Fenton's reagent.

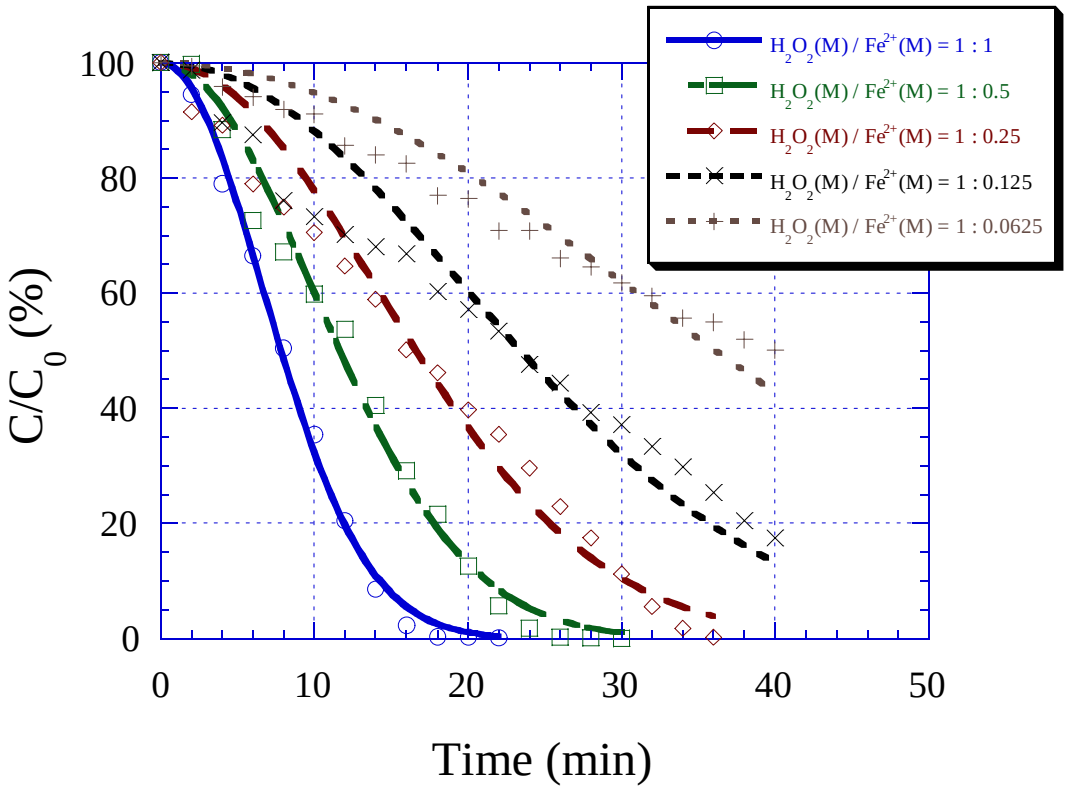

Figure 4.8. **Influence of molar ratio ($[H_2O_2]/[Fe^{2+}]$) on the decomposition of TCE by Fenton's reagent. Experimental conditions: room temperature (23.5 °C); pH = 3; ionic strength = 0.05M $NaClO_4$; H_2O_2 dosage rate = 1.16 x 10^{-4} M/min; $FeSO_4$ dosage rates = 1.16, 0.578, 0.289, 0.145, 0.072 (x 10^{-4}) M/min, corresponding to the molar ratios of 1:1, 1:0.5, 1:0.25, 1:0.125, 1:0.0625, respectively.**

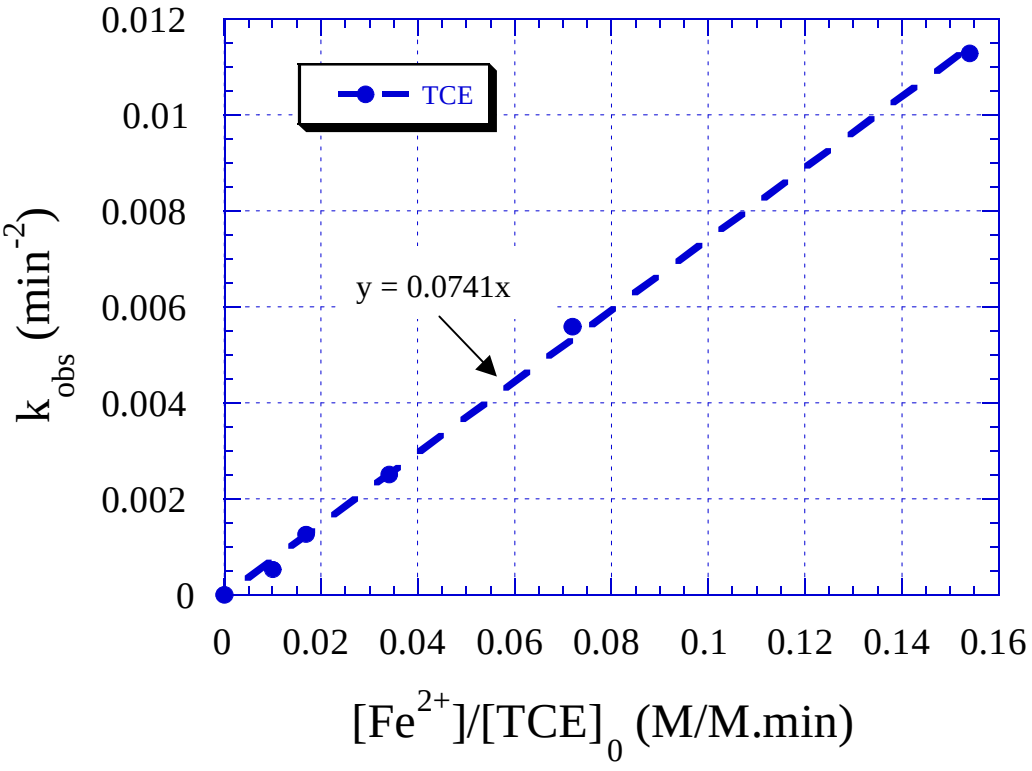

Figure 4.9. **Effect of $[Fe^{2+}]/[TCE]_0$ on the observed rate constant, k_{obs}, in the oxidation of TCE by Fenton's reagent.**

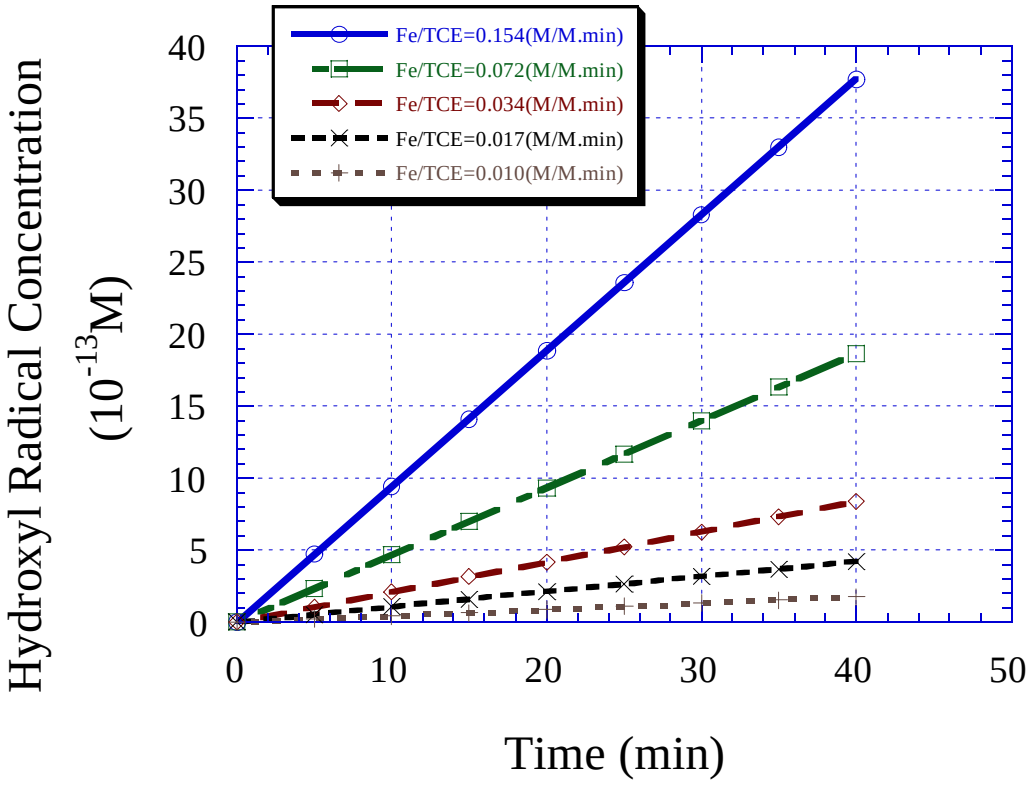

Figure 4.10. Hydrogen radical concentration as a function of reaction time in the oxidation of TCE by Fenton's reagent.

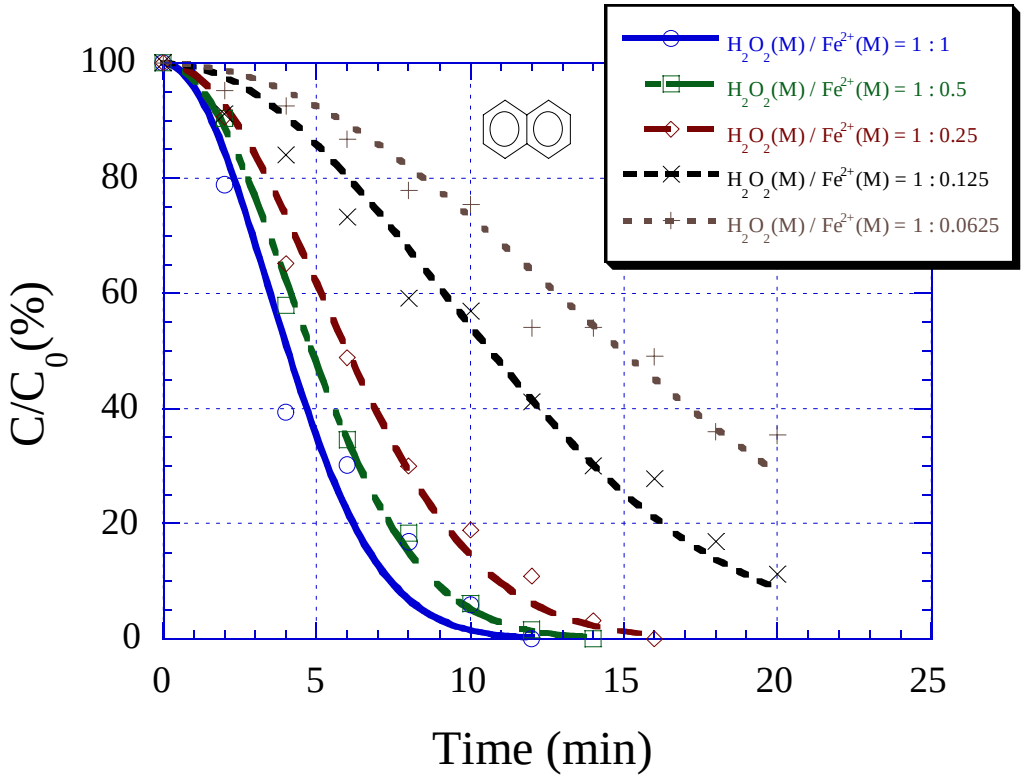

Figure 4.11. Influence of molar ratio ($[H_2O_2]/[Fe^{2+}]$) on the decomposition of naphthalene by Fenton's reagent. Experimental conditions: room temperature (23.5 ^{o}C); pH = 3; ionic strength = 0.05M $NaClO_4$; H_2O_2 dosage rate = 1.16 x 10^{-4} M/min; $FeSO_4$ dosage rates = 1.16, 0.578, 0.289, 0.145, 0.072 (x 10^{-4}) M/min, corresponding to the molar ratios of 1:1, 1:0.5, 1:0.25, 1:0.125, 1:0.0625, respectively.

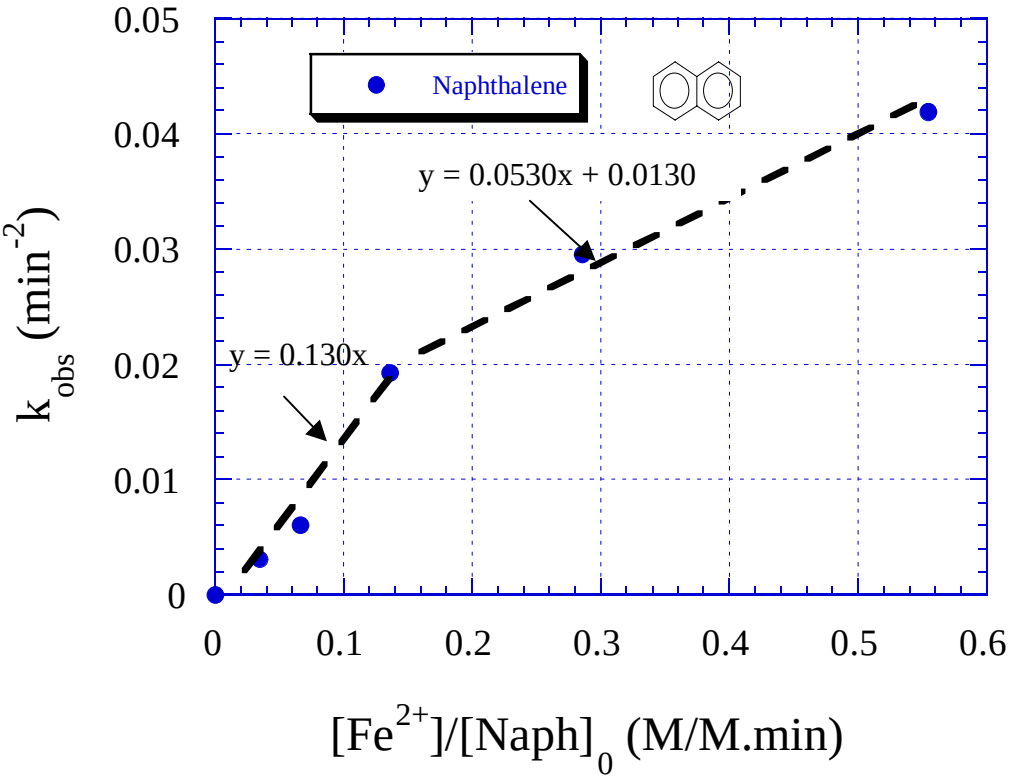

Figure 4.12. Effect of $[Fe^{2+}]/[Naph]_0$ on the observed rate constant, k_{obs}, in the oxidation of naphthalene by Fenton's reagent.

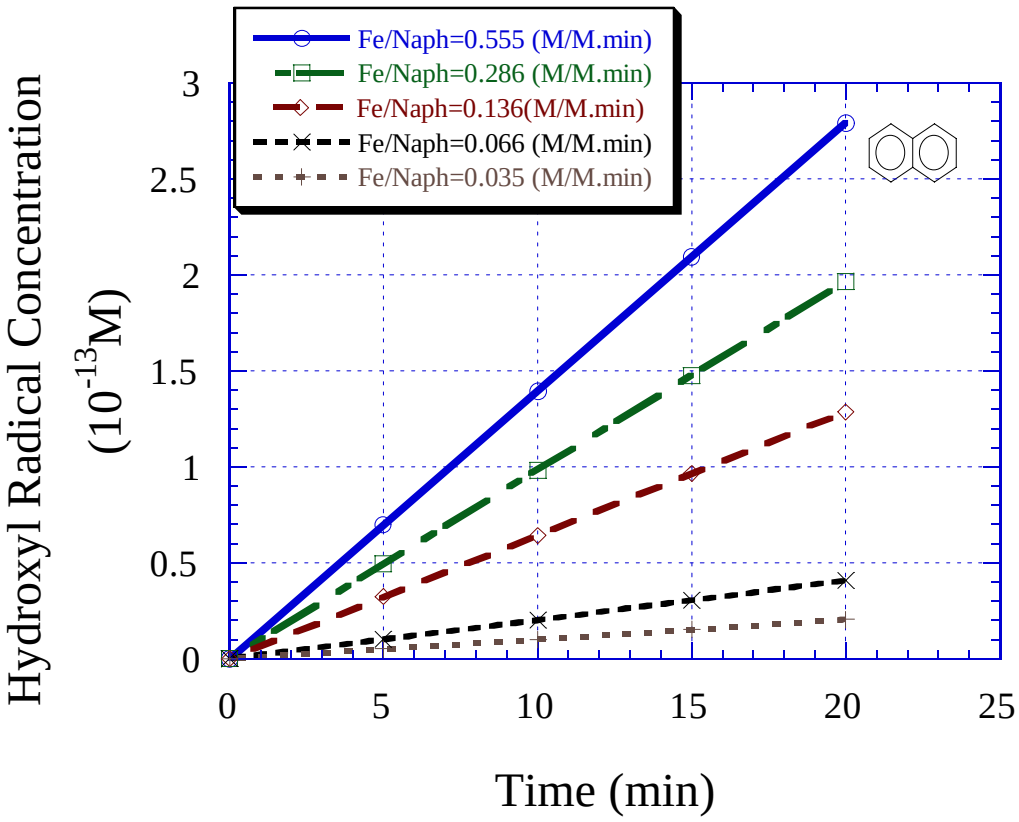

Figure 4.13. Hydrogen radical concentration as a function of reaction time in the oxidation of naphthalene by Fenton's reagent.

IV.3.3. Kinetic Modeling of Oxidation of Selected PAHs

As described above, the majority of PAHs degradation experiments by advanced chemical oxidation were carried out in organic solvent or in the mixture of water and organic solvent. However, the influence of organic solvent on the oxidation efficiency of target compound has not been clarified. Moreover, all PAHs are extremely hydrophobic compounds. In subsurface, they prefer to partition onto soil surfaces rather than dissolve in soil moisture or groundwater. This renders the soil and groundwater remediation for these compounds more difficult. As a consequence, cosolvents or surfactants have quite often been used to help desorption of PAHs from soil surfaces. Methanol is a typical cosolvent most frequently used for enhancing the washout of hydrophobic compounds in subsurface. However, the presence of methanol may seriously inhibit the further removal of organic contaminants in the water/methanol mixture. Experiments were carried out on the oxidation of selected PAHs either in the presence or in the absence of methanol (0.1% volume fraction).

Fluorene. The oxidation of fluorene at different dosage molar ratios ($[H_2O_2]/[Fe^{2+}]$) in the presence of methanol is shown in Figure 4.14. Hydrogen peroxide dosage rate was constant (1.32×10^{-4} M/min), and ferrous ion dosage rate varied as 1.32, 0.66, 0.33, 0.165, 0.083 ($\times 10^{-4}$) M/min, corresponding to the molar ratios of 1:1, 1:0.5, 1:0.25, 1:0.125, 1:0.0625, respectively. Results indicate that the ferrous ion dosage has little effect on the oxidation efficiency of fluorene. At the end of reaction (1 hour), the residue relative concentrations of fluorene are all in the range of 66 ~ 74%, though Fe^{2+} dosage changes by 16 times. Increasing dosage does not necessarily increase the oxidation efficiency. The optimal $[H_2O_2]/[Fe^{2+}]$ molar ratio is 1:0.125. Figure 4.15 shows the oxidation of fluorene at increasing hydrogen peroxide dosage rate, while ferrous ion dosage rate is kept constant (0.66×10^{-4} M/min). The removal efficiency is considerably improved with increasing hydrogen peroxide dosage. The minimum residue relative concentration is around 25% at the end of reaction. However, similar as in Figure 4.14, the removal efficiency decreases when the $[H_2O_2]/[Fe^{2+}]$ molar ratio exceeds the optimal value, 1:0.125. Therefore, in order to notably improve the removal efficiency of flurene in the presence of methanol, the only feasible way is to increase both dosages of hydrogen peroxide and ferrous ion simultaneously when the molar ratio is kept at the optimal value. Figure 4.16 shows that at the $[H_2O_2]/[Fe^{2+}]$ fixed optimal molar ratio (1:0.125), Fenton's reagent dosage exerts a significant effect on the oxidation efficiency of fluorene. When the dosage of hydrogen peroxide is increased to 1.06×10^{-3} M/min, all fluorene is decomposed. The oxidation of

fluorene without methanol interference was also investigated, as shown in Figure 4.17. Results indicate that fluorene can actually be oxidized very fast even at a low dosage rate of Fenton's reagent. All fluorene is gone at a reaction time of 6 minutes. Thus, it is obvious that the inhibition of methanol on the oxidation of fluorene is very significant. Walling *et al.* (1970) investigated the oxidation of alcohols (methyl, ethyl, isopropyl alcohols) by Fenton's reagent, and found that all of them could be oxidized by hydroxyl radical. He reported that the rate constant of methanol was ~1.29 x 10^9 $M^{-1}Sec^{-1}$, and the major products detected included HCHO (81%) and HCOOH (< 0.5%). Though the reactivity of methanol is not so high as that of fluorene (~10^{10} $M^{-1}Sec^{-1}$), methanol captures most of hydroxyl radials due to its high concentration. In our experiments, the initial concentration of methanol is 790ppm, which equals 24.7 mM. The water solubility of fluorene is only 1.84 ppm, which is equivalent to 11.1 μM. The concentration ratio of methanol to fluorene is as high as about 2500. Therefore, there is no doubt that methanol rather than fluorene captures most of hydroxyl radicals.

The oxidation of fluorene in the presence of methanol is very complicated. Many species compete for hydroxyl radical. Besides methanol, fluorene, hydrogen peroxide and ferrous ion, the intermediates and by-products of methanol, e.g., HCHO, can also react with hydroxyl radical. Unlike the relatively simple reaction systems as mentioned above in the oxidation of PCE, TCE and naphthalene, experiment data from this complicated system can not be fitted well by the proposed kinetic model. From the decreasing rate of fluorene decomposition, the concentration of hydroxyl radical actually decreases with reaction time. It is assumed that the major intermediate of methanol, HCHO, may react with hydroxyl radical more rapidly than the parent compound. Thus, the decrease of hydroxyl radical concentration retards the decomposition of fluorene. In the absence of methanol, the decomposition curve of fluorene has the similar shape as those of PCE, TCE and naphthalene. Experiment data can be fitted quite well by equation 4.18, as shown in Figure 4.17. The values of k_{obs} are 1.46 x 10^{-1} and 5.7 x 10^{-2} min^{-2} at different Fe^{2+} dosage rates, i.e., 0.66 x 10^{-4} and 0.33 x 10^{-4} M/min, respectively. Also, the increasing rate of hydroxyl radical can be calculated using equation 4.19, as 4.87 x $10^{-13}$and 1.90 x 10^{-13} M/min.

Phenanthrene. Figure 4.18 shows the influence of molar ratios ($[H_2O_2]/[Fe^{2+}]$) of Fenton's reagent on the oxidation of phenanthrene in the presence of methanol. Same experimental conditions were employed as those in the oxidation of fluorene. Results indicate again that the ferrous ion dosage has little effect on the oxidation efficiency. When Fe^{2+} dosage changes by 16 times, the final relative concentrations of phenanthrene remained in the reaction solution are within the range of 54 ~ 61%. It appears that the optimal $[H_2O_2]/[Fe^{2+}]$ molar ratio

is 1:0.25 or 1:0.125. Actually, the difference of oxidation efficiency is negligible. Figure 4.19 shows that at the fixed optimal molar ratio (1:0.25), the oxidation efficiency of phenanthrene significantly increases with increasing dosage of Fenton's reagent. After one hour reaction, 85% of phenanthrene was oxidized at the highest hydrogen peroxide dosage rate. The oxidation of phenanthrene in the absence of methanol is shown in Figure 4.20. Results indicate that all phenanthrene can be removed within 3~5 minutes of reaction time. The water solubility of phenanthrene is 6.1 μM, and the concentration ratio of methanol to phenanthrene is as high as about 4000. The inhibition of methanol is more serious on phenanthrene than fluorene due to a bigger methanol "concentration effect". The model fitting produces the values of k_{obs}, such as 7.85 x 10^{-1}, 5.24 x 10^{-1} and 1.50 x 10^{-1} min^{-2} at different Fe^{2+} dosage rates of 0.66, 0.33, 0.165 (x 10^{-4}) M/min, respectively. The corresponding *a* values are 2.62 x 10^{-12}, 1.75 x 10^{-12} and 5.0 x 10^{-13} M/min.

Fluoranthene. Figures 4.21 and 4.22 show the oxidation of fluoranthene at different $[H_2O_2]/[Fe^{2+}]$ molar ratios and at the fixed optimal molar ratio (1:0.125) in the presence of methanol, respectively. Since fluoranthene only has a water solubility of 1.2 μM, ferrous ion dosage exerts some effect on the oxidation efficiency. This means that the oxidation efficiency is not only controlled by $[H_2O_2]/[Fe^{2+}]$, but also significantly influenced by $[H_2O_2]/[RH]_0$ or $[Fe^{2+}]/[RH]_0$. The optimal $[H_2O_2]/[Fe^{2+}]$ molar ratio is 1:0.125, same as found in the oxidation of flurene and phenanthrene. Results in Figure 4.22 indicate that fluoranthene can be oxidized efficiently by Fenton's reagent at the optimal molar ratio. A total removal was achieved in less than 20 minutes when the dosage rate of hydrogen peroxide was 1.06 x 10^{-3} M/min. The oxidation of fluoranthene in the absence of methanol is shown in Figure 4.23. All phenanthrene was removed in 3 minutes of reaction time. The values of k_{obs} obtained by model fitting are 7.64 x 10^{-1}, 6.08 x 10^{-1} and 3.28 x 10^{-1} min^{-2}, corresponding to of 0.33, 0.165, 0.083 (x 10^{-4}) M/min of Fe^{2+} dosage rates, respectively. The corresponding *a* values are 2.55 x 10^{-12}, 2.03 x 10^{-12} and 1.09 x 10^{-12} M/min.

Pyrene. The oxidation of pyrene at different $[H_2O_2]/[Fe^{2+}]$ molar ratios and at the fixed optimal molar ratio (1:0.5) in the presence of methanol are shown in Figures 4.24 and 4.25, respectively. Pyrene has a water solubility of 0.67 μM. Ferrous ion dosage also exerts some effect on the oxidation efficiency of pyrene, as in the case of fluoranthene oxidation. The optimal $[H_2O_2]/[Fe^{2+}]$ molar ratio is 1:0.5, as shown in Figure 4.24. Results in Figure 25 indicate that Pyrene can be totally decomposed after 20 minutes reaction at the highest hydrogen peroxide dosage. Figure 4.26 shows the oxidation of pyrene in the pure solution. All pyrene was removed in 2.5 minutes of reaction time. The values of k_{obs} are 1.80, 0.81 and 0.48 min^{-2},

corresponding to of 0.66, 0.33, 0.165 (x 10^{-4}) M/min of Fe^{2+} dosage rates, respectively. The values of *a* are 6.00 x 10^{-12}, 2.70 x 10^{-12} and 1.60 x 10^{-12} M/min, correspondingly.

Anthracene. Figure 4.27 shows the oxidation of anthracene at different $[H_2O_2]/[Fe^{2+}]$ molar ratios in the presence of methanol. The oxidation rate of anthracene increases with increasing dosage rates of ferrous ion. There is no optimal $[H_2O_2]/[Fe^{2+}]$ molar ratio. The difference of oxidation efficiency between anthracene and other PAHs studied may be ascribed to its extremely low water solubility, which is 0.33 μM at 25 °C. Anthracene has the highest ratio of $[H_2O_2]/[RH]_0$ or $[Fe^{2+}]/[RH]_0$ among all the selected PAHs, which means Fenton's reagent dosage is the most sufficient. A complete decomposition of anthracene can be rapidly achieved, even seriously inhibited by methanol. Figure 4.28 shows the oxidation of anthracene without methanol inhibition. All anthracene was removed within 2~2.5 minutes. The values of k_{obs} are 1.45 and 1.28 min^{-2}, corresponding to of 0.33, 0.165 (x 10^{-4}) M/min of Fe^{2+} dosage rates, respectively. The values of *a* are 4.83 x 10^{-12} and 4.27 x 10^{-12} M/min, correspondingly.

Table 4.3 summarizes all kinetic information about the oxidation of selected PAHs by Fenton's reagent in the absence of methanol.

Table 4.3. Kinetic data for oxidation of selected PAHs by Fenton's reagent in the absence of methanol

$[H_2O_2]/[Fe^{2+}]$(M/M)*		1:0.5	1:0.25	1:0.125	1:0.0625
Fluorene	k_{obs} (10^{-1} min^{-2})	1.46	0.57	-	-
	a (10^{-12} M/min)	0.49	0.19	-	-
Phenanthrene	k_{obs} (10^{-1} min^{-2})	7.85	5.24	1.50	-
	a (10^{-12} M/min)	2.62	1.75	0.50	-
Fluoranthene	k_{obs} (10^{-1} min^{-2})	-	7.64	6.08	3.28
	a (10^{-12} M/min)	-	2.55	2.03	1.09
Pyrene	k_{obs} (10^{-1} min^{-2})	18.00	8.10	4.80	-
	a (10^{-12} M/min)	6.00	2.70	1.60	-
Anthracene	k_{obs} (10^{-1} min^{-2})	-	14.50	12.80	-
	a (10^{-12} M/min)	-	4.83	4.27	-

* H_2O_2 dosage rate = 1.32 x 10^{-4} M/min;
$FeSO_4$ dosage rates = 1.32, 0.66, 0.33, 0.165, 0.083 (x 10^{-4}) M/min;
corresponding to molar ratios of 1:1, 1:0.5, 1:0.25, 1:0.125, 1:0.0625 (M/M), respectively.

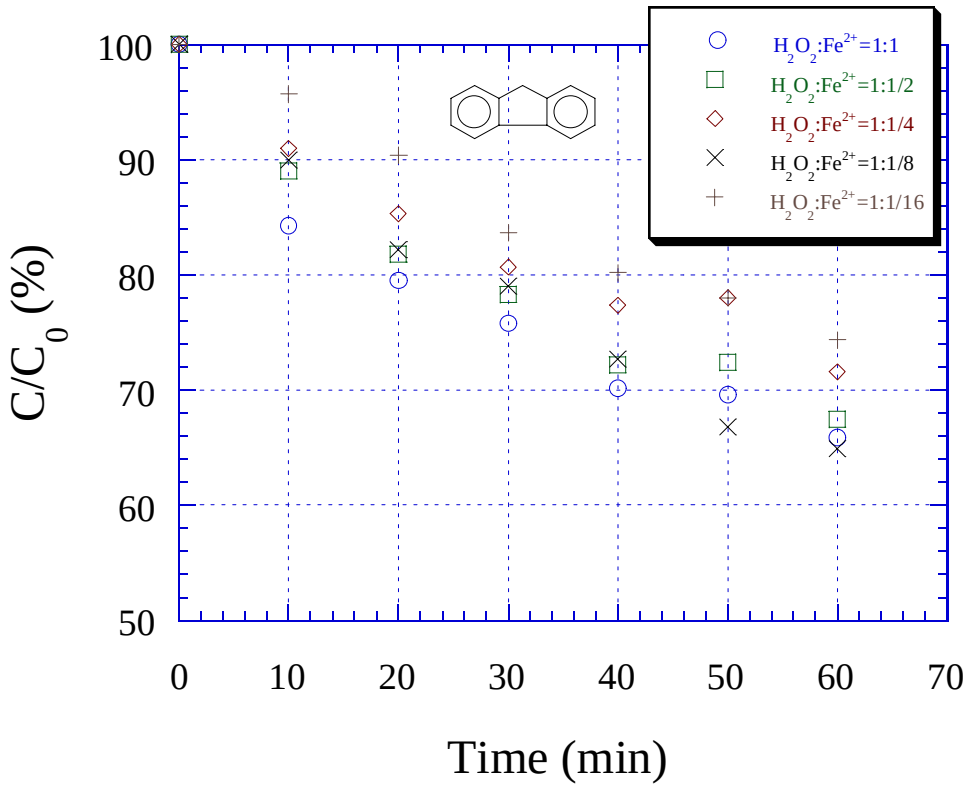

Figure 4.14. Influence of molar ratio ($[H_2O_2]/[Fe^{2+}]$) on the decomposition of fluorene by Fenton's reagent. Experimental conditions: [methanol] = 0.1% (v/v); room temperature (23.5 °C); pH = 3; ionic strength = 0.05M $NaClO_4$; H_2O_2 dosage rate = 1.32 x 10^{-4} M/min; $FeSO_4$ dosage rates = 1.32, 0.66, 0.33, 0.165, 0.083 (x 10^{-4}) M/min, corresponding to the molar ratios of 1:1, 1:0.5, 1:0.25, 1:0.125, 1:0.0625, respectively.

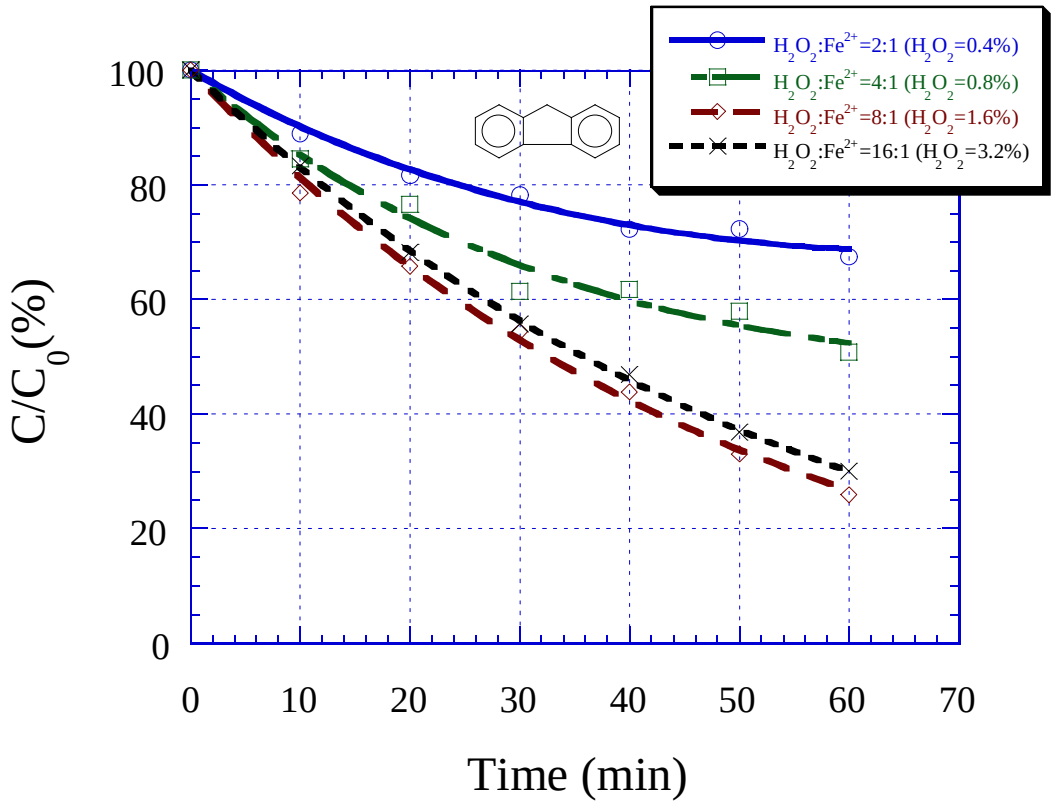

Figure 4.15. Influence of molar ratio ($[H_2O_2]/[Fe^{2+}]$) on the decomposition of fluorene by Fenton's reagent. Experimental conditions: [methanol] = 0.1% (v/v); room temperature (23.5 °C); pH = 3; ionic strength = 0.05M $NaClO_4$; $FeSO_4$ dosage rate = 0.66 x 10^{-4} M/min; H_2O_2 dosage rates = 1.32, 2.64, 5.28, 10.56 (x 10^{-4}) M/min, corresponding to the molar ratios of 2:1, 4:1, 8:1, 16:1, respectively.

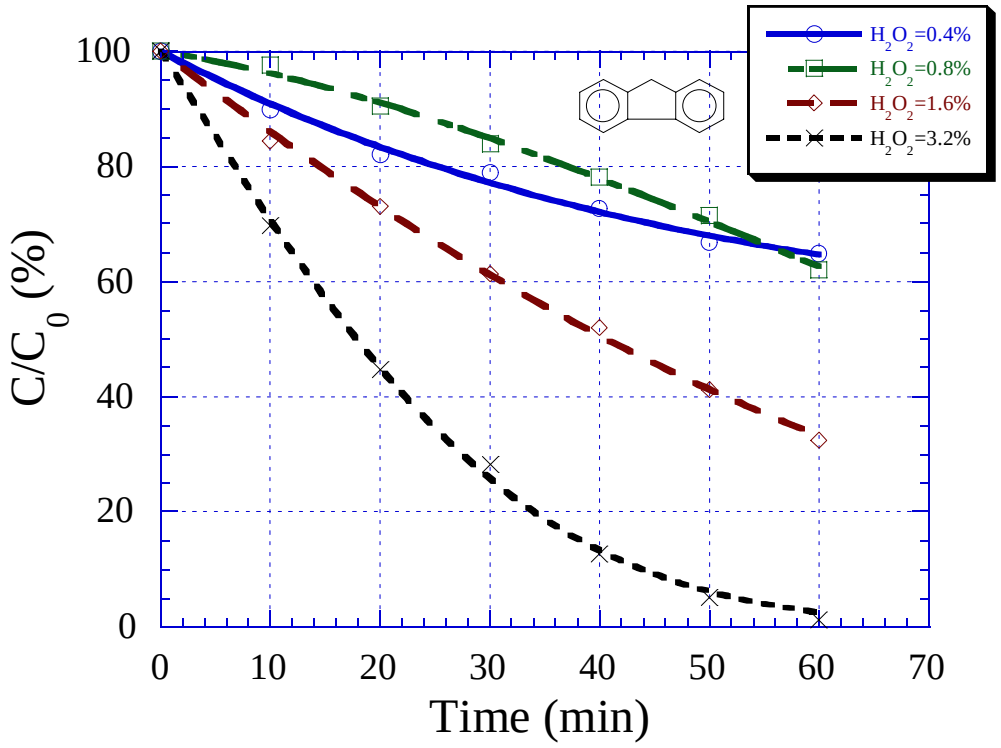

Figure 4.16. Influence of chemical dosage on the decomposition of fluorene by Fenton's reagent. Experimental conditions: [methanol] = 0.1% (v/v); room temperature (23.5 °C); pH = 3; ionic strength = 0.05M $NaClO_4$; fixed molar ratio ($[H_2O_2]/[Fe^{2+}]$) = 1:0.125.

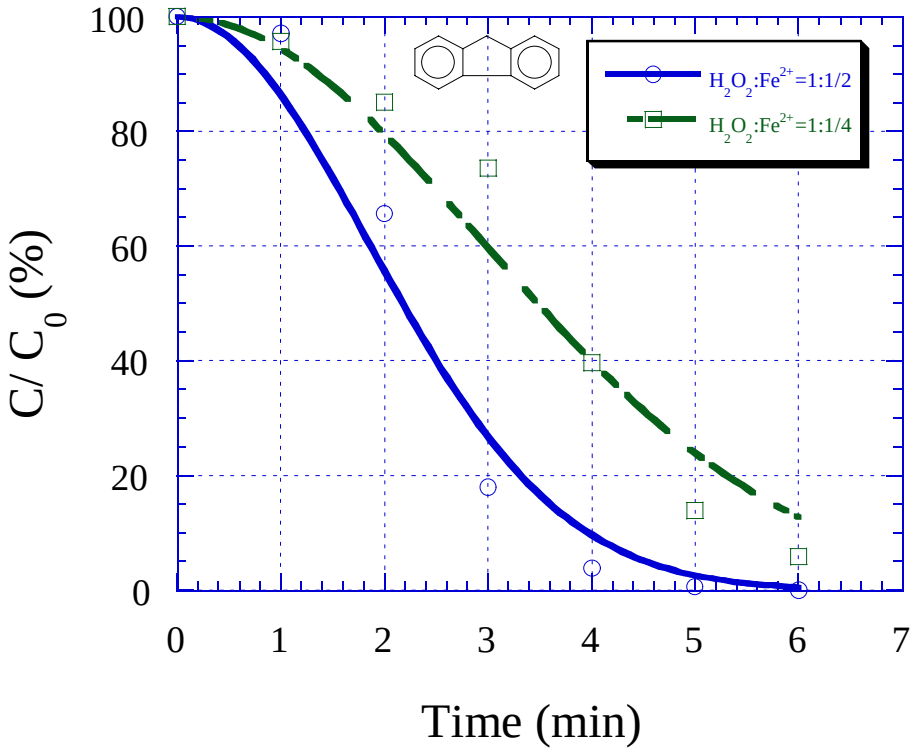

Figure 4.17. **Influence of molar ratio ($[H_2O_2]/[Fe^{2+}]$) on the decomposition of fluorene by Fenton's reagent. Experimental conditions: pure solution (no methanol); room temperature (23.5 ^{o}C); pH = 3; ionic strength = 0.05M $NaClO_4$; H_2O_2 dosage rate = 1.32 x 10^{-4} M/min; $FeSO_4$ dosage rates = 0.66, 0.33 (x 10^{-4}) M/min, corresponding to the molar ratios of 1:0.5 and 1:0.25, respectively.**

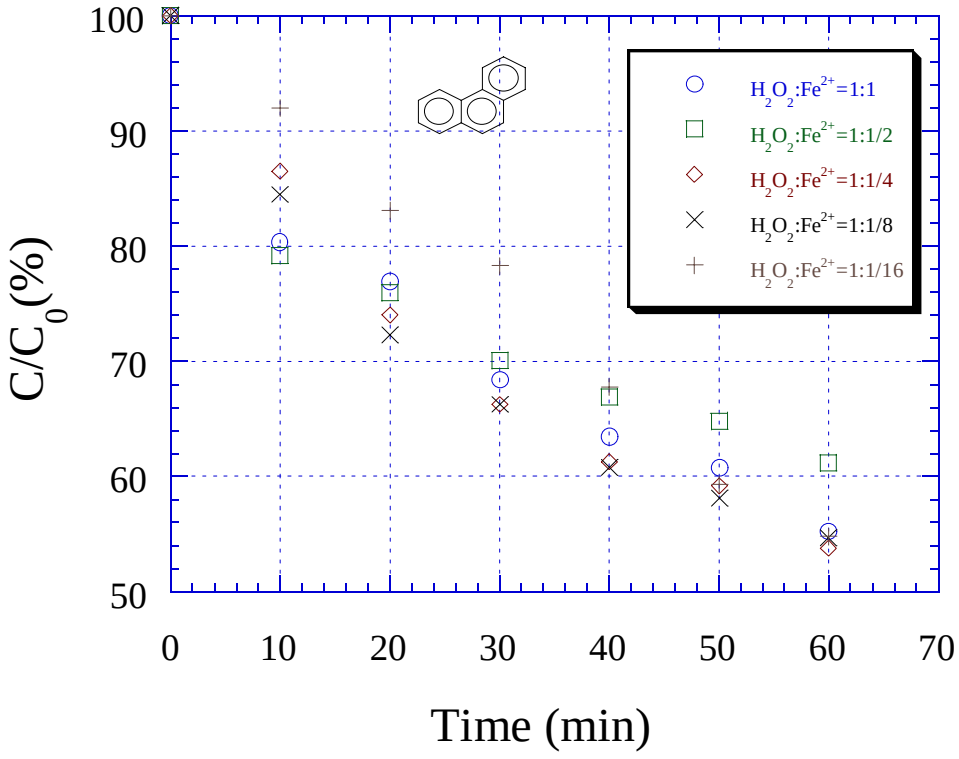

Figure 4.18. Influence of molar ratio ($[H_2O_2]/[Fe^{2+}]$) on the decomposition of phenanthrene by Fenton's reagent. Experimental conditions: [methanol] = 0.1% (v/v); room temperature (23.5 ^{o}C); pH = 3; ionic strength = 0.05M $NaClO_4$; H_2O_2 dosage rate = 1.32 x 10^{-4} M/min; $FeSO_4$ dosage rates = 1.32, 0.66, 0.33, 0.165, 0.083 (x 10^{-4}) M/min, corresponding to the molar ratios of 1:1, 1:0.5, 1:0.25, 1:0.125, 1:0.0625, respectively.

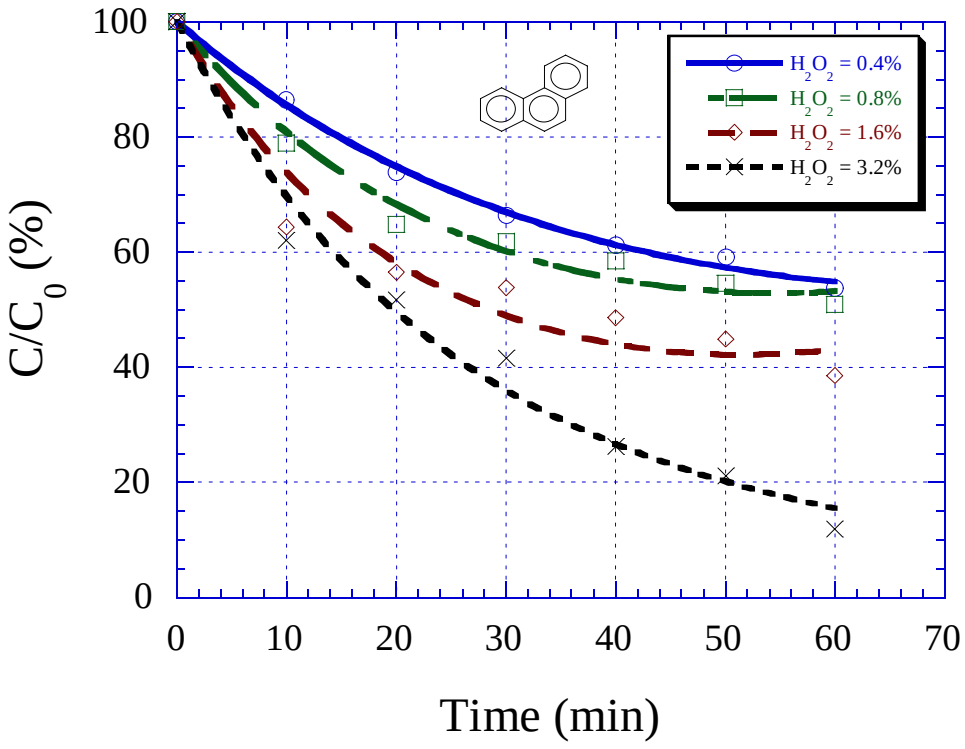

Figure 4.19. Influence of chemical dosage on the decomposition of phenanthrene by Fenton's reagent. Experimental conditions: [methanol] = 0.1% (v/v); room temperature (23.5 °C); pH = 3; ionic strength = 0.05M $NaClO_4$; fixed molar ratio ($[H_2O_2]/[Fe^{2+}]$) = 1:0.25.

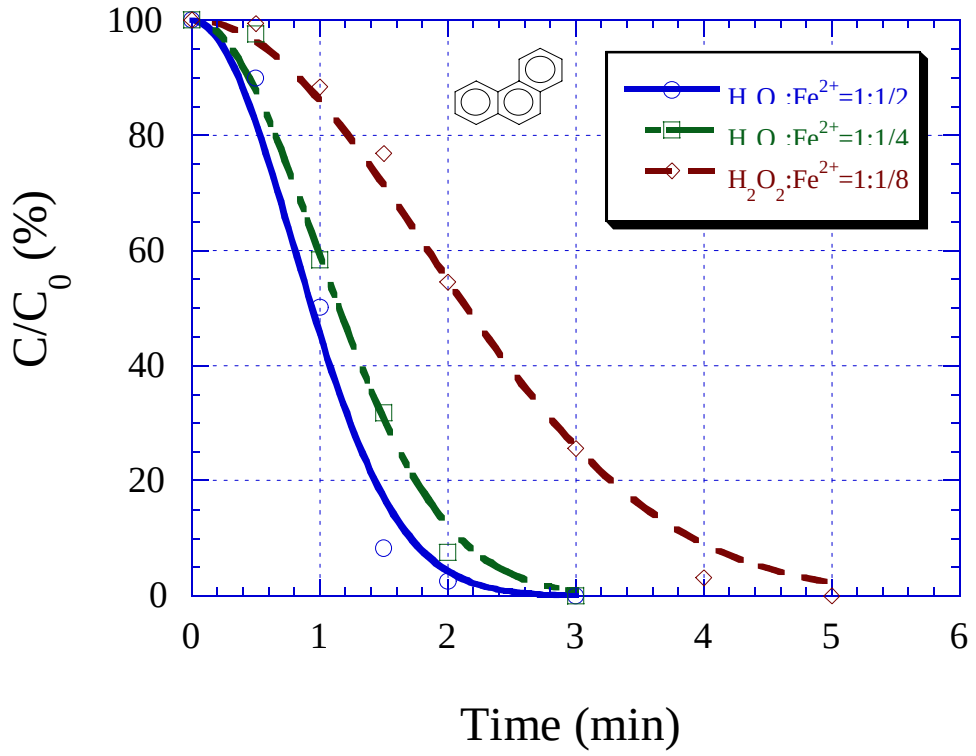

Figure 4.20. **Influence of molar ratio ($[H_2O_2]/[Fe^{2+}]$) on the decomposition of phenanthrene by Fenton's reagent. Experimental conditions: pure solution (no methanol); room temperature (23.5 °C); pH = 3; ionic strength = 0.05M $NaClO_4$; H_2O_2 dosage rate = 1.32 x 10^{-4} M/min; $FeSO_4$ dosage rates = 0.66, 0.33 (x 10^{-4}) M/min, corresponding to the molar ratios of 1:0.5, 1:0.25 and 1:0.125, respectively.**

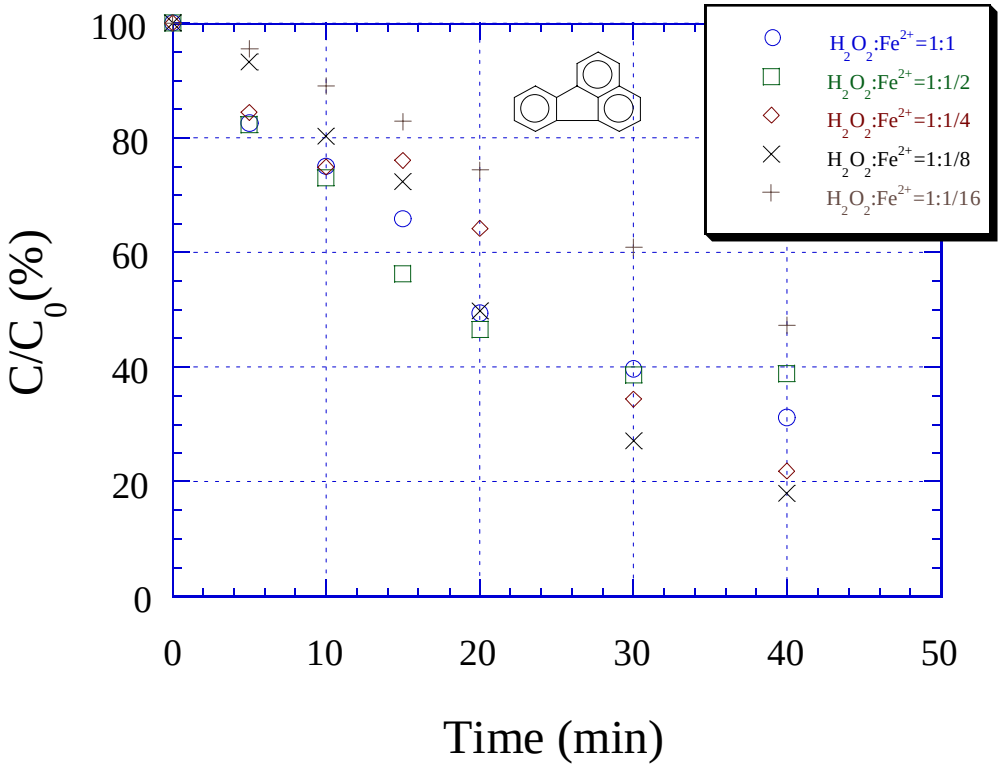

Figure 4.21. Influence of molar ratio ($[H_2O_2]/[Fe^{2+}]$) on the decomposition of fluoranthene by Fenton's reagent. Experimental conditions: [methanol] = 0.1% (v/v); room temperature (23.5 °C); pH = 3; ionic strength = 0.05M $NaClO_4$; H_2O_2 dosage rate = 1.32 x 10^{-4} M/min; $FeSO_4$ dosage rates = 1.32, 0.66, 0.33, 0.165, 0.083 (x 10^{-4}) M/min, corresponding to the molar ratios of 1:1, 1:0.5, 1:0.25, 1:0.125, 1:0.0625, respectively.

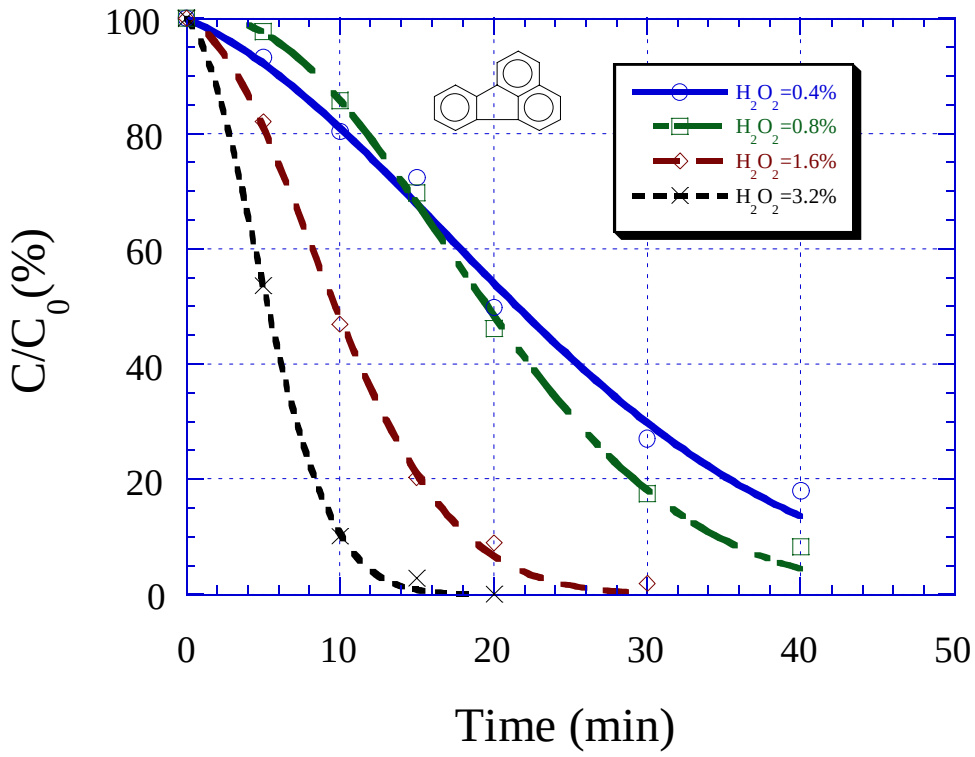

Figure 4.22. Influence of chemical dosage on the decomposition of fluoranthene by Fenton's reagent. Experimental conditions: [methanol] = 0.1% (v/v); room temperature (23.5 °C); pH = 3; ionic strength = 0.05M $NaClO_4$; fixed molar ratio ($[H_2O_2]/[Fe^{2+}]$) = 1:0.125.

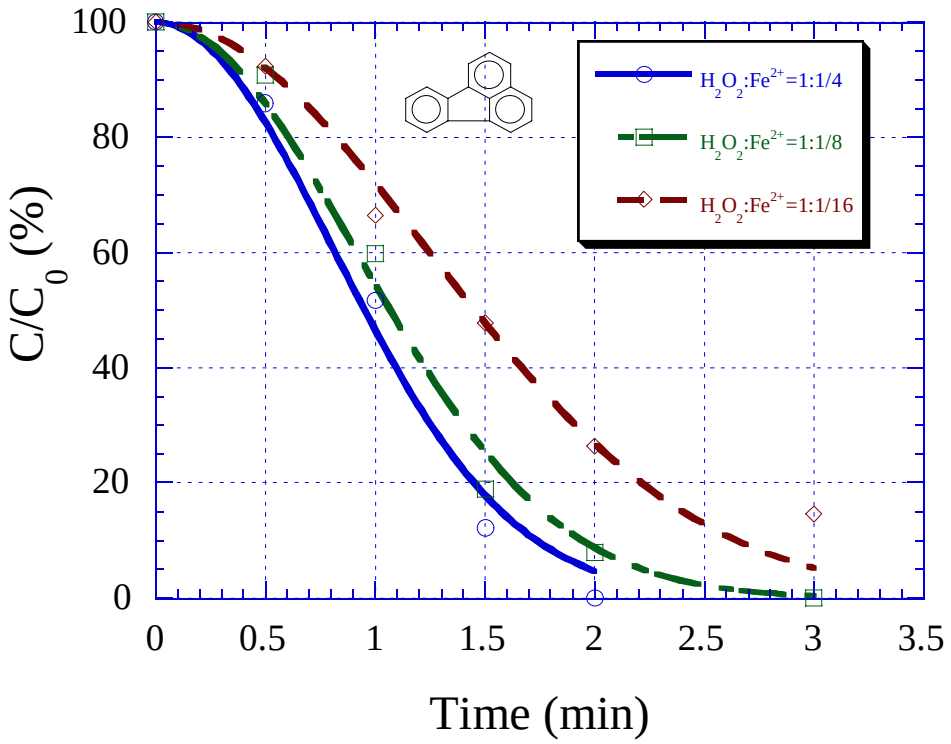

Figure 4.23. **Influence of molar ratio ($[H_2O_2]/[Fe^{2+}]$) on the decomposition of fluoranthene by Fenton's reagent. Experimental conditions: pure solution (no methanol); room temperature (23.5 °C); pH = 3; ionic strength = 0.05M $NaClO_4$; H_2O_2 dosage rate = 1.32 x 10^{-4} M/min; $FeSO_4$ dosage rates = 0.66, 0.33, 0.165 (x 10^{-4}) M/min, corresponding to the molar ratios of 1:0.25, 1:0.125 and 1:0.0625, respectively.**

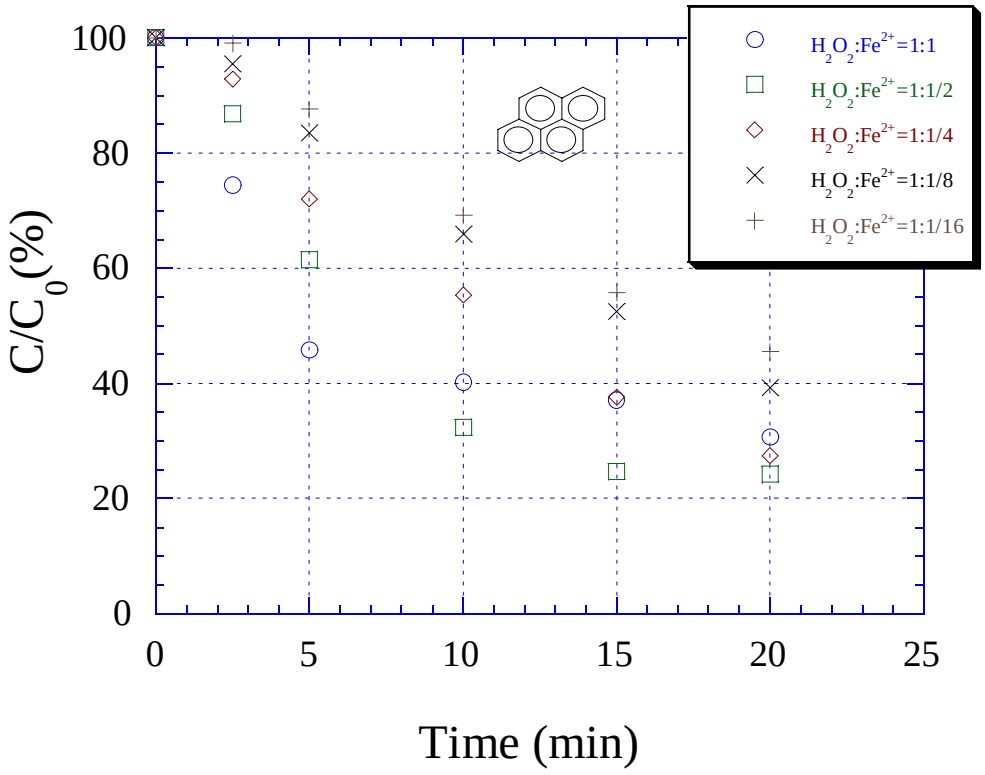

Figure 4.24. **Influence of molar ratio ($[H_2O_2]/[Fe^{2+}]$) on the decomposition of pyrene by Fenton's reagent. Experimental conditions: [methanol] = 0.1% (v/v); room temperature (23.5 ^{o}C); pH = 3; ionic strength = 0.05M $NaClO_4$; H_2O_2 dosage rate = 1.32 x 10^{-4} M/min; $FeSO_4$ dosage rates = 1.32, 0.66, 0.33, 0.165, 0.083 (x 10^{-4}) M/min, corresponding to the molar ratios of 1:1, 1:0.5, 1:0.25, 1:0.125, 1:0.0625, respectively.**

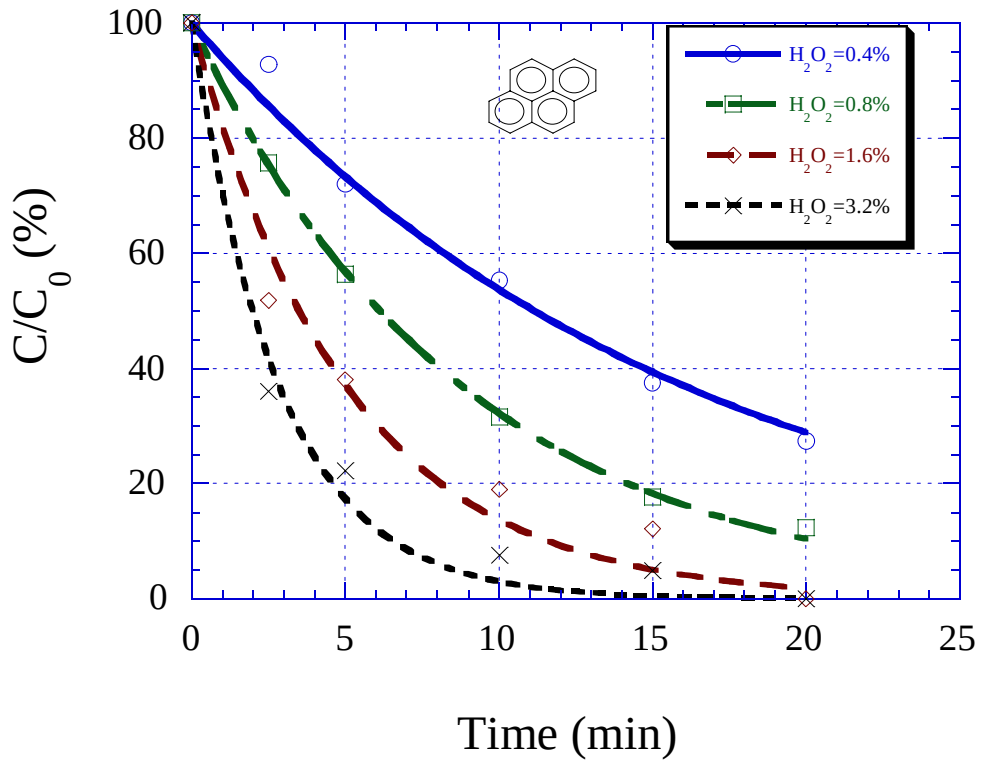

Figure 4.25. Influence of chemical dosage on the decomposition of pyrene by Fenton's reagent. Experimental conditions: [methanol] = 0.1% (v/v); room temperature (23.5 °C); pH = 3; ionic strength = 0.05M $NaClO_4$; fixed molar ratio ($[H_2O_2]/[Fe^{2+}]$) = 1:0.25.

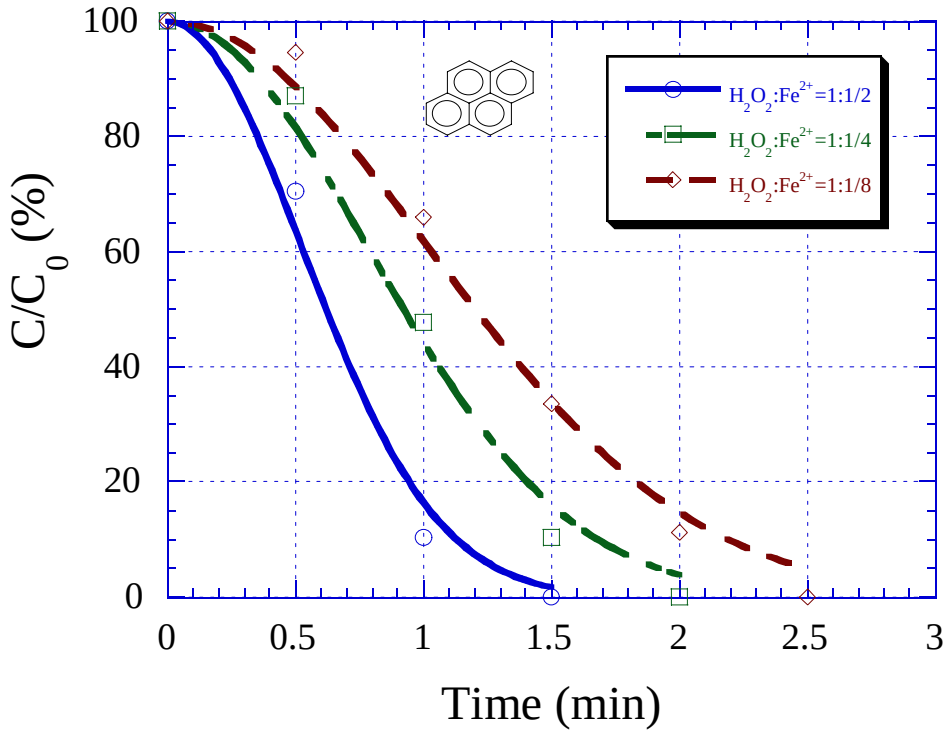

Figure 4.26. **Influence of molar ratio ($[H_2O_2]/[Fe^{2+}]$) on the decomposition of pyrene by Fenton's reagent. Experimental conditions: pure solution (no methanol); room temperature (23.5 °C); pH = 3; ionic strength = 0.05M $NaClO_4$; H_2O_2 dosage rate = 1.32 x 10^{-4} M/min; $FeSO_4$ dosage rates = 0.66, 0.33, 0.165 (x 10^{-4}) M/min, corresponding to the molar ratios of 1:0.25, 1:0.125 and 1:0.0625, respectively.**

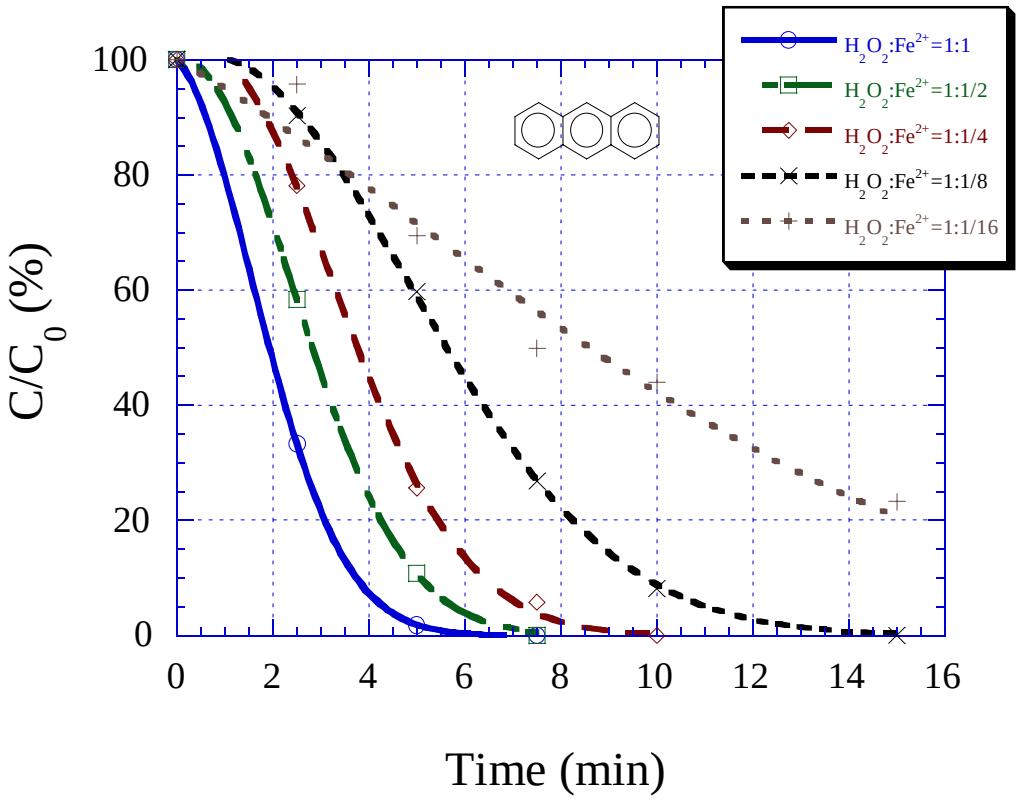

Figure 4.27. Influence of molar ratio ($[H_2O_2]/[Fe^{2+}]$) on the decomposition of anthracene by Fenton's reagent. Experimental conditions: [methanol] = 0.1% (v/v); room temperature (23.5 °C); pH = 3; ionic strength = 0.05M $NaClO_4$; H_2O_2 dosage rate = 1.32 x 10^{-4} M/min; $FeSO_4$ dosage rates = 1.32, 0.66, 0.33, 0.165, 0.083 (x 10^{-4}) M/min, corresponding to the molar ratios of 1:1, 1:0.5, 1:0.25, 1:0.125, 1:0.0625, respectively.

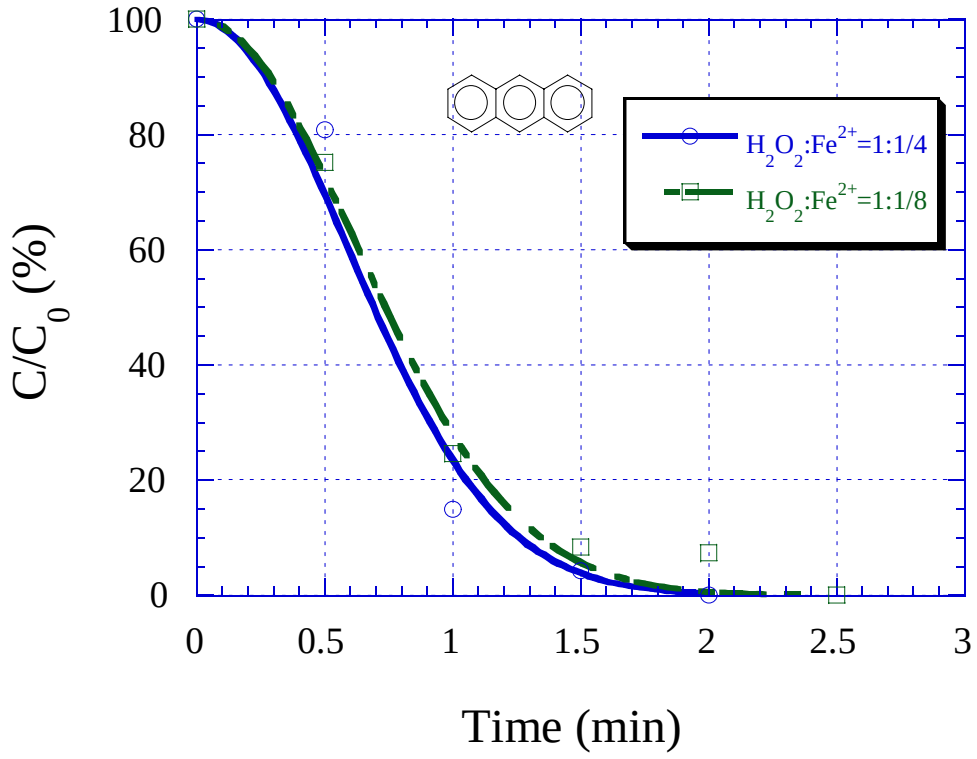

Figure 4.28. **Influence of molar ratio ($[H_2O_2]/[Fe^{2+}]$) on the decomposition of anthracene by Fenton's reagent. Experimental conditions: pure solution (no methanol); room temperature (23.5 °C); pH = 3; ionic strength = 0.05M $NaClO_4$; H_2O_2 dosage rate = 1.32 x 10^{-4} M/min; $FeSO_4$ dosage rates = 0.33, 0.165 (x 10^{-4}) M/min, corresponding to the molar ratios of 1:0.25 and 1:0.125, respectively.**

V. REFERENCES

1. Acar, Y. B., Hamed, J., Gale, R. J. and Putnam, G. (1991). Acid/Base Distribution in Electro-osmosis Transportation Research Record, Soils Geology and Foundations, Geotechnical Engineering, No. 1288, 23-34.
2. ATSDR Biannual Report to Congress: October 17, 1986 ~ September 30, 1988. Agency for Toxic Substances and Disease Registry, U. S. Public Health Service, Atlanta, GA, 1989.
3. Bailey, P. S., Kolsaker P., shiha, B., Ashton, J. B. Dobinson, F., Batterbee, J. E. (1964). Competing Reactions in the Ozonation of Anthracene, J. Org. Chem., 29, 1400.
4. Brideg, J. E. and Strestly, G. C. (1984). Decontamination of Hazardous Waste from Spills and Uncontrolled Waste Site by Radio Frequency In-Situ Heating, Proceedings, Hazardous Material Spills Conference, 9-65.
5. Brusseau, M. L., R. E. Jessup, and P. C. Rao (1991). Nonequilibrium Sorption of Organic Chemicals: Elucidation of Rate-Limiting Processes, Environmental Science and Technology, Vol. 25, No. 1, 134-142.
6. Brusseau, Mark, L., A. L. Wood, P. C. Rao (1991). Influence of Organic Cosolvents on the Sorption Kinetics of Hydrophobic Organic Chemicals, Environmental Science and Technology, Vol. 25, No. 5, 903-910.
7. Burgos, W. D., J. T. Novak, and D. F. Berry (1996). Reversible Sorption and Irreversible Binding of Naphthalene and α-Naphthol to Soil: Elucidation of Processes, Environmental Science and Technology, Vol. 30, No. 4, 1205-1211.
8. Burgreen, D. and F. R. Nakache (1964). Electrokinetic Flow in Ultrafine Capillary Slits, The Journal of Physical Chemistry, Vol. 68, No. 5, 1084-1091.
9. Burns, W. G. and Marsh, W. R. (1981). J. Chem. Soc. Farady Trans. 1, Vol. 77, 197-215.
10. Carmichael, L. M., R. F. Christman, F. Russell, and F. K. Pfaender (1997). Desorption and Mineralization Kinetics of Phenanthrene and Chrysene in Contaminated Soils, Environmental Science and Technology, Vol. 31, No. 1, 126-132.
11. Carroll, Kenneth M., M. R. Harkness, A. A. Bracco, and R. R. Balcarcel (1994). Application of A Permeant/Polymer Diffusional Model to the Desorption of Polychlorinated Biphenyls from Hudson River Sediments, Environmental Science and Technology, Vol. 28, No. 2, 253-2258.
12. Chivers, G. E. (1971). Survey in Industrial Wastewater Treatment: Petroleum and Organic Industries, Vol. 2, Noyes Data Co., Park Ridge, NJ.
13. Connaughton, Doreen F., J. R. Stedinger, L. W. Lion, and M. L. Shuler (1993). Description of Time-Varying Desorption Kinetics: Release of Naphthalene from Contaminated Soil, Environmental Science and Technology, Vol 27, No. 12, 2397-2403.

14. Cornell L. P. and Kuo, C. H. (1984). A Kinetic Study of Ozonation of Phenanthrene in Aqueous Solutions. Trans. Air Pollut. Control Association, March, 275-286.
15. Crank, J., The Mathematics of Diffusion, Second Edition, Clarendon Press, Oxford, 1975.
16. Esrig, M. I. (1964). Report of a Feasibility Study of Electro-kinetic Processes for Stabilization of Soils for Military Mobility Purposes, Research Report No. 1, School of Civil Engineering, Cornell University, Ithaca, New York.
17. Esrig, M. I. and S. Majtenyi (1966). A New Equation for Electroosmotic Flow and Its Implications for Porous Media, Highway Research Record, No. 111, 31-41.
18. Flaszer, B. and Sobkowiak A., (1983). Electrochem. Acta., 28, 1315.
19. Gauthler, Thomas D., W. R. Seltz, and C. L. Grant (1987). Effects of Structural and Compositional Variations of Dissolved Humic Materials on Pyrene K_{oc} Values, Environmental Science and Technology, Vol. 21, No. 3, 243-248.
20. Glaze, W. H., Kang, J. W., and Chapin, D. H. (1987). The Chemistry of Water Treatment Involving Ozone, Hydrogen Peroxide and Ultraviolet Radiation, Ozone Sci. & Technol, Vol. 9, No. 4, 335.
21. Gray, D. H. and J. K. Mitchell (1967). Fundamental Aspects of Electro-Osmosis in Soils, Journal of the Soil Mechanics and Foundations Division, ASCE, Vol. 93, No. SM6, Proceeding Paper 5580, November, 209- 236.
22. Helmholtz, H. (1879), Wiedemanns Annalen d. Physik, Vol. 7, 137.
23. Hoigne, J. and Bader, H. (1978). Ozone Initiated Oxidation of Solutes in Wastewater. A Reaction Kinetics Approach, Progress Water Technology, 10, 657-670.
24. Hoigne, J. and Bader, H. (1983). Rate Constant of Ozone with Organic and Inorganic Compounds in Water Non-dissociating Organic Compounds, Water Research, 17, 185.
25. Hoogendon, D. (1984). Review of Development of Remediation Action Techniques for Soil Contamination in Netherlands, Proceedings, Hazardous Material Spills Conference, 9-65.
26. Huang, C . P., Dong, C., Tang, Z. (1993). Advanced Chemical Oxidation: Its Present Role and Potential Future in Hazardous Waste Treatment, Waste Management, Vol. 13, 361-377.
27. Hunter, R. J. (1981). Zeta Potential in Colloid Science Principles and Applications, Academic Press, Orlando.
28. Ilnitsky, A. P., Khesina, A. Y., Cherkinsky, S. N. and Shabad, L. M. (1968). Effect of Ozonation of Aromatic, Particularly Carcinogenic Carbonhydrates, Gigiena I Sanitarija, 3, 8-11.
29. Kan, A. T., G. Fu, M. Hunter, W. Chen, C. H. Ward, and M. B. Tomson (1998). Irreversible Sorption of Neutral Hydrocarbons to Sediments: Experimental Observations and Model Predictions, Environmental Science and Technology, Vol. 32, No. 7, 892-902.
30. Kan, Amy T., G. Fu, and M. B. Tomson (1994). Adsorption/Desorption Hysteresis in

Organic Pollutant and Soil/Sediment Interaction, Environmental Science and Technology, Vol. 28, No. 5, 859-867.

31. Lapidus, L. and N. R. Amundson (1952). Mathematics of Adsorption in Beds. VI. The Effect of Longitudinal Diffusion in Ion Exchange and Chromatographic Columns, Journal of Physical Chemistry, Vol. 56, 984-988.
32. Legube, B., Guyon S., Sugimitsu, H. and Dore M. (1984). Ozonation of Some Aromatic Compounds in Aqueous Solution: Styrene, Benzaldehyde, Naphthalene, Diethylphthalate, Ethyl and Chlorobenzenes. Ozone: Sci. & Eng., 5, 151-169.
33. Legube, B., Guyon S., Sugimitsu, H. and Dore M. (1986). Ozonation of Naphthalene de l'Ozone et Produits de reaction, Water Research, 20, 197-208.
34. Mackay, D. M., and L. A. Smith (1990). Agricultural Chemicals in Groundwater: Monitoring and Management in California, Journal of Soil Water Conservation, Vol. 45, 253-255.
35. Martinez, D. (1986). Chemical Waste: Handling and Treatment, Springer-Verlag, Berlin.
36. Mckinnon, R. J. and Dykesen, J. E. (1984). Removing Organic from Groundwater through Aeration plus GAC, J. Am. Water Works Asso., 76, 42.
37. Michelcic J. r., and Luthy, R. C. (1988). Degradation of Polycyclic Aromatic Hydrocarbon Compounds under Various redox Conditions in Soil-Water Systems, Applied Environmental Microbiology, Vol. 54, 1182 – 1187.
38. Miller, Cass T. and J. A. Pedit (1992). Use of a Reactive Surface-Diffusion Model to Describe Apparent Sorption-Desorption Hysteresis and Abiotic Degradation of Lindane in a Subsurface Material, Environmental Science and Technology, Vol. 26, No. 7, 1417-1427.
39. Mitchell, J. K. (1986). Potential Use of Electrokinetics for Hazardous Waste Site Remediation, U. S. EPA - University of Washington, Workshop on Electrokinetics Treatment and Its Application in Environmental-Geological Engineering for Hazardous Waste Site Remediation, Seattle, WA, Aug 4-5, 20.
40. Mitchell, J. K. (1993). Fundamentals of soil behavior, 2nd edition, John Wiley & Sons, New York.
41. Moriconi, E. J. and Salce, L. (1967). Ozonolysis of Polycyclic Aromatics, J. Org. Chem., 32, 2829-2837.
42. Moriconi, E. J. and Salce, L. (1968). Carcinogenicity and K- and/or L-region Additivity towards Ozone, Advances in Chemistry Series, 77, 65-73.
43. Nzengung, V. A., P. Nkedi-Kizza, R. E. Jessup, and E. A. Voudrias (1997). Organic Cosolvent Effects on Sorption Kinetics of Hydrophobic Organic Chemicals by Organoclays, Environmental Science and Technology, Vol. 31, No. 5, 1470-1475.
44. Patric, R.(1983). Groundwater Contamination in the United States, National Academy Press, Washington, DC.
45. Pavlostathis, S. G. and K. Jaglal (1991). Desorptive Behavior of Trichloroethylene in

Contaminated Soil, Environmental Science and Technology, Vol. 25, No.2, 274-279.

46. Pignatello, J. J. and B. Xing (1996). Mechanisms of Slow Sorption of Organic Chemicals to Natural Particles, Environmental Science and Technology, Vol. 30, No. 1, 1-11.
47. Reid, B. J., G. L. Northcott, K. C. Jones, and K. T. Semple (1998). Evaluation of Spiking Procedures for the Introduction of Poorly Water Soluble Contaminants into Soil, Environmental Science and Technology, Vol. 32, No. 20, 3224-3227.
48. Schmid, G. (1950), Zur Electrochemie Feinporiger Kapollarsystems, Zhurnal fur Elektrochemie, Vol. 54, 424.
49. Schwarzenbach, R. P., Gschwend, P. M., and Imboden, D. M. (1993). Environmental Organic Chemistry, New York.
50. Sedlak, D. L., and Andren, A. W., (1991). Oxidation of Chlorobenzene with Fenton's Reagent, Environ. Sci. & Technol., Vol. 25, No. 4, 777-782.
51. Smoluchowski, M. (1914), Handbuch der Elektrizitat und des Magnetismus, Vol. 2.
52. Spiegler, K. S. (1958). Transport Processes in Ionic Membranes, Transactions, Faraday Society, Vol. 54, 1408-1428.
53. Steinberg, S. M., J. J. Pignatello, and B. L. Sawhney (1987). Persistence of 1,2-Dibromoethane in Soils: Entrapment in Intraparticle Micropores, Environmental Science and Technology, Vol. 21, No. 12, 1201-1208.
54. Stief, K. (1984). Remedial Action for Groundwater Protection, Proceedings, Hazardous Material Spills Conference, 9-65.
55. Strier, M. P. (1980). Pollution Treatability: A molecular Energy Approach, Environ. Sci. & Technol., Vol. 14, No. 28.
56. Sturrock, M. G., Cline, E. L. and Robinson, K. R. (1963). The Ozonation of Phenanthrene with Water as Participating Solvent, J, Org. Chem., 28, 2340.
57. U.S. Environmental Protection Agency, EPA-600/3-80-040 (1980). The Fate and Effect of Crude Oil Spilled on Subarctic Permafrost Terrain in Interior Alaska, Corvallis Environmental Research Laboratory, Corvallis, OR.
58. Walling, C. (1975). Fenton's Reagent Revisited, Acc. Chem. Res., Vol. 8, 125.
59. Walling, C. (1976). Fenton Chemistry Revisited, Acc. Chem. Res., Vol. 9, 175.
60. Walling, C. and Kato S. (1970). The Oxidation of Alcohols by Fenton's Reagent: the Effect of Copper Ion[1], J. American Chemical Society, 93:17, 4275-4281.
61. Walters, R. W. and G. E. Annette (1988). Sorption of 2,3,7,8-Tetrachlorodibenzo-p-dioxin to Soils from Water/Methanol Mixtures, Environmental Science and Technology, Vol. 22, No. 7, 819-825.
62. Watts, R. J. (1998). Hazardous Wastes: Sources, Pathways, Receptors. John Wiley and Sons, Inc., New York.

63. Weber, W. J., and W. Huang (1996). A Distributed Reactivity Model for Sorption by Soils and Sediments. 4. Intraparticle Heterogeneity and Phase-Distribution Relationships under Nonequilibrium Conditions, Environmental Science and Technology, Vol. 30, No.3, 881-888.
64. Werth, C. J. and M. Reinhard (1997). Effects of Temperature on Trichloroethylene Desorption from Silica Gel and Natural Sediments. 2. Kinetics, Environmental Science and Technology, Vol. 31, No. 3, 697-703.
65. Wood, P. R. (1980). Removing Potential Organic Precursors from Drinking Water, EPA - 600/2-80-130a.
66. Wu, S. C. and P. M. Gschwend (1986). Sorption Kinetics of Hydrophobic Organic Compounds to Natural Sediments and Soils, Environmental Science and Technology, Vol. 20, No. 7, 717-725.